The Dissertation Committee for Andrew Christopher Stolte Certifies that this is the approved version of the following dissertation:

Advancements in Direct-Push Seismic Testing

Committee:

Brady R. Cox, Supervisor

Ellen M. Rathje

Kenneth H. Stokoe II

Clark R. Wilson

Liam M. Wotherspoon

Advancements in Direct-Push Seismic Testing

by

Andrew Christopher Stolte

Dissertation

Presented to the Faculty of the Graduate School of

The University of Texas at Austin

in Partial Fulfillment

of the Requirements

for the Degree of

Doctor of Philosophy

The University of Texas at Austin

May 2018

Dedication

To my parents, for their enduring love, for their endless support, for fostering my love of learning.

Acknowledgements

First and foremost, I would like to express my deepest gratitude to my supervising professor, Dr. Brady Cox. I am thankful for his continual guidance and support throughout my doctoral studies. As a mentor he has shaped me into a better researcher, a better engineer, and a better human being. I have been inspired by his passion for quality work, his upmost professionalism, his abiding patience, and his genuine desire to help and teach others.

I would like to thank the members of my dissertation committee who have taken interest in my work and pushed me to achieve my academic goals. Thank you to Dr. Clark Wilson for teaching me the basics of signal processing. Thank you to Dr. Liam Wotherspoon supporting the development of my research and providing me the opportunity to conduct field work in New Zealand. Thank you to Dr. Ellen Rathje for her infectious enthusiasm and sharing her technical expertise. Thank you to Dr. Kenneth Stokoe, II for sharing his boundless knowledge of soil dynamics and providing insightful feedback at every step in the development of my research.

I would like to thank the other geotechnical engineering faculty at the University of Texas, including Dr. Chadi El Mohtar, Dr. Robert Gilbert, and Dr. Jorge Zornberg, who have taught me so much over the past few years and help develop the some of the best geotechnical engineers in the world.

I would like to thank the staff at the University of Texas who have helped me throughout my studies. Thank you to Robert Kent for sharing your knowledge of electronics and helping me to build various pieces of equipment in support of my research. Thank you to Andrew Valentine for help with field work and providing a thoughtful ear during our lunches together. Thank you to Dr. Farnyuh Menq sharing his expertise soil dynamics. Thank you to Alicia Zapata for helping me navigate the CAEE departmental structure and simplifying the system. Thank you to Chris Trevino for helping with orders

for obscure electronic parts. Thank you to Leslie McCroddan and Velma Vela for administrative support.

I would like to acknowledge the support and kindness of the many friends that I have made over my time at the University of Texas. I value your friendship and note the indelible impression each of you have made on my life. David Teague and Andrew Keene have been my steadfast and loyal companions along the journey of my doctoral studies. I have been fortunate to have your support and advice over our many years together. I must acknowledge the help and guidance of those students who came before me: Clinton Wood, Shawn Griffiths, and Trenton Ellis. You taught me the basics of soil dynamics and helped me grow as a researcher. I would like to thank Joe Vantassel, Ahmed Hussien, Reihaneh Hosseini, and Karly Summerlin, Joe Vantassel, and Michael Yust for making my last years at UT brighter and providing sanity during my writing crunch. I'd also like to acknowledge Jeremey Faker, Hande Gerkus, Mohamad Hallal, Sungmoon Hwang, Edward, Jaimes, Jillian Montevallo, Kaleigh McLaughlin, Chris Nelsen, Yuta Nakamura, Breanna Peterman, Aaron Potkay, Jon Rebuck, Julia Roberts and all the others who have made my time at UT enjoyable and memorable.

I would like to thank the many teachers, professors, mentors who encouraged me to seek knowledge and purse my studies in engineering. Bart Black, Forrest Campbell, Dr. Jim Carr, William Fitzgerald, Dr. Bob Watters, and many others have fostered my love of learning.

Lastly and most importantly, I would like to thank my family and lifelong friends for their everlasting support and love. My parents, Bruce and Kolleen, who fostered my thirst for knowledge and pushed me to do my best. My brother, Tim, who has always been there to challenge me and encourage me to adapt. My sister, Sarah, who has always been there to listen. My grandparents, who provided sagely advice and constant support in my youth. My aunt, Kari, who provided an ear for my concerns and offer frank advice. My lifelong friends, Alex, Chas, Cody, Jeff, Joe, Laura, and Nick, who have always been there to support me and kept my head on straight.

Abstract

Advancements in Direct-Push Seismic Testing

Andrew Christopher Stolte, Ph.D.

The University of Texas at Austin, 2018

Supervisor: Brady R. Cox

Invasive seismic testing methods are used to evaluate the in-situ small-strain stiffness of soil and rock for geotechnical earthquake engineering analysis and design. These methods provide localized measurements of the constrained compression and shear wave velocities, V_P and V_S, respectively. Early invasive testing methods, including crosshole (CH) and downhole (DH), were exclusively borehole-based (i.e., the test was performed in a pre-drilled borehole). The time and costs associated with the preparation of one or more boreholes are notable disadvantages of conventional CH and DH testing, significantly limiting their use. Direct-push variants of these testing methods have been developed, where the instrumentation can be installed in conical probes and a directly into the ground. This dissertation documents recent advancements in direct-push invasive seismic testing.

One such advancement is the development of the direct-push crosshole testing (DPCH) method where P- and S-waves are propagated between instrumented cones,

pushed directly into the ground. Each instrumented cone contains a sensor package including geophones to measure the seismic waveforms and a three-component MEMS accelerometer to track the cone deviation/position during the test. DPCH testing enables high-resolution profiles of V_P and V_S to be measured over the top 20 – 30 m of the subsurface.

In addition to developing a high-resolution velocity profile, it is important to quantify the epistemic uncertainty associated with these measurements. Often, a single velocity profile is provided to the engineer with no indication of uncertainty leaving the engineer to potentially over- or under-predict this uncertainty. Yet, through the consideration of multiple data reduction techniques and analysis methods, a robust and meaningful quantification of the epistemic uncertainty may be developed.

A direct application of DPCH high-resolution V_P and V_S measurements is the estimation of in-situ void ratio in granular soils using a relationship developed by Foti et al. (2002). The effectiveness of using DPCH measurements to estimate in-situ void ratio in granular soils is critically examined through comparisons with current in-situ penetration based estimates and laboratory measurements developed at several case history sites. The limitations associated with these estimates are explored in-depth.

Table of Contents

List of Tables

List of Figures

Chapter 1: Introduction

1.1 BACKGROUND

Near-surface, seismic testing methods are commonly used to evaluate in-situ soil and rock stiffness for engineering analyses and designs. Of particular interest are the small-strain constrained compression modulus (M_0) and shear modulus (G_0), which are proportional to the squares of primary constrained compression (P) and secondary shear (S) wave velocity, respectively. Generally, testing methods aimed at measuring P-wave velocity (V_P) and S-wave velocity (V_S) are broken into two distinct groups: (1) non-invasive/surface-based methods (e.g., seismic refraction and surface wave testing) and (2) invasive/borehole-based methods (e.g., downhole and crosshole testing).

Invasive seismic testing methods, the focus of the research presented herein, involve the placement of a seismic source and/or the receiver(s) below the ground surface. Initially, invasive seismic methods were used for deep exploration, typically to locate petroleum (McCollum and LaRue 1931, Dix 1939). These methods were subsequently adapted and developed for use in geotechnical engineering in the 1970's (Stokoe and Woods 1972, Woods 1978). During those early years, invasive testing methods, including downhole (DH) and crosshole (CH) seismic testing, were exclusively borehole-based (i.e., the source and/or receiver packages were lowered down a pre-drilled borehole). Later, direct-push variants of these testing methods were developed, for which the instrumentation could be installed in conical probes and directly advanced into the ground (e.g., seismic cone penetration testing (SCPT, Robertson et al. 1986) is the direct-push

equivalent of DH testing). These invasive seismic methods are further detailed in Chapter 2.

Non-invasive seismic testing methods are generally considered to be more uncertain/less reliable than invasive methods. However, a recent, comprehensive, blind-analysis study at three geologically-distinct sites in Europe revealed that V_S profiles derived from surface wave testing had coefficients of variation that were often similar to, and at times lower than, those derived from a combination of crosshole, downhole and PS suspension logging. The Garafalo et al. (2016b) study draws attention to the fact that uncertainties exist in *both* invasive and non-invasive methods and that those uncertainties need to be realistically quantified to aid subsequent engineering analyses. While this is not a new finding, it would be extremely rare at the present time for those conducting either invasive or non-invasive seismic testing to attempt to communicate this uncertainty to the end-user through statistics, or by providing multiple interpretations of the same dataset. Although still not common in practice, significant research has been devoted to quantifying uncertainty in V_S profiles derived from non-invasive surface wave testing (e.g., Marosi & Hiltunen 2004, Foti et al. 2009, Griffiths et al. 2016a, Teague & Cox 2016, Teague et al. 2018). On the other hand, comparatively little attention has been devoted to quantifying uncertainty in V_S profiles derived from invasive methods (Styler and Weemees 2016).

Two different types of V_S uncertainty need to be quantified for engineering analyses such as seismic site response (EPRI 2012): (1) aleatory variability, and (2) epistemic uncertainty. In terms of V_S, aleatory variability results from the inherent variability/randomness associated with the subsurface layering and shear stiffness across

the footprint of the site. Thus, aleatory variability is linked to the horizontal and vertical spatial variability of V_S. Aleatory variability can be estimated by the end-user of V_S data by considering the spatial variability of the invasive V_S profiles, which are essentially point-measurements. On the other hand, epistemic uncertainty results from data and modeling uncertainties. Thus, even for a single location, epistemic uncertainty in V_S exists due to factors such as data quality and method of analysis. As noted above, epistemic uncertainty in V_S is rarely quantified by those performing invasive seismic testing. Rather, a single, deterministic V_S profile is typically provided for a each testing location without consideration of uncertainty. Hence, end-users need to make assumptions about the epistemic uncertainty in V_S for use in subsequent analyses. For example, it is extremely common for engineers to account for epistemic uncertainty in seismic site response by creating upper- and lower-bound V_S profiles obtained by arbitrarily increasing and decreasing the reference V_S profile by a constant, depth-independent factor such as +/- 20% to 30% (Matasovic and Hashash 2012, Griffiths et al. 2016a). However, this methodology has recently been called into questions and has been shown to yield poor estimates of seismic site response (Griffiths et al. 2016b, Teague and Cox 2016). As such, methods for realistically quantifying epistemic uncertainty in V_S profiles derived from invasive seismic tests are needed. The epistemic uncertainty associated with invasive seismic measurements is further explored in Chapter 3.

A promising application of invasive seismic measurements is the evaluation of in-situ soil void ratio. Void ratio is fundamental to the understanding of soil behavior based on the critical state soil mechanics framework. Soil compressibility, permeability, and

shear strength are governed by the density (i.e., compactness) of the solid soil particles. Often, the in-situ void ratio is evaluated based on laboratory measurements on high-quality, "undisturbed" samples of soil. While "undisturbed" sampling of clayey-soils is commonplace in geotechnical practice, high-quality samples of granular soils are difficult and expensive to obtain. Hence, in-situ void ratio or relative density is often estimated using empirical relationships to in-situ measurements from penetration testing (e.g., CPT). CPT-based relationships are typically developed based on controlled testing of carefully prepared clean sand samples, limiting their application to similar soils. Void ratio relationships with strong theoretical underpinnings are needed for application to a wider range of soils. Using Biot's theory of linear poroelasticity as an underlying framework, Foti et al. (2002) derived a relationship that can be used to estimate soil porosity based on experimentally measured stress wave propagation velocities (i.e., V_P and V_S) and the physical properties of the soil, including the density (ρ_W) and bulk modulus (K_W) of water, the density (ρ_S) and bulk modulus (K_S) of the solid soil particles, and the Poisson's ratio of the soil skeleton (ν_{SK}). By using typical constant values for many of the parameters, which can be reasonably assumed in most cases, the relationship may be used to estimate in-situ void ratio from high-resolution measurements of V_S and V_P obtained via direct-push crosshole testing, as detailed in Chapter 4.

1.2 SCOPE OF RESEARCH

This dissertation details recent advancements in direct-push, near-surface, invasive seismic testing aimed at geotechnical engineering practice. First, the development and

refinement of the direct-push crosshole (DPCH) testing method is documented. In support of this work, several instrumented cones (including an in-ground source cone) were designed and fabricated by researchers at the University of Texas at Austin (UT). Recent cone designs have incorporated tri-axial MEMS accelerometers for tracking tilt angles and relative cone positon, thus allowing for the accurate calculation of the distance between cones at each measurement depth. The in-ground source cone uses six spring-loaded solenoids to generate stress waves in the vertical, horizontal in-line, and/or horizontal cross-line directions with positive or negative polarity. Using these cones, DPCH testing has been conducted by UT personnel at more than 90 sites. Insight gained from this testing has been used to refine the DPCH testing methodology and develop procedures for the acquisition and reduction of field data.

Second, this research investigates the epistemic uncertainty associated with the development of shear wave velocity profiles from seismic cone penetration testing (SCPT). This epistemic uncertainty has been quantified through the consideration of several shear wave travel time data reduction techniques and velocity analysis methods.

Lastly, this research examines the effectiveness and limitations of using seismic measurements to evaluate in-situ void ratio. Using Biot's theory of linear poroelasticity, Foti et al. 2002 developed a relationship to evaluate porosity (i.e., void ratio) based on seismic wave propagation velocities (i.e., V_S and V_P). This seismic-based relationship is used to develop in-situ void ratio estimates from high-resolution V_S and V_P profiles obtained at ten case history sites in Christchurch, New Zealand via direct-push crosshole

testing in predominantly clean sands. Relative comparisons are made between CPT-based estimates of in-situ void ratio those obtained from seismic measurements.

1.3 ORGANIZATION OF DISSERTATION

This dissertation is organized into three main body chapters (Chapters 2 through 4) along with an introduction (Chapter 1) and a conclusion (Chapter 5). Each main body chapter is a self-contained journal article that includes a literature review, research findings, and conclusions. All references are provided at the end of the dissertation.

Chapter 2 discusses the development of the direct-push crosshole testing method, an invasive, near-surface seismic testing method. The method combines the desirable characteristics of borehole-based crosshole seismic testing with the relative inexpense and speed of direct-push testing methods like cone pentation testing. This chapter documents the method in detail and establishes guidelines for appropriate field data acquisition and processing. Example DPCH datasets are presented with supporting geotechnical data, including borehole stratigraphy, soil classifications, and CPT sounding results. Challenges associated with DPCH testing are also discussed.

Chapter 3 discusses the depth-dependent epistemic uncertainty in V_S profiles obtained from seismic cone penetration testing. Epistemic uncertainty is quantified by considering both shear wave travel time data reduction techniques and analysis methods used to develop profiles of V_S. A detailed comparison of several V_S profiles is presented for two SCPT datasets. Also, the inter-method variability/bias between SCPT and DPCH

testing (as described in Chapter 2) is examined using 31 co-located datasets collected in Christchurch, New Zealand.

Chapter 4 examines the use of high-resolution V_S and V_P profiles obtained via DPCH testing (presented in Chapter 2) to evaluate in-situ void ratio using the Foti et al. (2002) porosity relationship. A simple parametric study is developed to evaluate the sensitivity of these void ratio seismic-based estimates to measured and assumed input parameters (e.g., V_P, V_S, ρ_W, K_W ρ_S, K_S, and v_{SK}). This seismic-based porosity relationship is then applied to ten clean sand case history sites with DPCH testing. Theses DPCH seismic-based estimates of void ratio are compared to those obtained via three CPT-based empirical relationships.

Chapter 5 provides closing remarks, summarizing important findings and proposing future research topics.

Chapter 2: A Direct-Push Crosshole (DPCH) Test Method for the In-Situ Evaluation of High-Resolution P- and S-wave Velocities

Brady R. Cox, Andrew C. Stolte, Kenneth H. Stokoe, II, and Liam M. Wotherspoon

This chapter contains a journal article that has been submitted to the ASTM Geotechnical Testing Journal and has been accepted with revisions. The full citation is listed below:

Cox, B. R., Stolte, A. C., Stokoe, K. H., II, and Wotherspoon, L. M., (2018). "A Direct Push Crosshole (DPCH) Test Method for the In-Situ Evaluation of High-Resolution P- and S-wave Velocities". *ASTM Geotechnical Testing Journal*. Manuscript in review.

As second author, I was responsible for approximately 33% of the concept development, 50% of the data acquisition, 100% of the data processing, and 50% of the results interpretation.

ABSTRACT

The direct-push crosshole (DPCH) test is a new, invasive, near-surface seismic testing method. DPCH combines the desirable characteristics of borehole-based crosshole seismic testing with the relative inexpense and speed of direct-push testing methods like cone penetration testing (CPT). At each measurement depth (typically every 20 – 50 cm), compression (P) and shear (S) waves are generated simultaneously using hammer taps on one of the CPT push rods (a pushable, in-ground seismic source can also be used). These P- and S-waves are propagated between two instrumented seismic cones (i.e, a source and receiver cone). The instrumented cones contain a sensor package with three orthogonally oriented geophones to measure the seismic waveforms, and a MEMS accelerometer to track the deviation/position of each cone as it is advanced into the ground. DPCH testing enables high-resolution profiles of P- and S-wave velocity to be measured over the top 20

– 30 m of the subsurface for use in geotechnical engineering analyses. It also allows for testing across/through ground improvement elements like stone columns. The DPCH instrumentation, testing methodology, and data reduction techniques are explained in detail in this paper, and results from several sites are discussed.

2.1 INTRODUCTION

Near-surface, seismic testing methods are commonly used to evaluate in-situ soil and rock stiffness for engineering analyses and designs. Of particular interest are the small-strain constrained compression modulus (M_0) and shear modulus (G_0), which are proportional to the squares of primary constrained compression (P) and secondary shear (S) wave velocity, respectively. Generally, testing methods aimed at measuring P-wave velocity (V_P) and S-wave velocity (V_S) are broken into two distinct groups: (1) non-invasive/surface-based methods (e.g., seismic refraction and surface wave testing) and (2) invasive/borehole-based methods (e.g., downhole and crosshole testing). Results from a thorough study documenting uncertainties within, and variability between, invasive and non-invasive methods at three blind study sites are presented in Garafalo et al. 2016a and 2016b. As this paper is concerned with invasive methods, only they will be discussed further herein.

Invasive seismic geophysical testing involves placement of instrumented receivers and/or seismic sources below the ground surface. The sensors and/or energy sources are either lowered into pre-drilled boreholes or directly pushed into the ground. Borehole-based seismic tests were initially developed and used in exploration geophysics. They were

then adapted for near-surface geotechnical engineering purposes in the 1970's (Stokoe and Woods 1972, Woods 1978). Two borehole-based seismic methods are commonly used for near-surface (depth ≤ 30 m) geotechnical site investigations: (1) crosshole seismic testing, and (2) downhole seismic testing. Each of these methods is briefly discussed below.

Crosshole seismic testing (ASTM D4428/D4428M-14, Stokoe and Woods 1972) is performed by lowering a source for generating seismic energy and one or two receivers incrementally down separate boreholes spaced 1.5 to 5 meters apart. The source and receiver(s) are advanced to a common measurement depth and coupled to the borehole wall to ensure good transmission of seismic waves. P- and S-waves are generated by the source and radially propagated through the soil. The waves traveling along a predominately horizontal path arrive at the receiver borehole(s) and are recorded using properly oriented transducers (geophones or accelerometers). The distances between the source and receiver boreholes at each measurement depth must be determined from a borehole deviation survey. The P- and S-wave arrival times are manually picked from the seismic waveforms recorded at the receiver(s). Typically, the use of two receivers is encouraged to allow the measurement of three different travel times: (1) source-to-receiver one, (2) source-to-receiver two, and (3) receiver one-to-receiver two. Examining these three different travel times allows identification of refracted wave travel paths and/or inhomogeneity in material properties between the boreholes. Using a single receiver is acceptable according to ASTM D4428, but it is crucial to: (1) properly calibrate the system to obtain trigger calibration factors, (2) record the trigger signal at each depth to verify consistent triggering since a true receiver-to-receiver interval measurement is not possible, and (3) properly orient the

horizontal, in-line receiver. To evaluate V_P and V_S at each measurement depth, the assumed horizontal wave travel path distance is divided by the corresponding wave travel times. The source and receivers are typically lowered at 1.0 to 1.5-m depth increments, although, the depth increment may be decreased near the ground surface, or in other layers of interest, to improve the spatial sampling of V_P and V_S.

The greatest advantages of crosshole seismic testing are: (1) maintaining a relatively consistent and short wave travel path, (2) preserving a strong signal-to-noise ratio as a function of depth, and (3) predominantly propagating waves through a single layer at each measurement depth. These three factors result in detailed wave velocity profiles with the potential to detect relatively thin layers. However, when testing in soft materials confined between stiffer materials, there is a potential for refracted waves traveling along stiffer layer boundaries to arrive faster than the direct waves through the soft material, leading to ambiguities in picking the correct wave arrival times. These refracted waves can mask the presence of thin, soft layers and/or lead to erroneously high velocities over transition zones. A priori knowledge of soil stratigraphy, limiting the horizontal distance between boreholes, and using small depth increments will help limit the impact of refracted waves. Furthermore, an experienced analyst can often identify early refracted wave arrivals by observing differences in polarity and amplitude relative to the direct arrivals. Another disadvantage of crosshole seismic testing is that it requires *two or three* boreholes to be drilled in close proximity to one another. The expense for three such boreholes is difficult to justify for many site characterization studies.

Downhole seismic testing is conducted by exciting a seismic energy source at the ground surface and measuring the wave arrivals at a receiver incrementally lowered into a single, cased borehole (ASTM D7400-14). The seismic source is horizontally offset from the top of the borehole and fluid is drained from the casing (at least over the top 10 m) to limit the potential for waves traveling directly down the borehole (i.e., tubes waves) and interfering with waves traveling through the geologic material. At the ground surface, P-waves are excited with a downward strike and S-waves are excited by hitting the ends of a rigid shear/traction plank. The receiver is coupled to the borehole wall at each testing location to ensure good transmission of seismic waves. The P- and S-wave arrival times are manually picked from the seismic waveforms recorded on properly oriented transducers within the receiver. The wave travel path is most often assumed as the straight-line/slant distance from the source at the ground surface to the receiver at depth. However, there are cases when this is not correct and the actual wave travel path is unknown, particularly over the top several meters of the subsurface. Typical shallow investigation testing increments range from 0.5 to 1.5 m.

A cased borehole is necessary to conduct traditional downhole seismic testing. Like traditional crosshole testing, drilling the borehole and properly installing/grouting the casing can be a slow and rather expensive undertaking. An alternative for soft ground conditions and shallow investigations (depth typically $\leq$ 30 m) is to directly push the sensor package into the ground, which ensures excellent coupling with the surrounding material and reduces costs associated with the borehole preparation. This is most commonly done by adding accelerometers or geophones to a standard cone used for cone penetration testing

(CPT; ASTM D5778-12), which allows seismic CPT (SCPT) downhole tests to be conducted. SCPT measurements are typically taken once every meter, when advancement of the cone is paused in order to add a 1-m long segment of push rod. In some cases, multiple receiver packages spaced at 0.5 to 1.0 m are installed in the cone, enabling a true interval measurement of wave arrival times.

There are multiple downhole/SCPT data reduction methods (e.g., true-interval, pseudo-interval (ASTM D7400-14), corrected vertical travel time/slope method (Redpath 2007, Boore and Thompson 2007), and ray tracing inversions (Baziw 2002)). While ASTM D7400-14 primarily discusses the pseudo-interval method, other methods are allowed provided they are accurately documented and scientifically sound. While a detailed discussion of these methods is beyond the scope of this paper, it should be noted that different processing methods can yield quite variable results even for the exact same wave arrival pick (refer to Chapter 3). Notably, the pseudo-interval method can result in velocity profiles that have apparently thin layers with large changes in velocity when triggering is inconsistent between measurement depths. Inconsistent triggering can be difficult to determine because the trigger signal is often not recorded during downhole or SCPT testing.

Downhole and SCPT are substantially less expensive than crosshole seismic testing, which requires two or three cased boreholes, more equipment, and somewhat more time to complete. As a result, downhole testing is generally performed more frequently than crosshole testing. However, it would be difficult to argue that downhole is advantageous over crosshole on any other technical basis. To begin with, during downhole

testing the length of the travel path consistently increases, the signal-to-noise ratio consistently decreases, and the high-frequency content of the signal is continually filtered out with increasing depth of investigation (Stokoe and Hoar 1978). These three factors result in decreasing resolution of V_P and V_S with depth and an increasing travel time, making it more difficult to obtain detailed velocity profiles and detect thin layers. Additionally, downhole results over the top several meters of the subsurface may be inaccurate due to unknown wave travel paths caused by the high angle of incidence and wave refractions through the near surface layers. This effect is greatly reduced as depth increases, the slanted travel path approaches vertical, and the angle of incidence decreases to small values. However, because borehole/cone deviation is not accounted for in downhole testing, the assumed travel path distances at depth are not completely accurate. Furthermore, it can be extremely difficult to obtain reliable P-wave velocities during SCPT testing because the compression waves tend to find their way into the steel push rods, travel vertically down the rod, and arrive at the receiver before the direct arrivals through the soil, obscuring the direct P-wave arrivals. Transmission of energy through the push rods generally does not obscure S-wave arrivals due to the difficulty in creating translational motion in the rods.

The resolution of V_P and V_S using both crosshole and downhole/SCPT testing is dependent upon several factors. Typically, V_P and V_S are evaluated assuming the seismic waves travel as rays. In reality, the waveforms observed at the receiver result from several waves constructively interfering inside a zone or volume of soil along the length of the ray path. The size of the Fresnel zone/volume is dependent upon both wavelength (i.e.,

frequency and propagation velocity) and the length of the ray path (Spetzler and Snieder, 2004). As either wavelength or ray path length increase, the P- and S-waves "see" or sample the material properties of larger volumes. The resolved P- and S-wave velocities represent the smearing or averaging of the sampled material properties (Backus 1962). In downhole/SCPT testing, the ever increasing ray path length and the increased attenuation of high-frequency waves due to anelastic damping effects, both result in increasing Fresnel zones/volumes and decreased resolution of V_P and V_S with depth. In crosshole testing, the P- and S-waves travel along a predominantly horizontal travel path that does not vary greatly with depth. The relatively consistent, short ray path length and limited attenuation result in smaller Fresnel volumes/zones and higher resolution of V_P and V_S, as compared to downhole/SCPT testing. The resolution of V_P and V_S are different, depending on the velocities and frequencies of each seismic wave. The identification of a thin layer is dependent on the frequency content of the source and the material properties of the layer.

A new, invasive, seismic testing method has been developed which combines the technical benefits of crosshole seismic testing with the ease and speed of direct-push downhole/SCPT methods. Direct-push crosshole (DPCH) testing uses a pair of instrumented seismic cones directly pushed into the ground. Waves are propagated from one cone (the source) to the other (the receiver) in order to evaluate the V_P and V_S of the material between the cones. The seismic energy is generated by either tapping on the top of the CPT push rod for the source cone, or by using a pushable, in-ground seismic source cone. Directly pushing the cones into the ground provides excellent coupling between the cones and the surrounding soil and eliminates the need for expensive cased boreholes.

DPCH testing was initially conceived in the late 1980's by Profs. Stokoe and Jamilokowski to conduct seismic crosshole testing in the Taranto clay using two truck-mounted CPT rigs, but was not developed beyond limited research purposes. Researchers at the University of Texas began using DPCH testing on a regular basis in conjunction with in-situ liquefaction tests conducted using large mobile shakers (Cox et al. 2009) in the early 2000's. The motivation behind these DPCH tests was primarily to investigate the in-situ degree of soil saturation, as inferred from P-wave velocity measurements. For example, Cox (2006) utilized DPCH testing to obtain profiles of V_P and V_S at high spatial resolution at the Wildlife Liquefaction Array and attributed abnormal dynamic pore pressure response at one location due to the presence of soils that were not saturated (as indicated by $V_P <$ 1500 m/s), even though they existed several meters below the hydrostatic ground water level.

The use of DPCH testing accelerated greatly in the aftermath of the Canterbury Earthquake Sequence, which caused unprecedented soil liquefaction damage to the city of Christchurch, New Zealand (Cubrinovski and Robinson 2016, Cubrinovski et al. 2017). Following these earthquakes, an extensive study was initiated to investigate the effectiveness of various shallow ground improvement methods at mitigating soil liquefaction damage to residential structures (Van Ballegooy et al. 2015, Wentz et al. 2015). DPCH testing played a key role in the ground improvement trails (Stokoe et al. 2014, Wotherspoon et al. 2015, Stokoe et al. 2016, Wotherspoon et al. 2017, Hwang et al. 2017), allowing for measurements of V_P and V_S at high spatial resolution in the unimproved soils, in the zones of improved soil between ground improvements, and directly across

ground improvement elements, which cannot be achieved with any other in-situ testing methodology. These tests revealed a number of important findings, including: the tendency for sandy and silty soils in Christchurch to be unsaturated well below the hydrostatic water table, patterns of desaturation caused by installation of certain ground improvements, patterns of decreasing soil shear stiffness due to installation of certain ground improvements, and patterns of soil type-/fines content-dependency on soil shear stiffening due to installation of certain ground improvements.

Following the ground improvement trials, DPCH testing was conducted at 31 sites in Christchurch, New Zealand specifically to contribute profiles of V_P and V_S at high spatial resolution at key liquefaction/no-liquefaction case history sites from the Canterbury Earthquake Sequence (McLaughlin 2017). Both the V_P and the V_S profiles played important roles in attempting to rectify a number of false positive liquefaction case histories predicted by CPT-based simplified liquefaction triggering analyses (Cox et al. 2017). The V_P profiles were used to account for the beneficial effects of partial saturation on the cyclic resistance of soils to liquefaction (Ishihara and Tsukamoto 2004), while the V_S profiles were used to perform simplified V_S-based liquefaction triggering analyses (Andrus and Stokoe 2000, Kayen et al. 2013) and to evaluate the presence of soil microstructure (Robertson 2015).

Given the expanding use of DPCH testing, this paper is meant to document the method in detail and establish key guidelines for appropriate field data acquisition and processing. Example DPCH datasets are presented with supporting geotechnical data,

including borehole stratigraphy and soil classifications, and CPT sounding results. Challenges associated with DPCH testing are also discussed.

2.2 METHODOLOGY OF THE DIRECT-PUSH CROSSHOLE TEST

A simplified DPCH test setup is shown schematically in Figure 2.1. In general, a DPCH test is conducted by pushing two instrumented cones, spaced approximately 1.5- to 2.5-m apart, to discrete, common measurement depths. At each depth, a measurement is performed by exciting seismic energy in the soil at the base of the source cone rod, which travels through the soil to the receiver cone. The seismic energy is excited either by tapping vertically downward on the top of the source cone rod or by using a pushable, in-ground source cone. The hammer tap method is the fastest and simplest means of conducting DPCH testing and is used below to illustrate the testing methodology. In-ground seismic source cones are not commonly available and add complexity to the testing methodology. However, they provide an opportunity for more advanced testing. Using measurements recorded at both instrumented cones (the source and the receiver), the travel time and travel distance of the seismic waves are calculated and used to determine the P- and S- wave velocities, resulting in profiles of V_P and V_S at each discrete measurement depth (typically every 20 – 50 cm). The equipment and testing methodology used for DPCH testing are described in detail below.

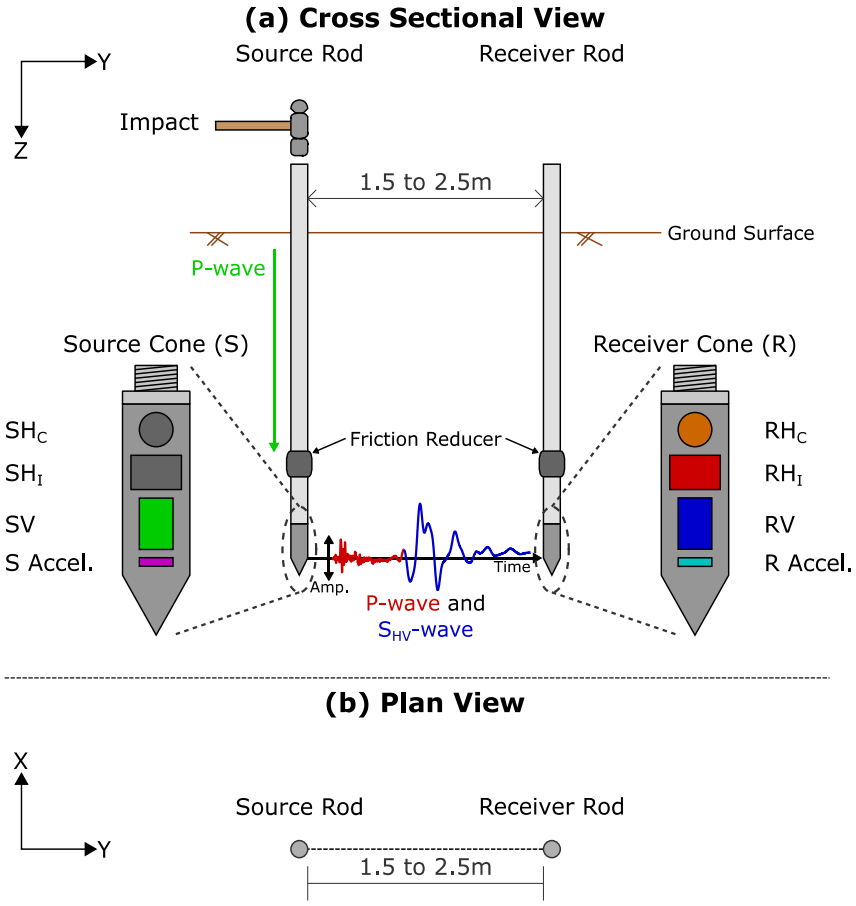

Figure 2.1: Schematic of the DPCH test: (a) Cross sectional view, and (b) plan view. A hammer strike excites a P-wave which travels down the source rod to the source cone (S). Data acquisition is triggered when the P-wave is measured on the vertical geophone in the source cone (SV). At the cone tip, the energy is transferred into the ground and travels as P_H- and S_{HV}-waves to the receiver cone (R), as indicated by the waveform. The P_H-wave is best observed on the receiver horizontal in-line geophone (RH_I) and the S_{HV}-wave is best observed on the receiver vertical geophone (RV). When using an in-ground source, S_{HH}-waves are best observed on the receiver horizontal cross-line geophone (RH_C). The MEMS accelerometers track the tilt of the source and receiver cone (S Accel. and R Accel., respectively) and are used to calculate the position of each cone.

2.2.1 Equipment and Instrumentation

The major components of the DPCH test equipment are: (1) the CPT-type, thrust-providing machines, (2) the instrumented seismic cones, (3) the dynamic source, and (4) the data acquisition system.

2.2.1.1 CPT-type Thrust-providing Machines

Two machines capable of providing controlled downward thrust via hydraulic rams are required to advance and retrieve the instrumented cones for DPCH testing. Standard CPT-type rigs are easily adaptable for this purpose. Large truck- or track-mounted CPT rigs are capable of providing the greatest reaction force (up to 20 tons) when advancing DPCH cones into the ground, but are not easy to maneuver and position in the relatively tight spacing (less than 2.5 m horizontal spacing) ideal for DPCH testing. Small, track-mounted CPT rigs that use auger anchoring systems, like the ones shown in Figure 2.2, have proven to be ideal for DPCH testing in relatively soft soils (< 15-20 MPa CPT tip resistance) down to 20-plus meters. Various combinations of large rigs, small rigs, and independent hydraulic rams with anchoring systems have been utilized successfully in the past.

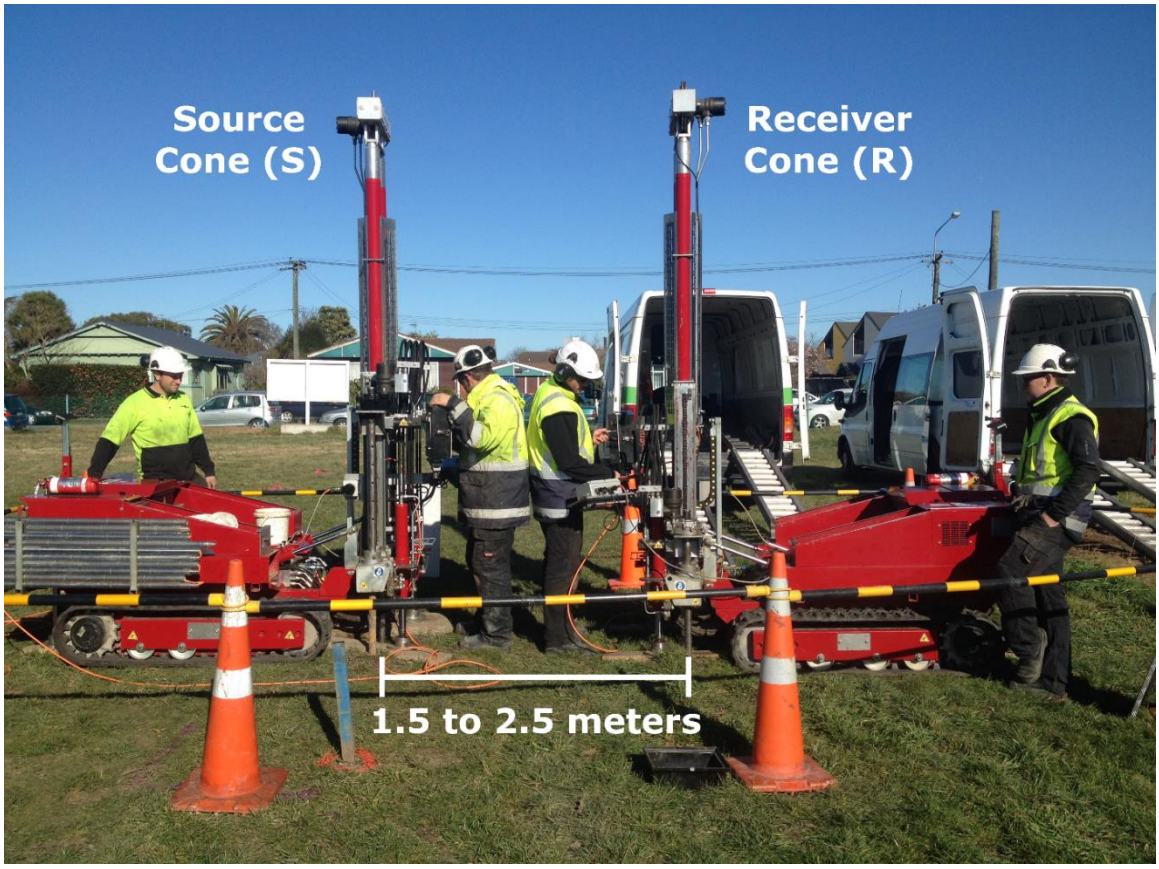

Figure 2.2: Photograph of two track-mounted CPT rigs advancing two DPCH cones for testing. The CPT rigs are positioned such that the DPCH cones are 1.5 to 2.5 meters apart.

The CPT-type push rods used to advance the DPCH instrumented cones should comply with ASTM D5778-12 *Standard Test Method for Electronic Friction Cone and Piezocone Penetration Testing of Soils.* Typical thick-walled, steel CPT cone rods are 1-m long and have a 3.6-cm diameter. The deviation of the rod from a straight axis should be minimized in order to limit cone drift from vertical during advancement into the ground. As discussed in the DPCH Testing Challenges section below, it is important to limit firm coupling between the push rods and the surrounding soil. This is achieved by using friction reducers. Friction reducers are commonly used in CPT testing (ASTM D5578-12) to

decrease the frictional resistance along the cone push rods. As shown in Figure 2.1, a friction reducer is a short length of oversized-diameter (~25% larger) push rod located above the cone tip. As the cone is advanced into the ground, the friction reducer develops a hole in the surrounding soil that is slightly larger than the diameter of the push rods. This effectively breaks the contact between the soil and the trailing push rods. While it is possible for soft soils to collapse into this gap, the coupling between the soil and the push rod is greatly reduced. This limits the transmission of waves along the rod-soil interface.

2.2.1.2 Instrumented Seismic Cones

In order to determine V_P and V_S as a function of depth, two cones outfitted with seismic instrumentation are advanced into the ground. While standard SCPT cones have been used in the past, cones custom built for DPCH testing have proven to be most useful. Since DPCH testing requires incremental measurements every 20-50 cm, standard measurements of CPT tip resistance, sleeve friction, and pore water pressure are best obtained using an accompanying CPT sounding nearby. Hence, there is no advantage to including instrumentation for standard CPT readings in the DPCH cones. Each DPCH cone must be capable of measuring several seismic waves radially propagating from the source cone with different polarities. So, ideally the cones should be outfitted with three orthogonally-oriented (vertical, horizontal in-line, and horizontal cross-line) vibration transducers.

Several versions of custom-built DPCH instrumented cones have been designed, constructed, and tested at the University of Texas at Austin, as detailed in Appendix A.

Each design iteration has incorporated changes based on valuable experience gained in the field during testing. The latest iteration of the custom-built DPCH instrumented cone is shown in Figure 2.3. Each DPCH cone contains a sensor package which is enclosed and protected by a removable, hardened steel housing. The outside diameter is 3.8 cm, which is just slightly larger than the diameter of a standard 10 cm^2 CPT cone. Future versions of the cones may be even larger in diameter, as this provides for a small annulus between the standard CPT push rods and the surrounding soil, which can be beneficial if friction reducers are not used. The apex angle of the cone tip is 60° and the length of the cone is 16.4 cm, not including the threading. The cones are attached to standard CPT rods using the threading at the top of the cone and an adaptor with threads matching that of the CPT rods. Markings on the exterior of the hardened steel jacket indicate polarity of the sensor package for proper orientation (X and Y markings in Figure 2.3) of the cones during testing.

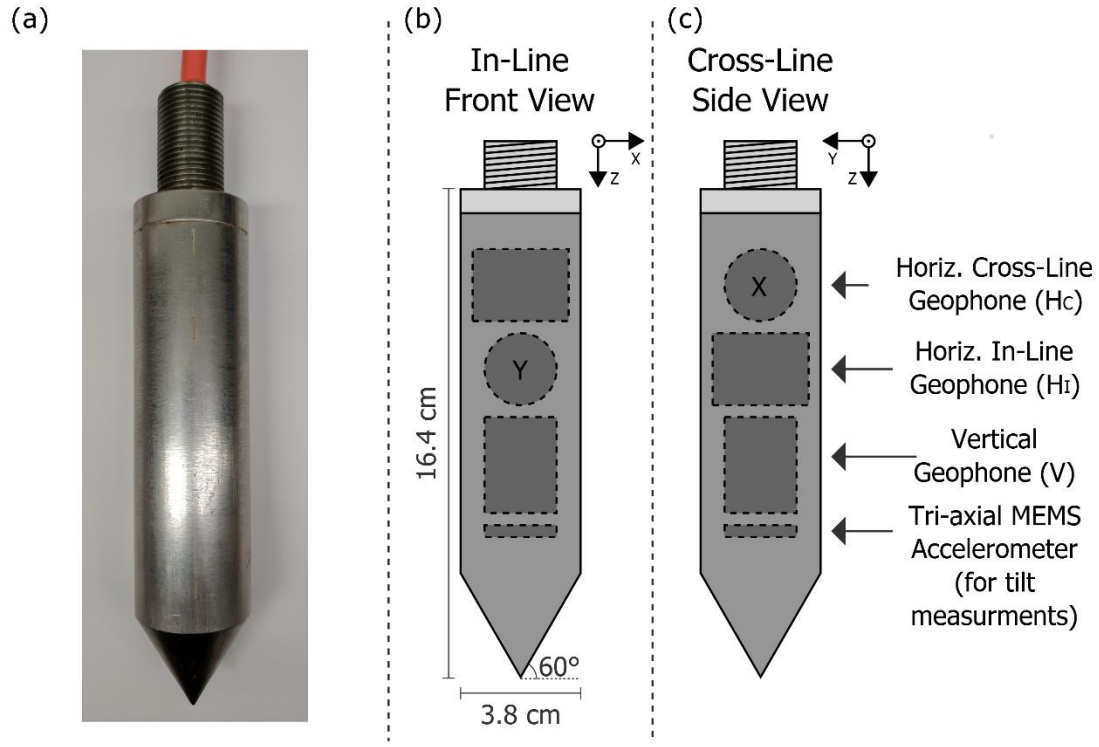

Figure 2.3: Instrumented cone used for DPCH testing. (a) Photograph of instrumented cone showing the exterior hardened steel jacket, the threaded connection to the rod adaptor, and the orange 6-pair cable. The positive horizontal in-line and cross-line directions are indicated by capital Y and X markings, respectively. Schematic of geophone and tri-axial accelerometer orientation inside the instrumented cone as viewed from the positive horizontal (b) in-line, and (c) cross-line directions.

The sensor package inside each cone includes three orthogonally-oriented 28-Hz geophones for the measurement of dynamic signals and a tri-axial MEMS accelerometer for tracking cone tilt. The 28-Hz geophones were selected because of their compact size, ability to function in any orientation while maintaining a constant response curve, robust shock resistance, and capacity to operate without requiring an external power supply. This particular model (GS-14 from Geospace Technologies) has a nominal sensitivity of 290 mV/ips, a damping factor of about 18%, and a height and diameter of approximately 17

mm. The voltage polarity of each geophone, as mounted in the cone, is carefully noted/controlled such that the analyst knows whether to expect a positive or negative voltage when the geophone is excited from a given direction. As discussed below, knowing the sensor polarity is critical for identifying S-wave arrivals, which are indicated by the first *major* change in voltage with the proper/*expected polarity* (e.g., a downward tap on the source rod will produce an S-wave with an initial downward/negative voltage departure at the receiver cone). The source vertical, horizontal in-line, and horizontal cross-line geophones are abbreviated as SV, SH_I, and SH_C, respectively (refer to Figure 2.1). Likewise, the receiver vertical, horizontal in-line, and horizontal cross-line geophones are abbreviated as RV, RH_I, and RH_C, respectively.

MEMS accelerometers were chosen to measure cone tilt and calculate sensor position because of their compact size, low power requirements, and ability to track tilt using gravity as a reference. Specifically, an Analog Devices ADXL335 MEMS accelerometer was pre-mounted on a printed circuit board for ease of installation. This model is a tri-axial MEMS accelerometer with a nominal sensitivity of 330 mV/g and a zero-g output of 1.65 V when supplied with a DC voltage of 3.3 V. The accelerometer has a full sensing range of ±3 g and a frequency bandwidth range from 0 to 50 Hz. This limited bandwidth is not suitable for the DPCH dynamic measurements; however, the DC offset is acceptable for static measurements of tilt. The recommended input supply voltage range for the accelerometer is 1.8 to 3.6 VDC. The MEMS accelerometers were calibrated in the laboratory for static tilt prior to use in the DPCH cones.

The electrical cable contains six shielded, twisted-pairs of stranded copper conductors, which are used to provide power and transmit signals from the sensor package to the data acquisition system. The waterproof, flexible, and tough polyurethane jacket protects the individual conductors and fits inside typical CPT rods. The end of the cable is terminated by a small 12-pin connector, which is mated to a custom-built breakout box to route the sensor signals to the data acquisition system and provide power to the MEMS accelerometer.

2.2.1.3 Dynamic Source

The source of dynamic energy used to generate the seismic waves traveling between the cones may be located either at the ground surface or inside a pushable source cone. At the ground surface, a tap on top of the source cone push rod generates a P-wave which travels down the push rod to the source cone, where the energy is transferred into the soil as radially propagating P- and S-waves. The horizontally propagating, horizontally polarized compression waves (P_H-waves) and horizontally propagating, vertically polarized shear waves (S_{HV}-waves) are of primary interest. A small metal hammer (e.g., a ballpeen hammer) is recommended to provide a crisp, high frequency wave. Ideally, each hit is consistent, quick, and strong enough to ensure the measurement of clear P- and S-wave arrivals at the receiver, yet soft enough to avoid over-ranging the vertical geophone in the source cone (SV). We have found that hammer taps on top of the source rod generate strong S_{HV}-waves but somewhat weak P_H-waves. If the soil is saturated, the P_H-waves are more energetic, contain high frequencies, and are easily recognized; however, they are

harder to identify when the soil is not saturated. Alternatively, various specialized energy generating mechanisms could be installed inside a pushable source cone in order to generate P- and S-waves directly in the ground (as discussed below in the testing challenges section).

2.2.1.4 Data Acquisition System

Ideally, every component of the 3D geophone array and MEMS accelerometer installed in each DPCH cone should be recorded during testing. To accomplish these measurements, a 12-channel data acquisition system (DAQ) is needed. However, if DAQ channels are limited, in proper combinations, fewer signals can be recorded without compromising data quality. At a minimum, three sensor signals from each DPCH cone must be recorded to accurately determine V_S: (1) the vertical geophone, (2) the horizontal in-line component of the accelerometer, and (3) the horizontal cross-line component of the accelerometer. To accurately determine V_P, the horizontal in-line geophone signals from the receiver cone must also be recorded. Dynamic measurements from a horizontal cross-line geophone are not necessary unless a source capable of generating S_{HH}-waves is used. Furthermore, the DC signal of the vertical component of the accelerometer is not used in the calculation of tilt and therefore does not need to be recorded if the number of channels is limited.

The minimum recommended DAQ sampling rate is based on the two following considerations: (1) Sampling theory dictates that the Nyquist frequency (i.e., half the sampling frequency) exceed the maximum frequency of interest in the sampled waveform.

We have observed P-waves with predominant frequencies as high as 3,000 Hz, thus requiring a minimum sampling frequency of 6,000 Hz. (2) Resolution in the time domain (i.e., the time increment, which is the inverse of the sampling frequency) is also important. The sampling frequency must allow adequate resolution of wave travel time relative to the minimum anticipated travel time of a P-wave propagating between the two DPCH cones. In saturated soil, a P-wave will travel at or above the V_P of water (~ 1,500 m/s). However, in saturated soils the stiffness of the soil skeleton also contributes to V_P, and velocities over 2,000 m/s have been recorded in saturated stiff sand and gravel layers. A P-wave traveling at 2,000 m/s will travel two meters in 1.0 ms. In order to resolve this travel time within 5%, the 1.0 ms travel time is divided into twenty samples, yielding a sampling rate of 0.05 ms. This corresponds to a minimum recommended sampling frequency of 20,000 Hz, exceeding the prior minimum of 6,000 Hz dictated by sampling theory. The minimum record duration is based on the following: (1) the maximum anticipated travel time of an S-wave traveling between the two DPCH cones, (2) the anticipated duration of the full wave train, and (3) a pre-trigger delay to measure the static DC voltage of the accelerometer components needed for tilt calculation. The slowest anticipated V_S is 50 m/s, measured in very soft clays or peats. The travel time of a 50-m/s S-wave over a distance of 2.0 meters is 40 ms. A minimum of another 40 ms is recommended to capture the remainder of the S-wave train. A pre-trigger delay of approximately 40 ms is sufficient to capture the static DC voltages output by the accelerometers. The pre-trigger delay also allows correction from the “zero” trigger time of the DAQ to the true departure of energy from the source

cone. Based on the three factors outlined above, the recommended minimum record duration is about 120 ms.

Most DAQs operate by storing the digitized signals in a buffer memory. The data in the buffer is continuously stored and overwritten until the system is triggered, at which point the desired data is retrieved and stored in an output data file. The triggering conditions are set by the user and typically include an input channel, a voltage level, and a slope. For DPCH testing, the data acquisition is triggered using the vertical geophone in the source cone (SV; refer to Figure 2.1), eliminating the need to determine the travel time of the P-wave down the source cone push rod. The consistent, downward hits of the metal hammer on the steel push rods result in a high frequency, downward polarized P-wave. The known polarity of the P-wave and the orientation of the geophone are used to set the trigger voltage level and slope (i.e., negative voltage with negative slope). The absolute value of the voltage level must be set high enough to prevent false triggers, but low enough to trigger on the first downward departure caused by the hammer hit. Time zero of the recording will correspond to the point in time where the voltage level threshold is exceeded with the correct slope. This recording of "time zero" will occur a few time samples after the arrival of the hammer hit and the departure of the waveform from the noise floor. Therefore, it is important to use a pre-trigger delay so the true arrival time of the P-wave at the source cone can be identified. This is further discussed below in the Data Analysis section.

When selecting a DAQ, it is also important to consider the range of expected signal amplitudes. Typically, we use a 24-bit DAQ to record the DPCH signals without the need for amplification prior to digitization. After conducting numerous DPCH tests, we have

found that S-wave amplitudes sensed by the 28 Hz geophones range from 0.25 to 2.5 millivolts (mV) and that P-wave amplitudes are on average an order of magnitude smaller, ranging from 0.025 to 0.25 mV. Many DAQs allow selection of the input voltage range for digitization; common ranges include ±0.1V, ±1.0V, and ±10V. Consider the impact of utilizing a DAQ with a ±1.0V range with three different digitization resolutions: 12, 16, and 24 bits. The smallest voltage that can be resolved with a 12-bit DAQ using a ±1.0V range is 0.5 mV, which is too large to resolve most S-waves and all P-waves. The smallest voltage that can be resolved with a 16-bit DAQ using a ±1.0V range is 0.03 mV, which is small enough to resolve all S-waves and some P-waves. The smallest voltage that can be resolved with a 24-bit DAQ using a ±1.0V range is 0.12 μV, which is small enough to resolve all S-waves but only some P-waves. The smallest voltage a 24-bit DAQ can resolve using a ±0.1V range is 0.012 μV, which is adequate to resolve all S- and P-waves. We have experimented with several different DAQs and get much better results when using a 24-bit digitizer with a ±0.1V range. It is possible to observe most S-wave arrivals using a 16-bit digitizer, but many P-wave arrivals cannot be detected.

2.2.2 Test Procedure

The generalized DPCH test procedure may be broken into four parts: (1) initial placement and orientation of both cones, (2) cone advancement, (3) wave propagation, signal measurement, and data collection, and (4) trigger calibration.

2.2.2.1 Initial Cone Placement and Orientation

Prior to testing, thoughtful placement of the DPCH cones at the ground surface is key to the proper measurement and interpretation of the P- and S-wave arrivals and vital to tracking the position of each cone during testing. As shown in Figure 2.1, a consistent local coordinate system is defined to aid in the proper orientation of the instrumented cones. For convenience, the origin of the coordinate system is defined as the center of the source cone at the ground surface. The vertical (Z) direction is a measurement of depth and positively increases into the ground. The horizontal in-line (Y) direction is zero at the center of the source cone and positively increases towards the receiver cone. In plan view, (Figure 2.1b) the positive horizontal cross-line (X) direction is 90 degrees counter-clockwise from the positive Y direction. This Cartesian coordinate system follows the right-hand rule.

The cones should be placed 1.5 to 2.5 meters apart. In soft soils, the cones can be pushed in relatively close proximity to one another with minimal disturbance of the soil between the cones. However, in dense soils it may be possible to disturb the soil between the cones if they are placed too close to one another. Body waves (i.e., P- and S-waves) geometrically attenuate as a function of squared distance from the source. Seismic energy is also absorbed and dissipated by the soil due to anelastic damping effects. The further the receiver cone is from the source cone, the more difficult it is to observe the attenuated P- and S-waves using the receiver geophones. Also, as length of the direct travel path between cones increases, the potential for measuring indirect refracted/head waves also increases (discussed in detail in the DPCH Testing Challenges section). Limiting the maximum

distance between the cones at the ground surface to 2.5 meters or less serves to limit both the geometric attenuation of the waves and the possibility of measuring refracted waves.

It is important to properly orient and level the cones prior to testing using the following steps. First, the cones are rotated such that the positive Y-components of the geophones and MEMS in each cone point in the positive Y direction of the local coordinate system (i.e., away from the source cone towards the receiver cone). Second, the CPT rigs are leveled such that the cones and the push rods will enter the ground vertically. The initial verticality of the push rods is verified using a carpenter's level. Finally, the cones and rods are adjusted to a uniform starting elevation (zero depth) and the distance between the cones at the ground surface is measured.

While the cones are at depth zero, initial reference tilt measurements (zero readings) are taken. The CPT rigs are turned off to limit noise and the data acquisition system is triggered to measure the static accelerometer response on all components. These initial accelerometer readings are used as the reference for all subsequent tilt measurements. After these initial readings are taken, the CPT rigs are turned on and uniformly advance the cones to the first measurement depth, typically 20 to 40 cm into the ground. The measured waveforms may be of low quality in the top half meter due to poor cone-to-soil coupling at low confining pressures and irregular weathering/desiccation patterns near the ground surface.

2.2.2.2 Cone Advancement

DPCH measurements are taken at discrete depths, resulting in non-continuous profiles of V_P and V_S. The CPT rigs are turned off during dynamic measurements in order to minimize rod and ground vibrations that contaminate the seismic waveforms. A constant depth increment is easiest to track and is used in general exploratory testing. In other cases, the depth increment may be varied to better characterize materials of interest. Small increments increase the depth resolution (i.e., finer spatial sampling) of the V_S and V_P profiles at the cost of additional testing time. We typically use 20-cm depth increments to profile the top 10 meters of soil. Once the CPT rigs are mobilized and the cones are ready at the ground surface, it takes 50 to 75 minutes to advance the cones to 10 meters in 20-cm increments. Each cone advancement and dynamic measurement takes 1 to 1.5 minutes to complete. Based on our field testing experiences, a 20-cm depth increment is a suitable compromise between spatial sampling and the total test duration. The DPCH measurement depth increment is easily altered to accommodate any number of variables such as changing layer thicknesses, additional testing in critical layers, specialized inclined travel paths, etc.

2.2.2.3 Wave Propagation, Signal Measurement, and Data Collection

After cone advancement, seismic waves are propagated from the source cone to the receiver cone and recorded using the DAQ. As mentioned previously, the seismic waves are most typically generated by tapping on the top of the source cone push rod with a small metallic hammer (refer to Figure 2.1). The metal-on-metal hit generates a high-frequency P-wave that travels down the push rod to the source cone. The P-wave arrives at the source

cone and is observed on SV geophone, which triggers the DAQ. The energy is transferred from the source cone into the surrounding soil as radially propagating P- and S-waves. Most often, horizontally propagating, horizontally polarized compression waves (P_H-waves) and horizontally propagating, vertically polarized shear waves (S_{HV}-waves) are measured, on the horizontal in-line (RH_I) geophone and vertical (RV) geophone, respectively. Optionally, for more advanced testing, the horizontal cross-line geophone (RH_C) is used to measure horizontally propagating, horizontally polarized shear waves (S_{HH}-waves), which can only be generated using an in-ground seismic source.

Signal stacking is a common seismic technique used to increase the signal-to-noise ratio. At a given measurement depth, waveforms from multiple hammer hits are averaged in the time domain. Consistent acquisition triggering is important to avoid averaging time-shifted signals, which otherwise results in unclear first arrivals. This impact on data quality underscores the need for a consistent trigger signal that is recorded for subsequent scrutiny. Many DAQs allow for visualization of recorded data in real-time. During testing, the trigger signal from the SV geophone should be inspected and compared with the stacked/average trigger signal to ensure consistent triggering. Poor or inconsistent individual records should be rejected prior to stacking. Typically, 3 to 10 stacked records are adequate for testing, depending on the noise level at the site and the signal amplitude. Small trigger timing inconsistencies can be further resolved through the cross-correlation of individual signals, using the evaluated time lag to align the signals prior to stacking if necessary. After sufficient stacking at the current measurement depth, the CPT rigs are re-started to advance the cones to the next measurement depth.

2.2.2.4 Trigger Calibration

When performing crosshole tests using only a source and single receiver cone, a trigger calibration is needed to correct for two factors. The first factor is the wave travel/compliance times inside of the cones. The second factor is timing issues between the cones and the DAQ, including mechanical-to-electrical signal conversion and digitization. As shown in Figure 2.4a, the measured travel time (t) includes the actual wave travel time in the soil between the cones (i.e., the corrected travel time; t_{cor}) as well as apparent time caused by the two factors noted above (i.e., the trigger calibration time; t_{cal}). The calibration time must be subtracted from the measured travel times to determine the actual P- and S-wave travel times through the soil.

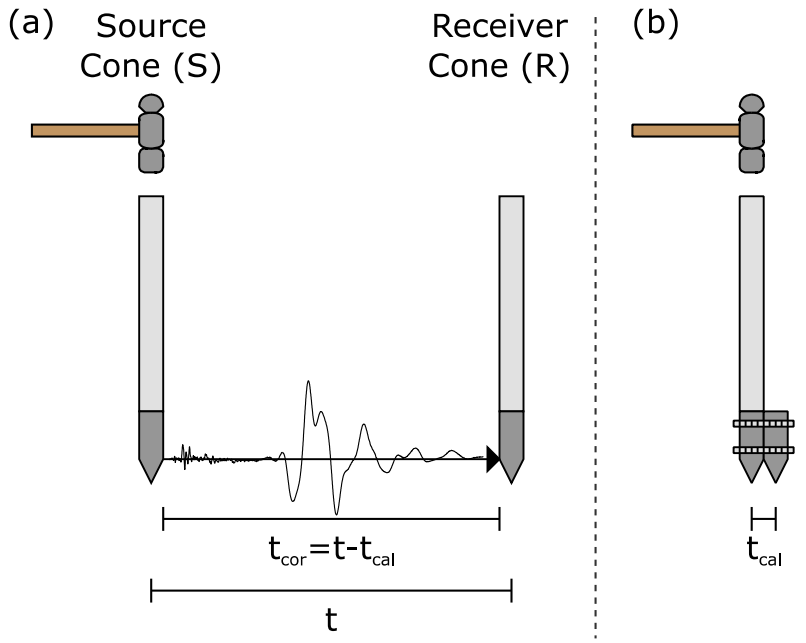

Figure 2.4: Overview of DPCH trigger calibration. (a) Generalized schematic of a DPCH measurement. The measured travel time (t) includes both the travel time through the soil (t_{cor}) and the travel time through the DPCH cone body to the internal geophones (t_{cal}). To correctly determine the P- and S-wave velocities through the soil, the t_{cor} must be calculated by subtracting t_{cal} from t. (b) Schematic of the trigger calibration. The travel time of the P- and S-waves through the cone bodies for DPCH testing can be determined by performing a calibration before testing. The cones are tightly clamped together. The hammer is used to tap on the source cone push rod and generate the seismic waves. Data acquisition is triggered by the source cone vertical geophone (SV). The P- and S-waves are measured by the receiver-geophones RH_I and RV, respectively. The difference in arrival times of the seismic waves at the source and receiver cones is t_{cal}, specifically t_{Pcal} for P-waves and t_{Scal} for S-waves.

The trigger calibration is performed prior to testing as follows. The cones are oriented in the same alignment used during testing, with zero spacing between the cones. Specifically, the positive horizontal in-line components of both cones are oriented such that they point from the source cone towards the receiver, with the tips of the cones pointing towards the ground. The cones are tightly clamped together using a pair of hose clamps at

the top and bottom, as shown in Figure 2.4b. To protect the threading at the top of the source cone, the cone push rod adapter or a short length of push rod should be attached. The source cone push rod is tapped with the hammer and the DAQ is triggered using the vertical geophone in the source cone, with all DAQ parameters identical to those used during testing. The trigger calibration times for P- and S-wave arrivals are picked from the appropriate stacked waveforms recorded on geophone signals SV, RH_I, and RV. The time difference between the P-wave arrival time recorded on RH_I and the initiation of energy recorded on SV is the calibration time for P-waves (t_{Pcal}). The time difference between the S-wave arrival time recorded on RV and the initiation of energy recorded on SV is the calibration time for S-waves (t_{Scal}). When the cones are clamped together in this manner, it is possible for the seismic waves to arrive at the receiver before the data acquisition is triggered using the chosen slope and voltage level. Meaning, it is possible for t_{cal} to be a negative value under certain conditions. Thus, using a pre-trigger delay when performing the trigger calibration is essential.

2.3 DATA ANALYSIS FOR THE DIRECT-PUSH CROSSHOLE TEST

The raw data recorded during DPCH testing consists of velocity and acceleration time histories from the source and receiver cone sensors at each DPCH measurement depth. The final processed data are profiles of V_P and V_S as a function of depth. The techniques used to evaluate P- and S-wave travel times, obtain travel path distances, and calculate velocities are presented in detail in the following sections. An example DPCH dataset

collected at the Cobra Reserve site in Christchurch, New Zealand is used to illustrate the data processing methodology.

2.3.1 Evaluation of Travel Time

The travel time of a particular type of seismic wave between the DPCH cones is simply the difference between the arrival time of the wave at the receiver cone and the departure time of the same wave from the source cone. To determine the travel times of the direct P- and S-waves at a given measurement depth, three points in time must be picked from the recorded waveforms as follows: (1) the initiation of energy/arrival time at the source cone (i.e., the trigger time), (2) the arrival time of the *direct* P-wave at the receiver cone, and (3) the arrival time of the *direct* S-wave at the receiver cone. The trigger time and direct arrival times are picked from the stacked waveforms recorded at each measurement depth. Preliminary trigger and arrival time picks are made in the field, during testing, using a display connected to the data acquisition system. These preliminary picks are refined in post-processing. The stacked waveforms from the entire test may be shown together in a waterfall plot by normalizing the amplitude and vertically offsetting each waveform by its measurement depth (as illustrated in Figure 2.5). Waterfall plots allow the analyst to observe changes in the direct wave arrival time, frequency content, and amplitude with depth. The observable trends from surrounding waveforms, and insight gained from other geotechnical data (e.g,. CPT testing), aid in the identification of the direct arrivals on difficult waveforms.

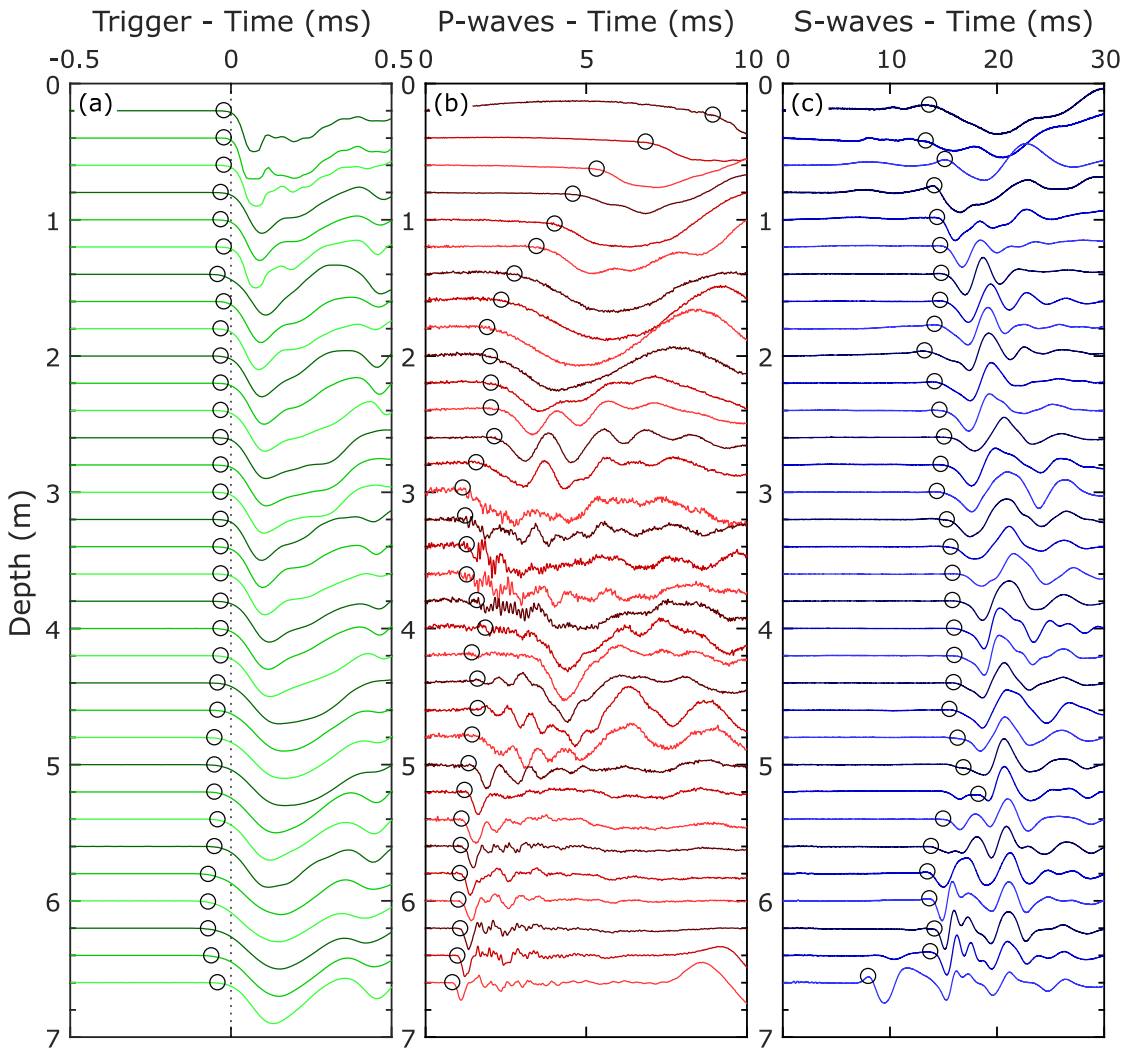

Figure 2.5: Example waterfall plots for: (a) the trigger, (b) the P-wave, and (c) the S-wave waveforms recorded on the source cone vertical (SV), receiver cone horizontal in-line (RH_I), and receiver cone vertical (RV) geophones respectively. Waveforms are normalized by absolute maximum amplitude and vertically offset in each plot by testing depth. The wave arrival picks are indicated by black hollow circles on the waveforms.

2.3.1.1 Processing Raw Waveforms

Before making arrival picks, pre-processing of the raw stacked waveforms may be necessary to clarify the waveforms and observe direct arrivals. The first step is to remove vertical offsets and low-frequency drift using linear detrending. There are a number of ways to do this in both the time and frequency domain. However, the easiest way is simply to calculate the average voltage/amplitude across the entire waveform and then subtract that average value from every point in the waveform. Next, filtering may be necessary to clarify wave arrivals at the receiver cone, but caution and discretion in the selection and application of filters is recommended. Prior to filtering, it is important to know the frequency band(s) of the signals, as evaluated on a case-by-case basis. From our database of DPCH results, we have observed S-waves with frequency content ranging between 100 and 700 Hz. When the soil is unsaturated, the frequency content of the P-waves ranges between 100 and 1,000 Hz. This range increases to between 750 to 3,000 Hz, when the soil is saturated. We typically do not need to filter our signals, but it sometimes is necessary to identify low-amplitude P-waves which become obscured by the noise floor of various DAQs. If filtering is needed, an acausal filter should be used to limit phase shifts in the time domain. Low-frequency drift and high-frequency noise may be removed using a bandpass filter to window the frequency range of the signal. Wave arrival picks made using filtered waveforms should be verified on the unfiltered waveforms to ensure phase shifts were not introduced by the filtering process.

After the data has been linearly detrended and/or filtered, waterfall plots are created by assigning a vertical offset to each waveform corresponding to its measurement depth.

When only determining the velocity of the waves traveling between the cones, the absolute amplitude of the waveform is unimportant. Thus, the amplitude of the waveforms may be adjusted to help in the identification of these arrivals by normalizing and/or scaling each stacked waveform. Each waveform is often normalized by the absolute maximum value of the waveform. Normalization ensures each waveform is uniformly scaled and has the effect of amplifying small signals, which may aid in picking the first arrivals. However, normalization removes any absolute trends in wave amplitude with depth, which may be indicative of changes in material type and material damping. Alternatively, scaling factors may be applied to uniformly amplify or de-amplify the amplitude values of each waveform. To improve readability of the waterfall plot, scaling factors are used to limit the vertical overlap of waveforms in the waterfall plot.

An example waterfall plot using data from the Cobra Reserve example dataset is shown in Figure 2.5 for: (a) the trigger, (b) the P-wave, and (c) S-wave waveforms recorded on the source cone vertical (SV), receiver cone horizontal in-line (RH_I), and receiver vertical (RV) geophones, respectively. For this data, the sampling frequency was 102.5 kHz, the record duration was 160 ms, and the pre-trigger delay was 20%. Each waveform was linearly detrended, normalized by the absolute maximum voltage amplitude over the time range shown, and uniformly scaled by a factor of 0.15 to limit vertical crossover of the waveforms. Additionally, the P-wave waveforms were bandpass filtered between 50 and 20 kHz. The arrival time picks are indicated on the waveforms by open, black circles. Subsets of waveforms from this dataset are shown in Figures 2.6 and 2.7 as examples for making correct P- and S-wave arrival picks, respectively.

2.3.1.2 Picking the Trigger Time (t_T)

Time zero on the digitizer does not necessarily correspond to the true first arrival of energy at the source cone (i.e., the trigger time, t_T). A pre-trigger delay is needed to pick the arrival of energy at the source, which is typically a few data points before the digitized zero time. As the length of cone push rod and material friction along the rod increases, the frequency content of the seismic energy arriving at the bottom of the rod changes, resulting in slight changes to the observed trigger time (refer to Figure 2.5a). Picking the true trigger time is necessary for obtaining the correct P-wave velocity, and to a lesser extent for the S-wave velocity. To illustrate the importance of picking the correct trigger time at the source cone, consider the potential error in V_P measured between the source and receiver cone for the example detailed as follows. A P-wave traveling 2000 m/s will travel 1.5 m in 0.75 ms. When sampling at 20 kHz, the travel time occurs over only fifteen samples. If the difference between the DAQ zero time and the true trigger time at the source is two samples, V_P will be over predicted by thirteen percent. As discussed below, this can be a significant difference when attempting to estimate geotechnical parameters such as void ratio and degree of saturation.

2.3.1.3 Picking the P-wave Arrival Time (t_{PA})

The P-wave arrival time (t_{PA}) at the receiver cone is best observed using the horizontal in-line (RH_I) geophone. P-waves will always arrive first at the receiver cone, followed by larger-amplitude S-waves later in the record. Therefore, the arrival time of the P-waves is picked at the first departure of the RH_I waveform from the noise floor. Two RH_I

waveforms, from the example DPCH dataset presented in Figure 2.5, are shown in Figure 2.6a. The top waveform was recorded at a shallow depth (1.4 m) in unsaturated soil, while the bottom waveform was recorded at a greater depth (6.2 m) in saturated soil. The P-wave arrivals are much smaller than the S-wave arrivals, which can clearly be observed arriving later on the RH_I waveforms. Zoomed-in views of the P-wave arrivals at a depths of 1.4 m and 6.2 m are shown in Figures 2.6b and 2.6c, respectively. The P-wave arrival at a depth of 1.4 m is gradual, occurring on a lower frequency wave. As such, picking the correct P-wave arrival is somewhat subjective, but should be based on the principle of picking the point where the waveform first departs from the pre-arrival trend. Once the soil becomes saturated, picking P-wave arrivals is much less subjective, as illustrated from the waveform at a depth of 6.2 m. In fully saturated soils, P-waves travel at or above the V_P of water (~ 1,500 m/s), depending on soil type and confinement. At 50+ sites, we have observed that P-waves travel in saturated soils at high frequencies up to 3,000 Hz and have clear, sharp arrivals.

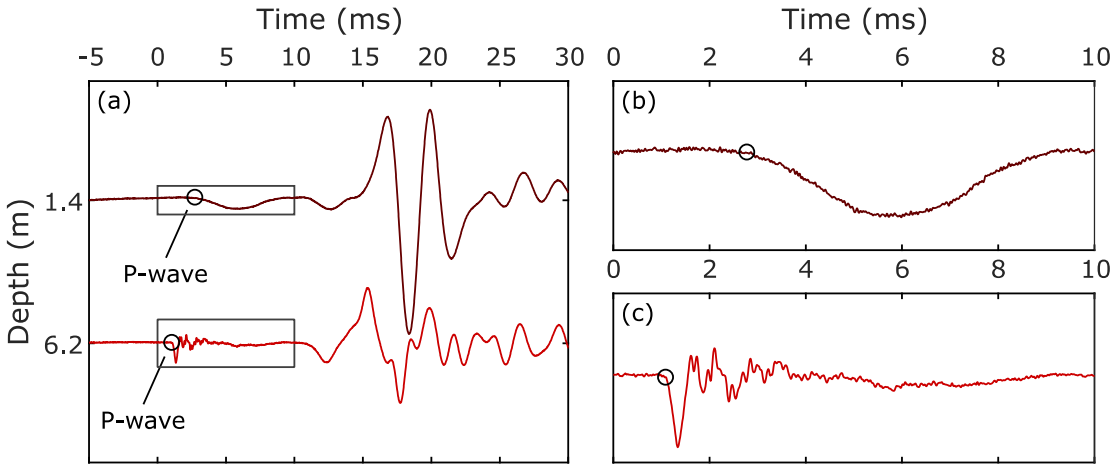

Figure 2.6: Example P-wave arrival picks shown as black open circles on waveforms measured with the receiver cone horizontal in-line (RH_I) geophone. (a) Two sample waveforms both recorded at the same site, but at different depths. The top waveform was recorded at a shallow depth (1.4 m) in unsaturated soil. The bottom waveform was recorded at a greater depth (6.2 m) in saturated soil. The rectangular boxes in part (a) show the extent of the zoomed-in windows presented in parts (b) and (c) on the upper and lower waveforms, respectively.

2.3.1.4 Picking the S-wave Arrival Time (t_{SA})

While the S-wave arrivals can often be observed, in a general sense, with the P-waves on the RH_I waveforms shown in Figure 2.6a, they are more reliably picked from waveforms recorded by a properly oriented sensor. The downward hammer taps at the top of the source rod induce S_{HV}-waves with an initial downward particle motion. Thus, the S-wave arrival time (t_{SA}) is most precisely observed on the receiver cone vertical (RV) geophone. A general guideline is to pick the arrival of S-waves as the first *major amplitude departure,* occurring after the P-wave arrival, *that has the correct polarity*. These custom built cones were wired such that a downward tap on the top of the cone produces a

downward voltage departure on the RV geophone. Therefore, the S_{HV}-wave arrivals should be picked as the *first major downward departure* after the P-wave arrivals. We cannot stress enough the importance of understanding the expected voltage polarities for a given set of equipment when performing DPCH testing, this is equally important in conventional crosshole and downhole testing.

Three RV waveforms, from the example DPCH dataset presented in Figure 2.5, are shown in Figure 2.7. These waveforms were recorded at three sequential measurement depths: 6.2, 6.4, and 6.6 m. The DPCH test was stopped at 6.6 m at the top of a dense gravel layer. The transition from a softer material into the stiffer gravel layer is apparent in the RV geophone waveforms shown in Figure 2.7. The top waveform measured at 6.2 m shows a clear downward S-wave arrival at ~14 ms. The bottom waveform measured at 6.6 m shows a clear downward S-wave arrival at ~8 ms. [Note that the downward departure at 6.6 m must be chosen as the direct S-wave arrival, not the preceding upward departure, because of the known downward particle motion of the S_{HV}-wave and the known negative voltage polarity of the RV geophone]. However, the middle waveform measured at 6.4 m shows two downward departures: a smaller amplitude arrival at ~10 ms followed by a larger amplitude arrival at ~14 ms. If the waveform at 6.4 m was considered alone, the analyst may be tempted to pick the smaller amplitude downward departure as the direct arrival of the S_{HV}-wave. However, when viewed together with the other waveforms in waterfall format it is evident that the earlier arrival at 6.4 m is caused by a refracted wave off the stiff gravel layer beneath. In general, refracted waves will have smaller amplitudes than direct waves and will not have a large reversal of polarity following their initial arrival.

In the context of the waveform at 6.4 m, the refracted wave has the correct downward polarity (e.g., negative/decreasing voltage), however, it is smaller than a later downward arrival and is not accompanied by a subsequent large upward cycle. Difficulties associated with picking correct arrivals times in the presence of refracted and other non-direct wave arrivals are discussed further in the DPCH Testing Challenges section below.

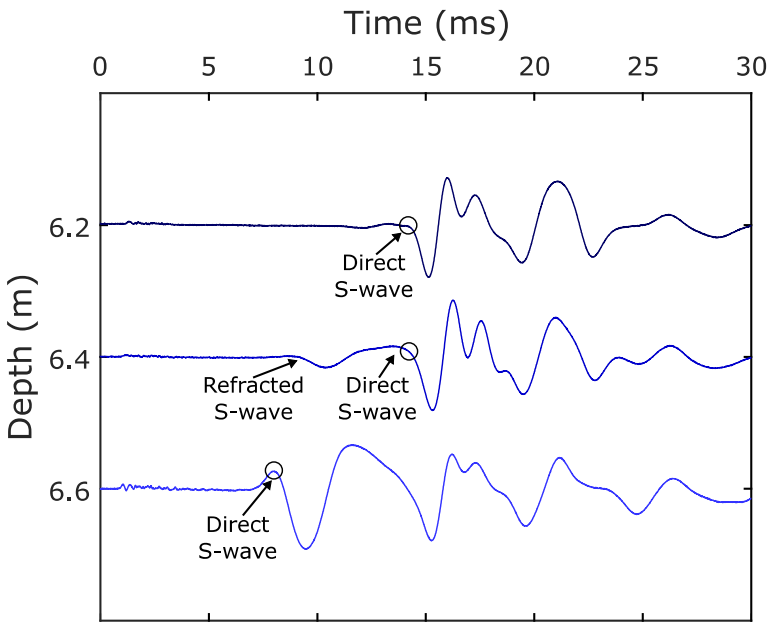

Figure 2.7: Example S-wave arrival picks shown as black open circles on waveforms measured on the receiver cone vertical (RV) geophone. The three sample waveforms were recorded at the same site, at three successive testing depths. The top and bottom waveforms show clear direct S-wave arrivals with the expected downward/negative polarity. The middle waveform shows an early arrival from a refracted travel path off of the stiffer material below. The direct S-wave arrival is picked as the stronger downward departure later in the waveform.

2.3.1.5 Determination of Corrected Travel Times

After the trigger time (t_T), P-wave arrival time (t_{PA}), and S-wave arrival time (t_{SA}) are picked from the DPCH waveforms, the actual travel times between the source and receiver cone are calculated. The actual travel time of the direct P-wave (t_P) is:

$$t_P = t_{PA} - t_T \tag{2.1}$$

Similarly, the actual travel time of the direct S-wave (t_S) is:

$$t_S = t_{SA} - t_T \tag{2.2}$$

The direct P- and S-wave travel times must be corrected using the trigger calibration values (t_{Pcal} and t_{Scal}, respectively) discussed earlier in conjunction with Figure 2.4. The corrected P- and S-wave travel times (t_{Pcor} and t_{Scor}, respectively) are determined using the following equations:

$$t_{Pcor} = t_P - t_{Pcal} \tag{2.3}$$

$$t_{Scor} = t_S - t_{Scal} \tag{2.4}$$

These corrected travel times are used to calculate V_P and V_S, once the direct wave travel path distance is determined.

2.3.2 Calculation of the Travel Path Distance

To calculate the distance between the DPCH cones at each measurement depth, the 3D subsurface position of each cone must be known. The 3D position of each cone is tracked from the surface down to the final measurement depth by using the tilt angles observed at each depth in conjunction with the known push increments. The tilt angles of the cones are tracked using the horizontal in-line (y) component and horizontal cross-line (x) component of the MEMS accelerometer. The DC voltage of each MEMS accelerometer signal is proportional to the measured acceleration parallel to the direction of the individual component. The vertical downward acceleration due to Earth's gravity provides a reference from which to track tilting of the cone. When the accelerometer is oriented such that the positive vertical (z) component points downward, the z-component measures 1 g (~9.81 m/s^2) of positive static acceleration and both horizontal components measure 0 g. As the accelerometer is tilted about the x-axis (in the yz-plane) the voltage of the y-component changes as it measures a fraction of ±1g relative to the direction (up or down) and angle of tilt. Similarly, as the accelerometer is tilted about the y-axis (in the xz-plane) the voltage of the x-component changes as it measures a fraction of ±1g relative to the direction and angle of tilt.

The MEMS accelerometers are calibrated for tilt in the laboratory using a tilt table to fix the accelerometer at known tilt angles. The calibration is performed by limiting rotation to one plane, xz- or yz-plane, at a time and measuring the DC output voltage on the appropriate component of the accelerometer. When rotation is limited to one plane perpendicular to either the x- or y-component, there should be no change in the voltage on

that component. The DC voltage of the z-component changes due to tilt in any vertical plane, therefore, it is not used to track the position of the cone. The known tilt angles and corresponding DC offset voltages are used to develop relationships to determine the tilt of the cone based on measured DC voltages. The relationship between tilt angle and measured DC offset for both components is sinusoidal. However, in the range of ±25° of tilt for either horizontal component (i.e., rotating the cone from vertical), a linear relationship adequately fits the tilt angle versus DC voltage trend. For reference, in CPT testing it is common to limit tilt angles to 10-15° from vertical to avoid damaging the push rods or the cones. Thus, using a simple linear trend to relate the measured voltages to degrees of tilt is acceptable, because testing would be stopped before exceeding the reasonable range of angles for the linear trend. The slope of this trend in units of volts/degree is used as a calibration factor (CF) to determine the change in cone tilt between measurement depths.

At the ground surface, the CPT rigs are leveled to initially advance the cones vertically into the ground with zero tilt about the x- and y-axes, as verified using a carpenter's level. Therefore, the initial tilt angles $\theta_{xz,0}$ and $\theta_{yz,0}$ (the tilt about the y-axis in the xz-plane and the tilt about the x-axis in the yz-plane, respectively) are assumed to be zero. As discussed in the testing methodology, initial accelerometer x- and y-component DC voltages ($DC_{x,0}$ and $DC_{y,0}$) are taken at the ground surface and used as a reference to calculate changes in tilt from vertical. Equations 2.5 and 2.6 are used to calculate the tilt angles ($\theta_{xz,i}$ and $\theta_{yz,i}$) at each measurment depth where i is an integer denoting increasing measurement depth number. In the xz-plane, cone tilt about the y-axis is determined using the accelerometer x-component measurements according to:

$$\theta_{xz,i} = \theta_{xz,i-1} + \frac{DC_{x,i} - DC_{x,i-1}}{CF_{xz}} \quad (2.5)$$

where $\theta_{xz,i}$ is the tilt angle in xz-plane at the current depth, $\theta_{xz,i-1}$ is the tilt angle at the previous depth, $DC_{x,i}$ is the measured DC voltage of the x-component accelerometer signal at the current depth, $DC_{x,i-1}$ is the measured DC voltage at the previous depth, and CF_{xz} is the tilt calibration factor for the x-component of the accelerometer.

Similarly in the yz-plane, cone tilt about the x-axis is determined using the accelerometer y-component measurements according to:

$$\theta_{yz,i} = \theta_{yz,i-1} + \frac{DC_{y,i} - DC_{y,i-1}}{CF_{yz}} \quad (2.6)$$

where $\theta_{yz,i}$ is the tilt angle in yz-plane at the current depth, $\theta_{yz,i-1}$ is the tilt angle at the previous depth, $DC_{y,i}$ is the measured DC voltage of y-component accelerometer signal at the current depth, $DC_{y,i-1}$ is the measured DC voltage at the previous depth, and CF_{yz} is the tilt calibration factor for the y-component of the accelerometer.

At the ground surface, the relative 3D positon of the cones is known. The source cone is set at the origin of the coordinate system and the positive y-axis (the in-line horizontal direction) points towards the receiver cone, which is placed at a measured distance away in the positive y-direction. After each cone is pushed into the ground, their positions at each measurement depth are tracked using the known cone push distances, the

measured tilt angles, and their initial placement at the ground surface. The position of the cone at each measurement depth is defined by the vector:

$$P_i = \langle P_{x,i}, P_{y,i}, P_{z,i} \rangle \tag{2.7}$$

where $P_{x,i}$, $P_{y,i}$, and $P_{z,i}$ are the cone positions in the x-, y-, and z-direction at depth i, respectively. If there was no deviation from vertical, the change in position of either cone (P_i-P_{i-1}) would simply be the change in depth (d_i-d_{i-1}), which is equal to the cone advancement distance, as represented by the vector:

$$P_i - P_{i-1} = \langle 0,0, d_i - d_{i-1} \rangle \tag{2.8}$$

In reality, the cones deviate from vertical and the change in positon vector must be rotated based on the tilt of the cone. Pure rotation about the vertical (z-axis) cannot be measured using the MEMS accelerometer and for simplicity are not considered in the following calculations. Therefore, precautions should be taken to ensure the CPT rods are not twisted during advancement. At each depth, a vertical change in positon vector (Equation 2.8) is rotated using standard rotation matrices in three-dimensional Cartesian space. Using linear algebra, the initial change in the positon vector, and the rotation matrices, the following three equations may be defined to calculate the position of each cone at measurement depth increment (i) in the x-, y-, and z- directions:

$$P_{x,i} = P_{x,i-1} + (d_i - d_{i-1}) * \sin(\theta_{xz,i}) * \cos(\theta_{yz,i}) \quad (2.9)$$

where $P_{x,i}$ is the x-coordinate of the cone position at the depth increment of interest(d_i) and $P_{x\text{-}i}$ is the x-coordinate of the cone position at the previous depth increment ($d_{i\text{-}1}$);

$$P_{y,i} = P_{y,i-1} - (d_i - d_{i-1}) * \sin(\theta_{yz,i}) \quad (2.10)$$

where $P_{y,i}$ is the y-coordinate of the cone position at the depth increment of interest and $P_{y\text{-}i}$ is the y-coordinate of the cone position at the previous depth increment;

$$P_{z,i} = P_{z,i-1} + (d_i - d_{i-1}) * \cos(\theta_{xz,i}) * \cos(\theta_{yz,i}) \quad (2.11)$$

where $P_{z,i}$ is the z-coordinate of the cone position at the depth increment of interest and $P_{z\text{-}i}$ is the z-coordinate of the cone position at the previous depth increment.

Once the positions of both cones at each measurement depth are known, the distance between the cones (i.e., the direct wave travel path) is determined for each DPCH measurement depth using the standard equation to calculate the distance between two points in 3D Cartesian space:

$$dist_i = \sqrt{(P_{x2,i} - P_{x1,i})^2 + (P_{y2,i} - P_{y1,i})^2 + (P_{z2,i} - P_{z1,i})^2} \quad (2.12)$$

This distance is used in the calculation of the V_P and V_S of the material between the two cones.

2.3.3 Evaluation of P- and S-Wave Velocity

The values of $V_{P,i}$ and $V_{S,i}$ are determined from the corrected travel times and direct, travel-path distances at each depth increment (i) using the following equations:

$$V_{P,i} = \frac{dist_i}{t_{Pcor,i}} \tag{2.13}$$

$$V_{S,i} = \frac{dist_i}{t_{Scor,i}} \tag{2.14}$$

The V_P and V_S profiles for the example dataset collected at the Cobra Reserve site are shown in Figure 2.8 and are discussed below.

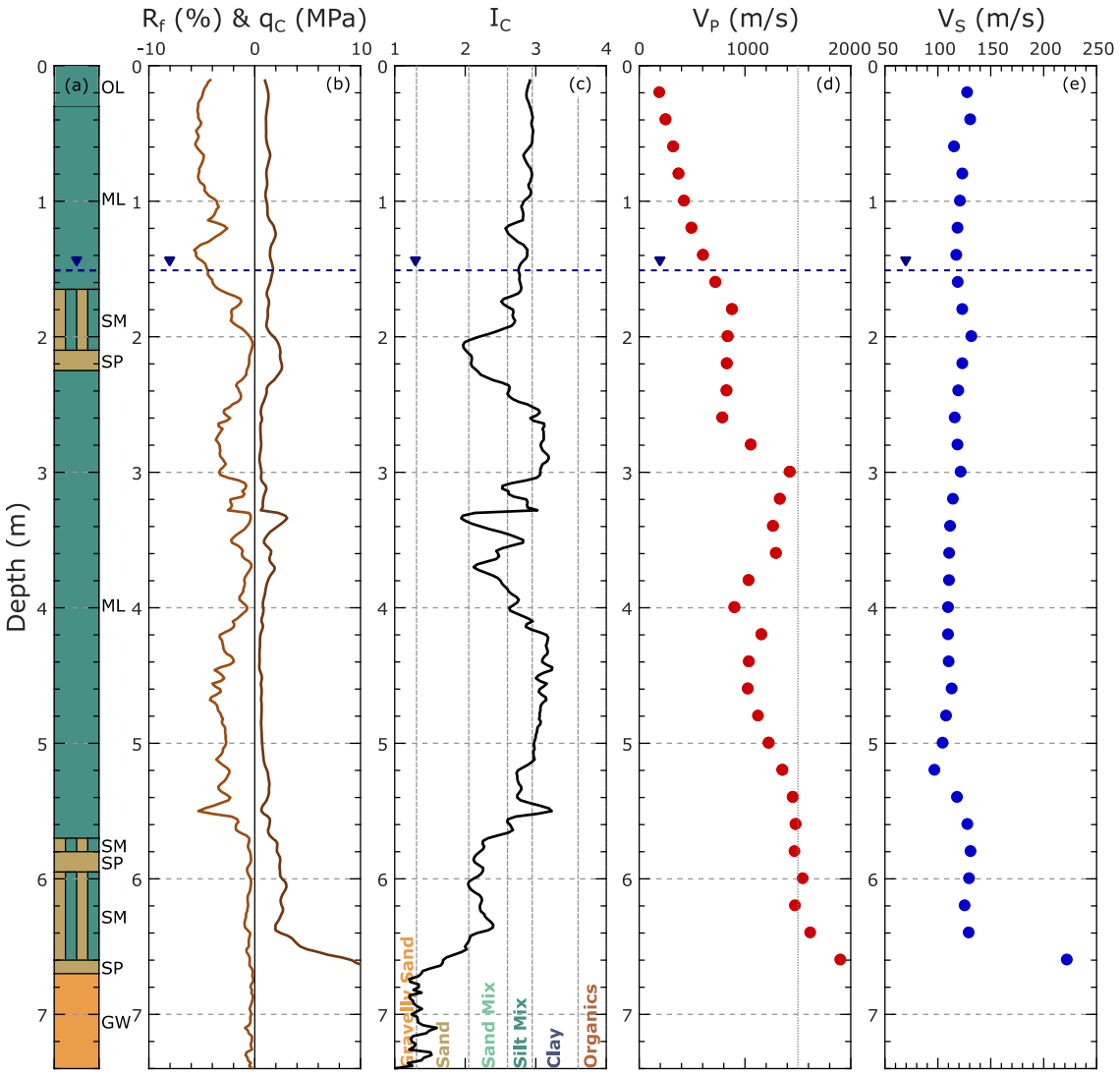

Figure 2.8: Comparison of various site investigation data at the Cobra Reserve site: (a) soil classification from sonic borehole samples, (b) friction ratio (R_f) and cone tip resistance (q_C) from CPT testing, (c) normalized soil behavior type index (I_C) from CPT testing, (d) V_P from DPCH testing, and (e) V_S from DPCH testing. The observed ground water table based on piezometer readings is indicated by a horizontal dashed line and an inverted triangular symbol in each panel.

2.4 EXAMPLE RESULTS FROM DIRECT-PUSH CROSSHOLE TESTING

The DPCH V_P and V_S profiles obtained at the Cobra Reserve site are compared in Figure 2.8 to other geotechnical data collected at the site, including the following: (a) detailed boring log from continuous sonic borehole samples; (b) CPT friction ratio (R_f) and tip resistance (q_C); (c) normalized CPT soil behavior type index (I_C); (d) DPCH V_P; and (e) DPCH V_S. The ground water level (GWL) on the day of testing was 1.51 meters below the ground surface. However, based on a permanent piezometer at the site, the GWL is known to seasonally fluctuate between approximately 1.1 and 2.3 m. In most conventional geotechnical analyses, soil is assumed to be saturated below the ground water table. However, at this site, the DPCH measurements of V_P indicate the soil is not fully saturated, with V_P less than 1,500 m/s until about 5.5 m, where the soil begins to transition from silt to sand. Multiple laboratory studies have been conducted relating measurements of V_P to the degree of soil saturation, Skempton's B-value, and increased resistance to liquefaction (Kokusho 2000, Tsukamoto et al. 2002, Ishihara and Tsukamoto 2004, Valle-Molina 2006, Hossain et al. 2012). However, accurate profiles of V_P are rarely measured in situ during geotechnical site investigations.

The borehole log indicates that the soil profile is composed mostly of a silty soil to a depth of 5.7 meters, except for two thin zones of sand to silty sand around depths of 2.1 and 3.1 meters. These sandy layers are slightly stiffer, as indicated by the increase in CPT cone tip resistance in each of the zones. The increase in stiffness is also observed in the V_S profile, which peaks at 132 m/s at 2 meters, before gradually decreasing to an average of 110 m/s in the thick, soft silty layer. Another sandy zone is found between 5.7 and 6.7

meters, which is underlain by a gravel layer. The CPT cone tip resistance gently increases between the 5.5 and 6.4 meters and steadily increases below 6.4 meters as the stiff gravel layer begins to influence the q_c readings. Similarly, V_S increases to 130 m/s below 5.4 meters, indicating the presence of the stiffer silty-sand and sand layer. The DPCH cones met refusal below 6.6 meters, and a V_S of 223 m/s was measured at the last testing depth. In general, observed changes in V_S correspond well to observed changes in cone tip resistance and soil type. DPCH testing is complimentary to CPT testing and provides V_S profiles with higher spatial resolution than typical SCPT testing.

2.5 DPCH TESTING CHALLENGES

DPCH testing has been successfully conducted at 50+ sites using above-ground hammer taps to propagate P- and S-waves between instrumented cones. All of these tests were conducted near CPT soundings, and in many cases near sonic boreholes with continuous, disturbed soil sampling. At sites with interlayered soil profiles containing stiff layers overlying very soft, thin layers (as indicated by CPT and/or borehole data), it is sometimes challenging to resolve the proper V_S of the underlying thin, soft layers by DPCH testing. Depending on the thickness and the stiffness contrast of these soft materials, the waveforms can be complicated/contaminated by indirect wave arrivals, which may arrive faster than the waves traveling directly between the cones. Thus, strictly following the S-wave arrival identification rule of thumb (i.e., pick the first major departure with the correct polarity after the P-wave) can in some instances result in shear wave velocities that are too high and nearly equivalent to those measured in the underlying and/or overlying stiff

material. Without a deeper consideration of the waveforms, the soft layer can be hidden in the resulting DPCH V_S profile even though it is apparent in the CPT tip resistance. However, a closer look at the DPCH waveforms reveals that waves are propagating in-part through the stiff layer and arriving earlier than the S-waves traveling directly through the soft soil. Potential causes of the early arrivals include: (1) refracted waves traveling along the stiff layer boundary, and (2) communication of energy between the push rods through the overlying stiff material. The direct travel path, a potential refracted travel path, and a potential travel path indicative of communication between the rods through an overlying stiff layer are shown in Figure 2.9 for a simplified two layer system.

The potential early arrival of refracted waves, called head waves in geophysics, is a known issue for seismic crosshole testing (ASTM D4428/D4428M-14). When the hammer tap energy is transferred into the ground at the source cone, the energy is propagated as both P- and S-waves in all directions. While measuring wave propagation along the horizontal direct travel path between the cones is desired, waves traveling along inclined paths (either upward or downward) can be refracted along the layer boundaries. The refracted waves travel along the layer boundary at the V_P or V_S of the stiffer material, before refracting back through the soft soil toward the receiver cone. Both the direct and refracted P-waves are significantly faster and smaller in amplitude than the direct S-waves and typically do not complicate the identification of the S-wave arrivals. However, refracted S-waves may arrive earlier than the direct waves and complicate the waveforms. This possibility depends on many factors including: (1) differences in V_S, (2) the distance

between the cones, and depth of the cones below or above the layer boundary with the stiffer material.

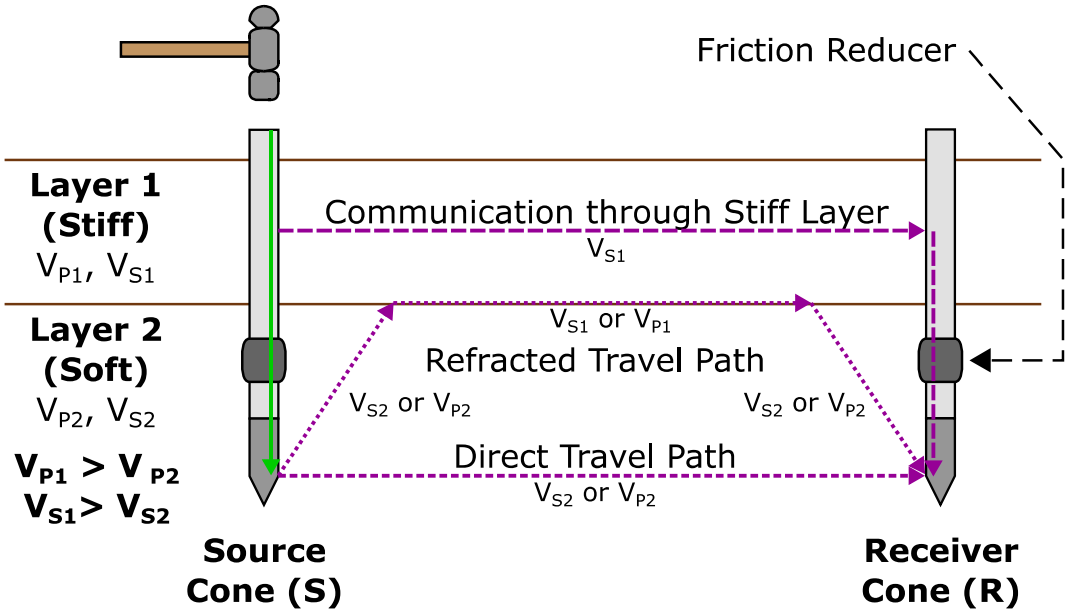

Figure 2.9: An idealized DPCH test in a two layer system consisting of a layer of stiff material with V_{P1} and V_{S1} overlying a layer of softer material with V_{P2} and V_{S2}. The DPCH cones have been advanced into the softer layer. The potential travel paths of waves between the cones include the direct travel path, a refracted travel path, and communication of waves between the cone push rods through the stiff layer due to the shedding of energy along the source cone rod.

Mode conversion from S_{HV}-waves to P-waves may also contribute to the early arrival of refracted energy. When seismic energy traveling as S_{HV}-waves impinge upon a horizontal layer boundary, the vertical particle motion produces refracted S_{HV}-waves and P-waves (Richart et al. 1970). These S_{HV}-to-P mode conversions produce waves which travel the majority of the refracted travel path at the P-wave velocities, arriving later than direct and refracted P-waves, but earlier than direct or refracted S-waves.

Another potential cause of waves arriving earlier than the direct S_{HV}-waves traveling between the instrumented cones is communication of shear wave energy through the overlying stiff layer. If the diameter of the cone and rod are similar, the rod will be in contact with the soil material above the cone. The downward hammer tap at the top of the source cone rod produces a shearing motion at the rod-soil interface, transferring some of the hammer tap energy into the stiff layer of soil above the soft soil layer of interest. This energy will travel through the overlying stiff soil as S-waves, into the receiver cone rod, and down to the receiver cone, as illustrated in Figure 2.9. As discussed above, using friction reducers placed above the cones (see Figure 2.9) will minimize the coupling of the rods with the surrounding soil and limit this indirect communication of wave energy. Hence it is imperative that friction reducers be used when conducting DPCH testing.

To study the potential for early arrival of shear wave energy in soft, interlayered soils, a custom-built, in-ground source cone was developed at the University of Texas at Austin. This source cone uses six spring-loaded solenoids to individually tap the cone body in the vertical, horizontal in-line, and horizontal cross-line directions with either positive or negative polarity. Specifically, the ability to generate S_{HH}-waves (which do not mode convert into P-waves during refraction) and reverse the polarity of both S_{HH}- and S_{HV}-waves is advantageous over using hammer taps alone. Additionally, using an in-ground source prevents communication of seismic energy through the rods between stiff overlying layers. The diameter of the source cone is 5.33 cm, which is larger than the push rods and the 3.81-cm receiver cones. This large diameter increases the horizontal stresses and the extent of the zone of potential soil disturbance during cone advancement. However, it also

reduces the coupling between the trailing push rod and the surrounding soil, further limiting any possible communication of energy between the push rods.

The in-ground source cone and a three-component receiver cone were used to perform DPCH testing at a site with known interlayered sands and silts. The DPCH tests were conducted using traditional hammer taps to generate downward polarized S_{HV}-waves, immediately followed by using the in-ground source cone to generate both S_{HV}- and S_{HH}-waves with positive and negative polarities. The S_{HH}-waveforms obtained with the in-ground source are of particular interest because S_{HH}-waves do not convert modes at horizontal layer boundaries and are therefore expected to be the least influenced by indirect wave paths. In Figure 2.10, the following information is presented together: (a) the borehole log, (b) the CPT q_C and DPCH $V_{S,HH}$ profiles, and (c) the S_{HH}-waveforms. The S_{HH} butterflied waveforms are plotted such that waves with negative initial voltage polarity are indicated by solid lines and waves with positive initial voltage polarity are indicated by dashed lines. The direct arrivals of the S_{HH}-waves are indicated on the waveforms by a filled, circular marker. Generally, the data quality was excellent and first arrival picks were unambiguous. The resulting $V_{S,HH}$ profile is plotted with the cone tip resistance in Figure 2.10b. While absolute values of q_C and V_S are not uniquely related to one another, changes in q_C are accompanied by changes in $V_{S,HH}$ over the entire depth range. The strong agreement between trends in q_C and $V_{S,HH}$ are really quite remarkable and there was no difficulty in identifying the soft soil interlayers using the S_{HH}-waveforms. Furthermore, remarkably similar results were obtained using the S_{HV}-waveforms from the hammer taps

at most testing depths, lending confidence to using the simple hammer source in most situations, as discussed below.

Two, stiff-to-soft soil transition zones, denoted as Zones A and B, are highlighted on the geotechnical data shown in Figure 2.10. These zones were selected for further scrutiny because of the potential contamination of the measured waveforms by indirect waves (e.g., waves refracted along stiff layer boundaries). Zone A ranges from 1.2 to 2.2 meters, while Zone B ranges from 4.0 to 5.0 meters. For Zones A and B, the S_{HV}-waveforms generated using hammer taps (bold, solid lines) and the S_{HH}-waveforms generated using the in-ground source (thin, dashed lines) are shown together in Figure 2.11. Note, that for clarity purposes, only the S_{HH}-waveforms with an initial negative voltage polarity are shown. Thus, the expected voltage polarity for the direct S-wave arrival on both sets of waveforms is the same. Assuming minimal influence from either stress- or structural-induced anisotropy in these young, soft soils, the direct shear wave arrivals determined from the S_{HV}- and S_{HH}-waveforms should be similar. In Zone A, the S_{HH} arrival picks from the in-ground source often agree quite well with the location of a negative voltage departure on the S_{HV}-waveforms obtained from the hammer taps. This is particularly true at 1.2 m and 1.4 m, where the soil is sandy and relatively stiff. At these two depths, it is quite easy to pick unambiguous S_{HV} arrivals from the hammer taps as major negative voltage departures that agree well with the timing of the S_{HH} arrivals from the in-ground source. However, with increasing depth/distance into the soft silt layer, earlier low-amplitude and low-frequency downward arrivals from non-direct wave paths (indicated by arrows) are evident in the S_{HV} waveforms. While it is still possible to pick

the direct S_{HV} wave arrivals later in the waveforms, it could be more challenging for inexperienced analysts. Nonetheless, as long as the early negative voltage departures are avoided, the differences between the $V_{S,HH}$ and $V_{S,HV}$ velocities are less than 10%. The only exception occurs at 2.2 m, where it is difficult to pick a strong negative departure on the S_{HV} waveform in the vicinity of the S_{HH} arrival. At this depth the difference between the $V_{S,HH}$ and $V_{S,HV}$ is greater than 20%.

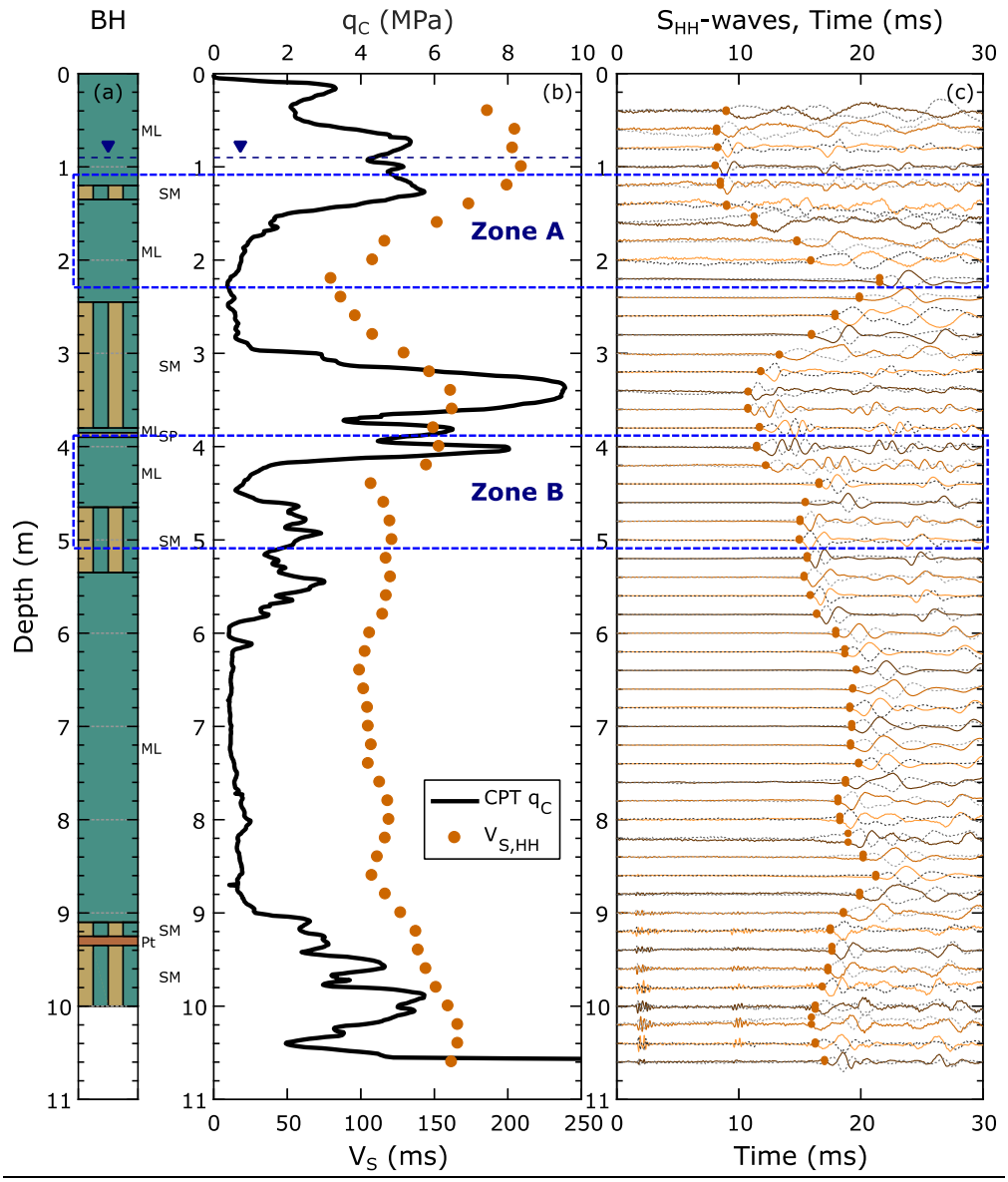

Figure 2.10: A comparison of DPCH S_{HH}-waveforms and S_{HH}-wave velocities at an interlayered silt/sand site with other geotechnical site investigation data. (a) Borehole log from sonic drill rig with continuous disturbed soil sampling. (b) CPT cone tip resistance (q_C, top axis values) and S_{HH}-wave velocity, ($V_{S,HH}$, bottom axis values). (c) Butterflied S_{HH}-waveforms with downward (solid lines) and upward (dashed lines) polarities. The average S_{HH} first arrival picks are shown on the waveforms, as indicated by filled, circular markers. Zones A and B are indicated by dashed-line boxes for further discussion in Figure 2.11.

Zone B contains another transition from stiff sand into soft silt between depths of 4.0 – 5.0 m. In this case, the S_{HV} waveforms from the hammer taps are not as complicated as those from Zone A, and it is relatively easy to pick negative voltage departures that agree well with the S_{HH} arrivals from the in-ground source. The only exceptions occur in the softest materials at 4.4 m and 4.6 m, where there are some weak early arrivals from non-direct waves, and the major negative departures from the S_{HV} waveforms occur a bit earlier than the arrival times picked from the S_{HH} waveforms. Even at these depths the maximum difference between the $V_{S,HH}$ and $V_{S,HV}$ is less than 9%.

From the example DPCH waveforms shown in Figure 2.11, it is evident that early, non-direct wave arrivals can sometimes complicate picking direct S_{HV} wave arrivals generated by hammer taps when testing in soft soil layers underlying stiff soil layers. However, given positive qualitative comparisons with other measurements of soil stiffness (i.e., q_C) and generally good agreement between in-ground source $V_{S,HH}$ and hammer tap $V_{S,HV}$ profiles (less than 10% difference even in challenging zones) we believe it is possible to obtain high-quality velocity profiles using DPCH testing provided that the following guidelines are adhered to: (1) Use friction reducers to minimize the coupling between the push rods and the surrounding soil. (2) Look for soft soil layers in the CPT q_C data and scrutinize the S_{HV} waveforms in these zones for evidence of early wave arrivals. (3) Pick S_{HV} departures that have the correct initial voltage polarity (e.g., negative for the waveforms presented in this paper, based on our particular equipment) immediately followed by a polarity reversal (e.g., a positive cycle for the waveforms presented in this

paper). By following this approach, it will be possible to obtain very good measurements of V_P and V_S using simple hammer taps without needing to use an in-ground source. This type of velocity resolution is not possible using downhole/SCPT. While high-resolution measurements may not be needed for every engineering application, DPCH testing provides engineers with a tool for making more accurate measurements when needed.

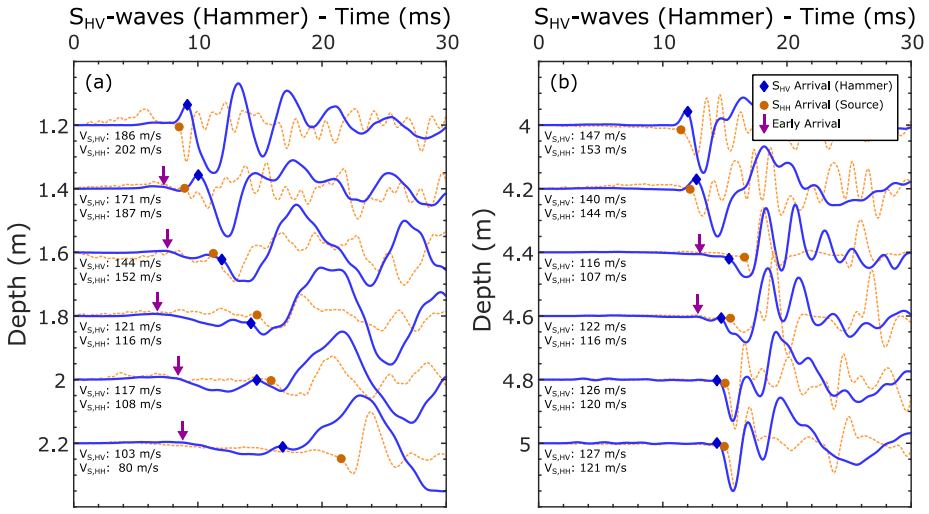

Figure 2.11: S_{HV}-waveforms (bold, solid lines), generated with a hammer tap on top of the push rods, and S_{HH}-waveforms (thin, dashed lines), generated by the in-ground source, are shown in waterfall format from two different depth zones, highlighted in Figure 2.10. (a) The depth range in Zone A is 1.2 to 2.2 meters, and the soil transitions from a stiff, near-surface crust to a softer silty layer. (b) The depth range in Zone B is 4 to 5 meters, where the soil transitions from a stiff sandy material to a softer silty to a stiff silty-sand. The S_{HH}-wave first arrival picks (filled, circular markers) are shown on the S_{HH}-waveform and used to inform the S_{HV}-wave first arrival picks (filled, diamond markers), shown on the associated S_{HV}-waveforms. An initial negative departure is expected for the direct wave arrivals for both sets of waveforms. The S-wave velocities associated with the S_{HH}-wave and S_{HV}-wave arrival picks are provided for reference. Early wave arrivals (that might be incorrectly picked and not representative of direct wave arrivals) are indicated on the S_{HV}-waveforms by arrows.

2.6 CONCLUSIONS

An invasive seismic testing method called direct-push crosshole (DPCH) testing has been developed. DPCH combines the technical benefits of crosshole seismic testing with the ease and speed of direct-push downhole/SCPT methods. DPCH testing uses a pair of instrumented seismic cones pushed into the ground with two closely-spaced CPT rigs. Pushing the cones into the ground provides excellent coupling with the soil and eliminates the need for expensive cased boreholes. The relative position of each cone is tracked using tilt angles obtained from MEMS accelerometers, thus allowing for accurate calculations of the distance between cones at each measurement depth. The seismic energy required for testing is easily generated by tapping a hammer on top of the CPT push rod connected to the source cone. In this manner, both P-waves and S-waves are propagated from one cone (the source) to the other (the receiver). A significant advantage of DPCH testing is the ability to maintain a consistent wave travel path and strong signal-to-noise ratio as a function of depth. These two factors allow for consistent resolution of V_P and V_S as a function of depth, resulting in detailed wave velocity profiles with the potential to detect thin layers.

Using the methodology detailed in this paper, DPCH field data can be collected at a rate of approximately 1.0 to 1.5 minutes per test depth. Thus, using a depth increment of 20 cm, it is possible to simultaneously collect V_P and V_S data down to a depth of 10 m in 50 to 75 minutes. The maximum DPCH testing depth to date is just over 20 m, but it is possible to go deeper. In order to avoid potential problems with non-direct wave paths, the cones should be placed no more than 1.5 to 2.5 meters apart and friction reducers should

be used on the cone rods. Other strategies for dealing with complicated wave arrivals in interlayered soil deposits have been discussed.

DPCH testing has thus far been used for in-situ evaluation of various ground improvement methods, allowing for measurements of V_P and V_S directly across/through vertical elements such as stone columns, which cannot be achieved with any other in-situ testing methodology (Stokoe et al. 2014, Wotherspoon et al. 2015, Stokoe et al. 2016, Hwang et al. 2017, Wotherspoon et al. 2017). DPCH has also been used in soil liquefaction studies to account for the beneficial effects of partial saturation, which can be inferred from high quality measurements of V_P, and soil microstructure, which can be inferred from high quality measurements of V_S (Cox et al. 2017, McLaughlin 2017). An area of ongoing research is the in-situ evaluation of soil porosity and void ratio, which requires extremely precise values of V_S and V_P (Foti et al. 2002, Foti and Lancellota 2004). It is anticipated that DPCH testing will play a key role in eventually being able to measure soil void ratio in situ, which is currently obtained only by correlations to penetration test results. These applications, and no doubt others yet to be discovered, make DPCH testing an important in-situ site characterization tool for geotechnical engineering in the future.

2.7 ACKNOWLEDGEMENTS

This work was partially supported by U.S. National Science Foundation (NSF) grant CMMI-1547777. However, any opinions, findings, conclusions, or recommendations expressed in this material are those of the authors and do not necessarily reflect the views of NSF.

Financial support was also provided by the New Zealand Earthquake Commission (EQC) under the Capability Building Fund at the University of Auckland and QuakeCoRE through Technology Platform 2.

Chapter 3: Epistemic uncertainty in shear wave velocity measurements obtained via SCPT

Andrew C. Stolte and Brady R. Cox

This chapter contains a journal article that is in preparation. The full citation is listed below:

Stolte, A. C., and Cox, B. R, (2018). "Epistemic uncertainty in shear wave velocity measurements obtained via SCPT". Manuscript in preparation.

As first author, I was responsible for approximately 50% of the concept development, 90% of the data processing, and 50% of the results interpretation.

ABSTRACT

Seismic cone penetration testing (SCPT) combines the benefits of CPT testing (e.g., the speed of directly advancing instrumentation into the ground and the effectively continuous measurement of tip resistance, sleeve friction, and pore pressure) with the ability of borehole-based downhole seismic testing to measure the in situ shear wave velocity, V_S (i.e., small-strain stiffness). Four different imprecation techniques are used to evaluate shear wave travel times from SCPT measurements, including: (1) first arrival picks, (2) peak/trough picks, (3) crossover picks, and/or (4) the time delay associated with the peak response of the cross-correlation function. The V_S profiles are developed using three different velocity analysis methods: (1) the pseudo-interval method, (2) true-interval method, and (3) the corrected vertical travel time slope-based method. Commonly, a single V_S profile is developed from SCPT measurements and the end-user is left to estimate the associated epistemic uncertainty. However, through the consideration of multiple data

reduction techniques and analysis methods, a more robust and meaningful qualification of the epistemic uncertainty may be developed. A comparison of several SCPT V_S profiles is considered for two datasets. Finally, inter-method variability/bias between SCPT and direct-push crosshole (DPCH) testing is examined using 31 co-located datasets collected in Christchurch, New Zealand.

3.1 INTRODUCTION

Careful characterization of near-surface soil and rock is an important part of all geotechnical engineering projects. Measuring the stiffness of these materials is essential for evaluating their response to dynamic loads such as earthquakes and machine vibrations. Furthermore, measurements of soil stiffness can be used for other geotechnical engineering applications, including the evaluation of foundation settlement, in-situ degree of saturation, and soil porosity. The small-strain constrained compression modulus (M_0) and shear modulus (G_0) are of principal interest. These moduli are directly proportional to the square of the primary constrained compression (P) wave and secondary shear (S) wave velocity, respectively. While laboratory measurements of P- and S-wave velocity (V_P and V_S) may be performed on soil and rock specimens using techniques such as bender element and resonant column testing, it is important to make in-situ measurements of V_P and V_S using field seismic testing methods.

Seismic testing requires a source of stress wave energy, whether actively-generated or passively-observed, and receivers with transducers (e.g., geophones or accelerometers) to sense the propagation of the stress waves. In practice, field seismic testing methods are

divided into two categories: (1) non-invasive, surface-based methods, and (2) invasive, borehole-based/direct-push methods. Non-invasive seismic methods are those which involve placement of the source and receivers along the ground surface, such as seismic refraction and surface wave testing. The resulting V_S and V_P profiles (whether directly measured or inverted) represent a spatial average of material stiffness for layers identified within the bounds of the receiver array.

Invasive seismic testing methods involve the placement of a seismic source and/or the receiver(s) below the ground surface, inside of the material tested. Initially, invasive seismic methods were used for deep exploration, typically to locate petroleum. These methods were subsequently adapted and developed for use in geotechnical engineering in the 1970's (Stokoe and Woods 1972, Woods 1978). During those early years, invasive testing methods, including downhole (DH) and crosshole (CH) seismic testing, were exclusively borehole-based (i.e., the source and/or receiver packages were lowered down pre-drilled boreholes). Later, direct-push variants of these testing methods were developed, for which the instrumentation could be installed in conical probes and directly advanced into the ground (e.g., seismic cone penetration testing (SCPT) is the direct-push equivalent of DH testing).

Non-invasive seismic testing methods are generally considered to be more uncertain/less reliable than invasive methods. However, a recent, comprehensive, blind-analysis study at three geologically-distinct sites in Europe revealed that V_S profiles derived from surface wave testing had coefficients of variation that were often similar to, and at times lower than, those derived from a combination of crosshole, downhole and PS

suspension logging (Garafalo et al. 2016). The Garafalo et al. (2016b) study draws attention to the fact that uncertainties exist in *both* invasive and non-invasive methods and that those uncertainties need to be realistically quantified to aid subsequent engineering analyses. While this is not a new finding, it would be extremely rare at the present time for those conducting either invasive or non-invasive seismic testing to attempt to communicate this uncertainty to the end-user through statistics, or by providing multiple interpretations of the same dataset. Although still not common in practice, significant research has been devoted to quantifying uncertainty in V_S profiles derived from non-invasive surface wave testing (e.g., Marosi & Hiltunen 2004, Foti et al. 2009, Griffiths et al. 2016a, Teague & Cox 2016, Teague et al. 2018). On the other hand, comparatively little attention has been devoted to quantifying uncertainty in V_S profiles derived from invasive methods (Kim et al. 2004, Bang et al. 2014, Styler and Weemees 2017).

Two different types of V_S uncertainty need to be quantified for engineering analyses such as seismic site response (EPRI 2012): (1) aleatory variability, and (2) epistemic uncertainty. In terms of V_S, aleatory variability results from the inherent variability/randomness associated with the subsurface layering and shear stiffness across the footprint of the site. Thus, aleatory variability is linked to the horizontal and vertical spatial variability of V_S. Aleatory variability can be estimated by the end-user of V_S data by considering the spatial variability of the invasive V_S profiles, which are essentially point-measurements. On the other hand, epistemic uncertainty results from data and modeling uncertainties. Thus, even for a single location, epistemic uncertainty in V_S exists due to factors such as data quality and method of analysis. As noted above, epistemic

uncertainty in V_S is rarely quantified by those performing invasive seismic testing. Rather, a single, deterministic V_S profile is typically provided for a single testing location without consideration of uncertainty. Hence, end-users need to make assumptions about the epistemic uncertainty in V_S for use in subsequent analyses. For example, it is extremely common for engineers to account for epistemic uncertainty in seismic site response by creating upper- and lower-bound V_S profiles obtained by arbitrarily increasing and decreasing the reference V_S profile by a constant, depth-independent factor such as +/- 20% to 30% (Matasovic and Hashash 2012, Griffiths et al. 2016a). However, this methodology has recently been called into questions and has been shown to yield poor estimates of seismic site response (Griffiths et al. 2016b, Teague and Cox 2016). As such, methods for realistically quantifying epistemic uncertainty in V_S profiles derived from invasive seismic tests are needed.

This paper examines the depth-dependent epistemic uncertainty in V_S profiles obtained from seismic cone penetration testing (SCPT). While the datasets used herein originate from SCPT, the same principles can be applied to traditional downhole testing. Epistemic uncertainty is quantified by considering both data processing and data analysis methods. Specifically, four different ways of obtaining shear wave travel times from SCPT waveforms are investigated: (1) first arrivals, (2) first peaks/troughs, (3) first crossovers, and (4) the time delay associated with the peak of the cross-correlation function between pairs of waveforms. Then, three data analysis techniques are used to develop V_S profiles: (1) the true-interval method, (2) the pseudo-interval method, and (3) the corrected vertical travel time slope-based method. Combinations of the four data interpretation techniques

and three data analysis methods produce a total of eleven V_S profiles for each SCPT dataset (noting that the cross-correlation time delay is not compatible with the slope-based method). These eleven V_S profiles are developed at each site using the commonly-assumed straight-line, slanted travel path from the source to the receiver. Additionally, a raytracing algorithm was used by an independent, well-regarded CPT contractor to develop an additional V_S profile for each SCPT dataset. The epistemic uncertainty associated with the travel path is considered by comparing the V_S profile from raytracing to the other SCPT V_S profiles. Finally, inter-method variability/bias between SCPT and direct-push crosshole (DPCH) testing is examined using 31 co-located datasets collected in Christchurch, New Zealand.

3.2 SCPT/Downhole Seismic Testing

3.2.1 General Testing Methodology

Conventional downhole seismic testing is conducted by exciting a seismic energy source at the ground surface and measuring the wave arrivals at a receiver incrementally lowered into a cased borehole (ASTM D7400-14). The time and costs associated with preparation of a borehole, including grouting the casing in place and pumping out borehole fluid to avoid measurement of tube waves, are undesirable aspects of conventional DH testing. Thus, when relatively soft soil conditions exist, it is common to conduct downhole seismic testing in conjunction with CPT testing (ASTM D5778-12). This combined test is called seismic cone penetration testing (Robertson et al. 1986).

A simplified SCPT testing layout is shown in Figure 3.1. At the ground surface, the source is horizontally offset a distance X (typically 1 to 3 meters) from the cone push rods. Vertically propagating, horizontally polarized (S_{VH})-waves are typically excited using horizontal sledgehammer strikes on a rigid shear/traction plank oriented perpendicular to the horizontal offset from the borehole. The polarity of the shear waves may be reversed by striking opposite ends of the plank; this helps when trying to identify the arrival of the shear waves at the receiver. These waves are best observed on transducers (e.g., geophones or accelerometers) oriented in the crossline-horizontal direction parallel to the wave particle motion and the traction plank, as indicated inside of the cones by highlighted circular symbols in Figure 3.1a. P-waves are typically generated using vertical, downward sledgehammer hits on a metal strike plate, and are best observed using vertically-oriented transducers in the cone. Directly advancing an instrumented receiver cone into the ground provides excellent coupling with the surrounding soil and ensures transmission of seismic energy from the soil into the cone. However, compression waves generated at the ground surface often make their way into the steel cone push rod and obscure the direct arrival of the P-waves through the soil. These "rod" waves are difficult to eliminate and therefore reliable measurements of V_P from SCPT testing are difficult to obtain. Typically, SCPT cones contain a seismic sensor package consisting of two or three orthogonally-oriented transducers. In some cases, the receiver may contain a pair of sensor packages vertically offset at a fixed distance (typically 0.5 to 1.0 meters apart). These dual-sensor cones allow measurement of true-interval velocities. However, true-interval seismic cones are less

common because they are more expensive and require additional wiring and data acquisition channels.

CPT measurements of cone tip resistance and skin friction are taken as the cone is advanced into the ground. Seismic measurements are typically taken once every meter, when cone advancement is paused to add a push rod segment. Many commonly used DH analysis methods (as discussed in the next section) assume a straight-line seismic wave travel path from the source to the receiver, as indicated by rays L_1 and L_2 in Figure 3.1 for testing depths D_1 and D_2, respectively. The deviation of the borehole(s)/cone(s) are almost never considered in DH testing analyses.

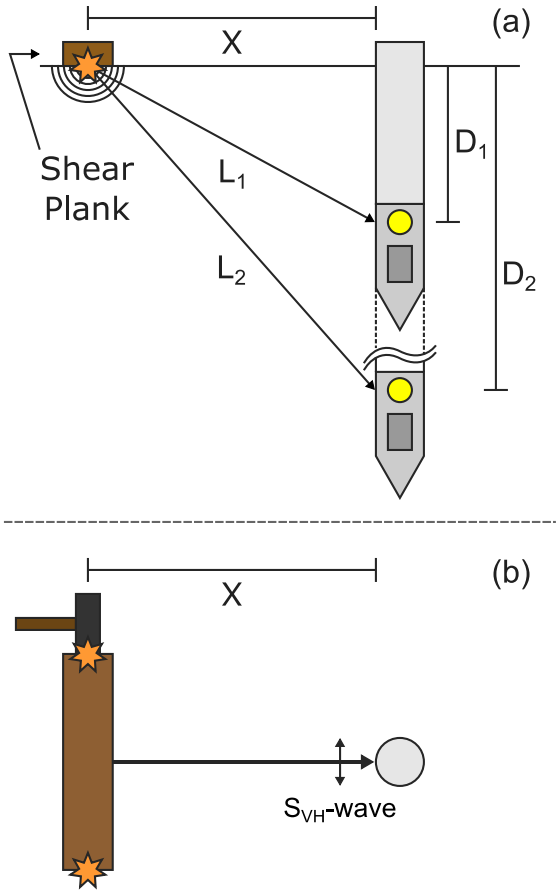

Figure 3.1: Schematic of a SCPT test: (a) Cross sectional view and (b) plan view. The SCPT cone is advanced into the ground and stopped at successive measurement depths (D_1, D_2, etc). The shear plank is horizontally offset a distance X from the cone push rod at the ground surface and oriented crossline/perpendicular to the offset. S_{VH}-waves are excited by horizontally striking the ends of the shear plank. The S_{VH}-waves propagate from the source into the ground along assumed ray paths (L_1, L_2, etc.) and arrive at the seismic transducers inside of the SCPT cone. The S_{VH}-waves are best observed on the transducer components aligned in the crossline-horizontal direction, as indicated by the highlighted circles.

3.2.2 Data Reduction and Analysis Techniques

With the goal of developing profiles of V_S (and less frequently V_P), the first step in SCPT data reduction is travel time evaluation of the seismic waves; either the direct travel time from the source to the receiver, or the relative travel time between two measurement depths. Barring early rod wave arrivals, the P-wave is the first to arrive at the receiver. Therefore, the P-wave arrival time is picked as the first departure from the noise floor, regardless of voltage polarity. The S_{VH}-wave, referred to as an S-wave hereafter, arrives at the receiver after the P-wave. At times, the S-wave arrival may be difficult to clearly identify, as it may be obscured or complicated by the preceding P-wave. However, the initial polarity of the S-wave (i.e., a positive or negative voltage caused by a left or right strike on the traction plank) should be maintained as the wave travels through the soil. Therefore, S-wave first arrivals are picked as the *first major departure with the correct voltage polarity* following the P-wave arrival. As noted above, both ends of the shear plank may be used to generate S-waves, producing two S-waves with opposite polarity. When examined together, the waveforms with opposite polarity will exhibit similar P-wave traces and diverge (or "butterfly") at the arrival of the S-wave, roughly mirroring each other. Each pair of reversed waveforms may be plotted with their associated measurement depth in a waterfall-style plot. The analyst may choose to pick a single representative S-wave arrival time from the butterflied waveforms ("averaging" by eye), or pick a separate S-wave arrival time for both polarities, which is subsequently averaged. A sample S-wave waterfall plot is shown in Figure 3.2, with the associated average S-wave first arrival (FA) picks indicated by circular markers on the waveforms. In a perfect world, the FA picks would be

preferred, as they are indicative of the initial arrival of the shear waves at the receiver, but in practice they may be difficult to identify, requiring the subjective judgment of the analyst. In such cases, later points in the S-wave traces are often picked, such as the first peak/trough (PT) or first crossover (CO) of the reversed waveform pairs, as indicated in Figure 3.2 by square and diamond markers, respectively. A benefit of picking first PT and CO times is that they may be semi-automated, requiring less subjectivity than making FA picks by eye. For example, PT times can be obtained by numerically searching for local maxima/minima and CO times can be obtained by searching for the local minimum difference between the amplitude of the two waveforms.

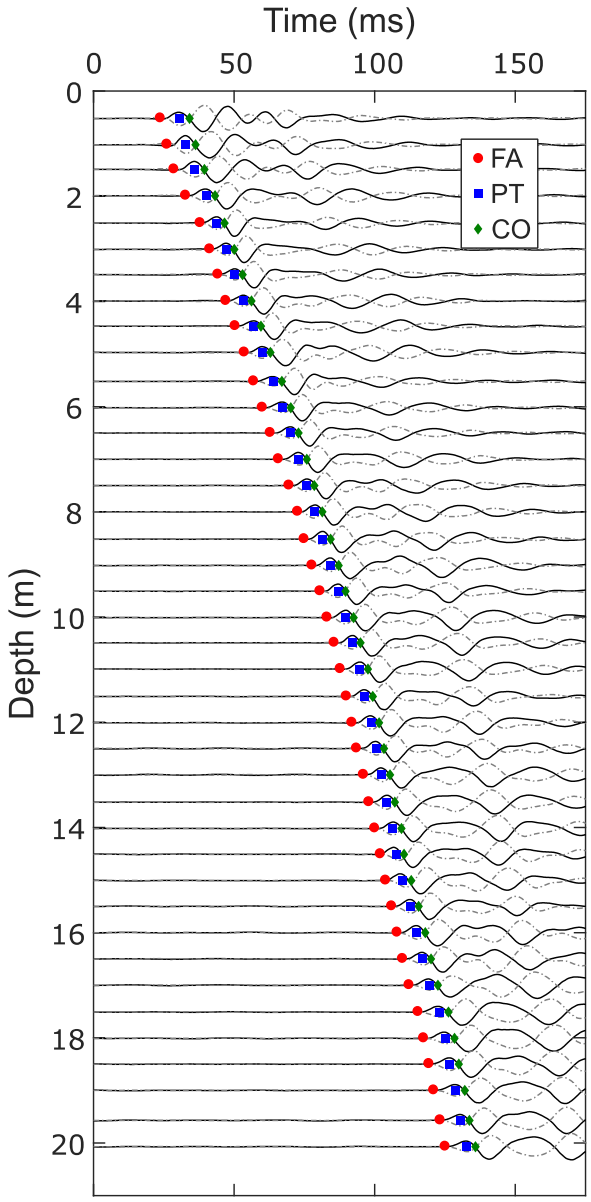

Figure 3.2: Waterfall plot of SCPT reversed S_{VH}-waveform pairs from the Avondale Playground dataset. Waveforms with initial positive voltage (upward) departures are indicated by solid lines, and those with initial negative voltage (downward) departures are indicated by dash-dotted lines. Symbols associated with three commonly-picked shear wave arrival times are indicated in the legend: first arrivals (FA), first peaks/troughs (PT), and first crossover (CO) times.

When the relative (e.g., interval) wave travel time (Δt) between two measurement depths is desired for subsequent data analyses, it is obtained by taking the difference between the FA, PT, or CO travel times obtained at each measurement depth. To clearly illustrate the process of obtaining Δt, two sets of reversed waveform pairs are plotted together in Figure 3.3a. These particular waveforms were taken from measurement depths five meters apart so that the Δt values are large enough to see. The FA, PT, and CO travel times are indicated on each pair of waveforms by circle, square, and diamond markers, respectively. The interval travel time for each picking method is visually indicated in-between the waveforms and the Δt values are tabulated in the legend. Alternatively, the time delay associated with the peak response of the cross-correlation (CC) function between two waveforms recorded at different measurement depths may be used to evaluate the interval travel time. Baziw (1993) recommends using CC to obtain Δt, as it eliminates the subjectivity associated with making manual picks and uses the full-waveform rather than discrete points. The cross-correlation function of the positive voltage polarity waveforms from Figure 3.3a is shown in Figure 3.3b. The peak response is indicated by a triangle marker. Note the similarities and differences in the Δt values from the four different methods (i.e., FA, PT, CO, and CC) used to obtain the shear wave travel times from the exact same waveforms, as illustrated in Figure 3.3.

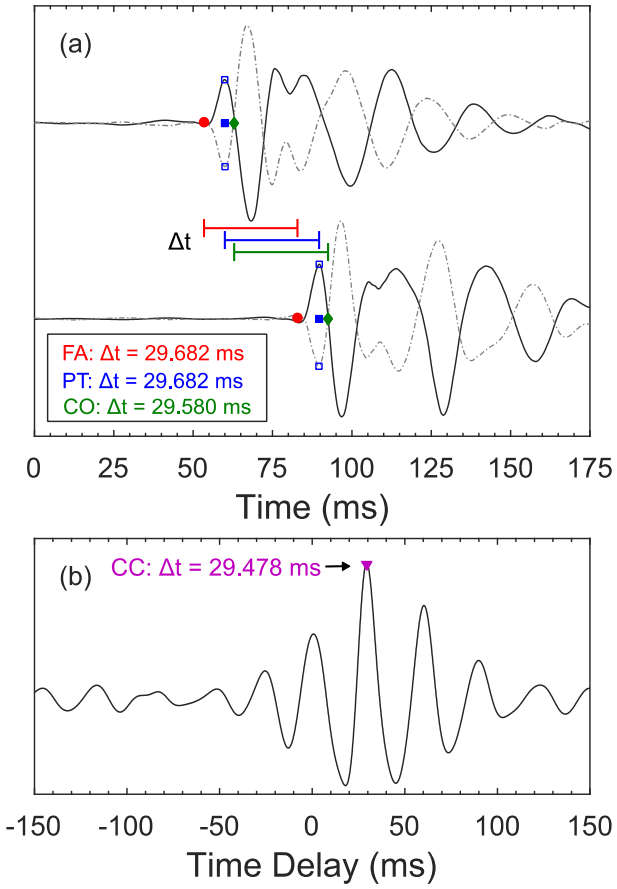

Figure 3.3: Interval travel time evaluation example from: (a) Butterflied S_{VH}-waveform pairs (solid line for initial positive voltage departure and dash-dotted line for initial negative voltage departure) recorded at different measurement depths. The picked first arrivals (FA), first peaks/troughs (PT), and first crossover (CO) times are indicated on the waveforms by circle, square, and diamond markers, respectively. The interval times (Δt) associated with each travel time picking method are indicated in the legend. (b) The cross-correlation function between the two positive voltage polarity waveforms in (a) is indicated by the solid line. The time delay (i.e., the product of the time lag and the sampling rate of the waveforms) associated with the peak of the cross-correlation function is the Δt value between the two measurement depths, as indicated by the triangle marker.

Once the travel times have been obtained from the seismic waveforms, a variety of analysis techniques may be employed to process SCPT data and develop profiles of V_P and

V_S, including the true- and pseudo-interval methods (TI and PI, respectively), the corrected vertical travel time slope-based method (SM), and raytracing algorithms (RT). The interval methods (TI or PI) are described in the downhole seismic testing ASTM standard (ASTM D 7400-14) and are the most common methods used to reduce SCPT data. Interval methods are used to develop profiles of V_S and V_P by evaluating the velocity between pairs of measurements, whether obtained by successive advancements of a single receiver (pseudo-interval) or collected simultaneously using two vertically-offset sensor packages in a dual receiver (true-interval). First, the interval (i.e., relative) wave travel time, Δt, between two measurement depths is evaluated, as discussed above relative to Figure 3.3. Next, the change in wave travel path, ΔL, is evaluated for the two measurement depths. Typically, a simple straight-line travel path (see Figure 3.1) is assumed from the source at the ground surface to the receiver. However, the ASTM standard strongly recommends that refracted travel paths should be considered at shallow testing depths and across layer boundaries with significant stiffness contrasts. In these cases, Snell's law should be used to evaluate the refraction angles and length of the travel path. In practice, it is not common for refracted ray paths to be considered in conjunction with the interval analysis methods. Therefore, many SCPT V_S profiles will not accurately represent the near-surface velocity structure. However, the straight-line ray path assumption becomes reasonable as depth increases and the travel path approaches vertical.

The interval velocity is evaluated for each successive pair of measurements using the following equation:

$$V_S = \frac{L_i - L_{i-1}}{t_i - t_{i-1}} = \frac{\Delta L}{\Delta t} \quad (3.1)$$

where i is the current, deeper measurement, i-1 is the previous, shallower measurement, L is the travel path length, and t is the picked wave arrival time. If a dual receiver cone is used to simultaneously record a pair of waveforms from a common source excitation, the resulting velocity is considered a true-interval velocity. Otherwise, if a single receiver cone is used to incrementally record waveforms at two different depths using different source excitations, the resulting velocity is considered a pseudo-interval velocity. Slight differences in the source excitations and data acquisition triggering may introduce timing errors into the evaluated PI velocities. Robertson et al. (1986) noted a maximum 10% error associated with PI velocities as compared to TI velocities, both evaluated from a true-interval cone dataset.

The corrected vertical travel time slope-based method is used to develop a shear wave velocity profile by examining linear trends in corrected vertical travel time with depth (Kim et al. 2004, Redpath 2007, Boore and Thompson 2007), as shown for an example SCPT dataset in Figure 3.4. The average first arrival picks are taken directly from the waterfall plot in Figure 3.2. First, the FA shear wave travel times at each measurement depth, indicated by hollow circular markers in Figure 3.4, are corrected to vertical travel times (solid circular markers), effectively removing the horizontal source offset and adjusting the travel time at the ground surface to zero. This correction is accomplished using the assumed triangular testing geometry (refer to Figure 3.1a) and the following equation:

$$t_{vert} = t_a \cdot \frac{D}{\sqrt{D^2+X^2}} \quad (3.2)$$

where t_a is the picked first arrival time, D is measurement depth, and X is the horizontal source offset. If later features of the waveform (e.g., first peak/trough or first crossover point) are picked, they must be adjusted to an equivalent first arrival time (refer to Redpath 2007 for details). V_S profiles are developed by fitting linear trends to groups of data (i.e., layers) separated by distinct changes in slope. If changes in slope are subjective, subtle, or difficult to discern, the layer boundaries observed in the CPT sounding or boring log should be used to establish logical slope breaks. In Figure 3.4, the CPT cone tip resistance (q_C) and normalized soil behavior type index (I_C) were used to guide the selection of the layer boundaries, as indicated by the dashed horizontal lines. Once the layer boundaries are identified, linear trends are fitted to the corrected vertical travel time data for each individual layer using a least squares regression. Travel time outliers may be weighted less or removed from the regression if needed. The slope of the fitted linear trend is the constant S-wave velocity of the corresponding layer. In Figure 3.4, the resulting shear wave velocities are reported to the nearest meter per second. The velocities above and below the layer boundary defined at 14.25 meters are 241 and 246 m/s, respectively. These velocities are essentially the same for practical purposes, however, the increase in cone tip resistance at this depth warrants consideration of a change in shear stiffness. As noted by Boore and Thompson (2007), velocity profiles developed from this slope-based method are less prone to large fluctuations (i.e., swings) in velocity (as compared to the pseudo-interval method). The effects of inconsistent triggering and other small errors are averaged out by fitting a liner trend to multiple data points.

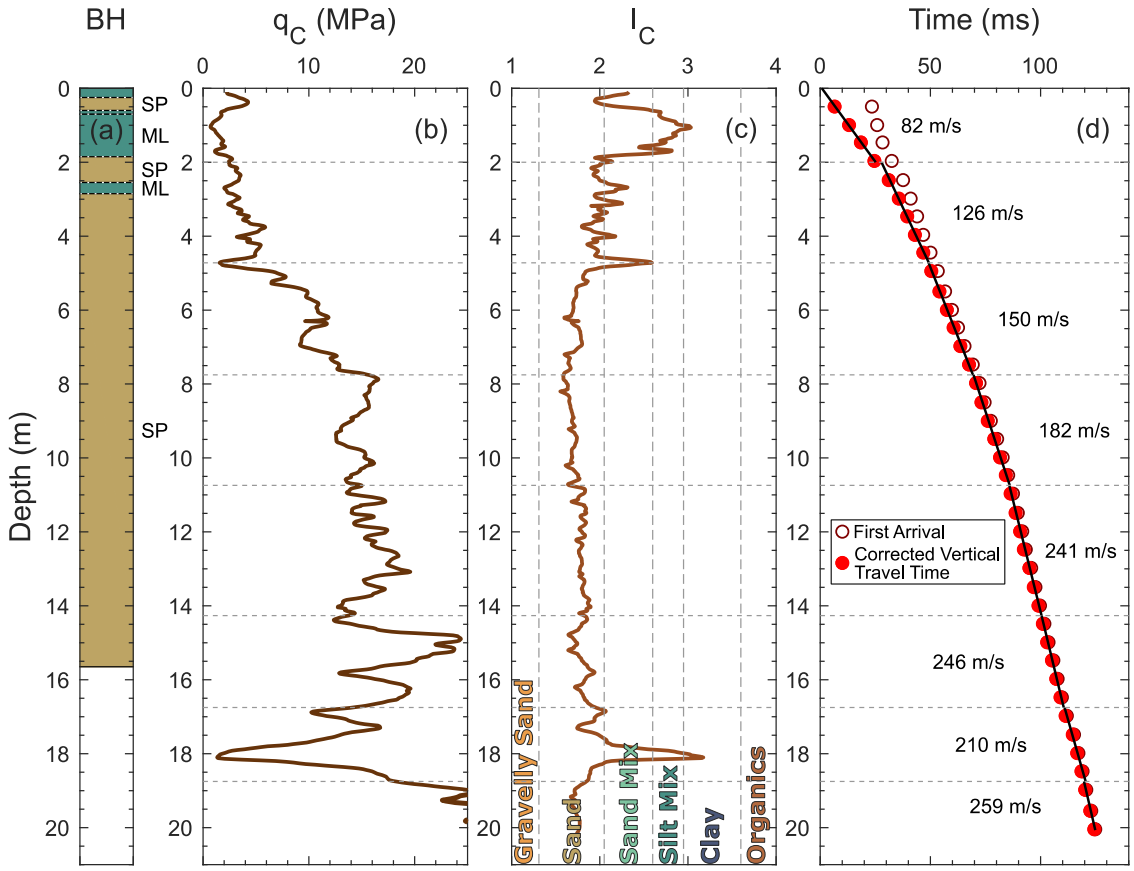

Figure 3.4: Slope-based SCPT V_S evaluation method for the Avondale Playground dataset. Potential layer boundaries are defined based on supporting geotechnical data at the site including: (a) the continuous core sonic borehole log, (b) the raw cone tip resistance, q_C, and (c) the normalized soil behavior type, I_C. In panel (d), the shear wave first arrival (FA) times (hollow circular markers) have been corrected to vertical travel times (solid circular markers) using the SCPT testing geometry. Note that the correction is more pronounced in the near surface, with the apparent vertical travel time at the ground surface equal to zero. Linear slopes are fitted to vertical travel times to evaluate the associated V_S values of layers identified using the supporting geotechnical data.

As noted above, the S- (and P-) wave travel path between the source at the ground surface and the downhole receiver is typically assumed to be a simple, straight-line. As receiver depth increases, the travel path of the seismic energy is nearly vertical (i.e., the

angles of incidence with near-horizontal layer interface is negligible) and the assumed straight-line travel path is reasonable. However, near the ground surface the angles of incidence of the waves with near-horizontal layers increase, causing the waves to follow a non-linear, refracted travel path. A third possible method of velocity analysis attempts to account for these refracted travel paths. Chandler (1977) developed a raytracing algorithm to evaluate the downhole travel times along refracted travel paths through an assumed horizontally layered velocity model by using Snell's law to determine refraction angles at layer interfaces. Baziw (2002) developed a forward modeling, downhole simplex method (FMDSM) to invert for the V_S profile by iterating layer velocities and comparing measured S-wave travel times to theoretical travel times calculated using Chandler's raytracing algorithm. Typically, the FMDSM assumes a horizontally layered profile with fixed layer interfaces either defined by a constant depth increment (e.g., one horizontal layer for every downhole measurement depth) or a priori geotechnical data (e.g., CPT or borehole logs).

In summary, wave arrival times can be obtained from FA, PT, and CO picks, as well as the CC function. Velocity profiles can be developed from these wave arrival times using TI, PI, SM, and raytracing (RT) analysis methods. When a single wave arrival time and a single analysis method are used to develop a single, deterministic velocity profile, the epistemic uncertainty involved in selecting the wave arrival time and analysis method is not reflected in the end results. For the case history sites discussed below, epistemic uncertainty in V_S is investigated by using all possible combinations of these wave arrival time and data analysis methods.

3.3 Analysis of SCPT Datasets

Following the 2010-2011 Canterbury Earthquake Sequence, a study aimed at resolving discrepancies between the observed manifestation (or lack thereof) of liquefaction induced by the earthquakes and the liquefaction predicted by simplified CPT-based liquefaction triggering relationships was undertaken by an multi-national team of researchers (Cox et al. 2017, McLaughlin 2017). As a part of this effort, a thorough near-surface geotechnical site characterization was completed at 31 sites. Site characterization included continuous, disturbed soil sampling from a sonic borehole, a SCPT sounding, and direct-push crosshole (DPCH) testing (as documented in Chapter 2). At each site, these investigation methods were conducted no more than 2 meters apart to allow direct comparison of the geotechnical data. The results from each of these tests are publically available on the New Zealand Geotechnical Database (https://www.nzgd.org.nz).

The SCPT soundings were collected and initially processed by a well-regarded, independent, international CPT contractor. The SCPT data included typical CPTu measurements of cone tip resistance, sleeve friction, and pore pressure response at the U2 location. A true-interval SCPT cone was used with two sets of sensors vertically offset by 0.5 meters. Each sensor set consisted of a vertical and crossline-horizontal geophone. Seismic measurements were taken every meter when cone advancement was halted to add a segment to the cone push rod. The use of a true-interval cone allowed measurement of waveforms every half meter, while only stopping to collect waveforms every meter. The shear plank was horizontally offset 1.7 meters from the cone rod and held in place by one of the cone rig leveling jacks. The waveforms were digitized at a 9.8 kHz sampling rate

(time interval of 0.102 ms). Data acquisition was triggered when the contact between the hammer and metallic shear plank closed the triggering circuit. At each measurement depth, the S-waves were reversed by striking both sides of the shear plank. Typically, three waveforms were stacked for each S-wave polarity. Measurements of P-waves were attempted at a few sites using vertical downward hammer strikes, but the recorded waveforms were of insufficient quality to process due to early rod wave arrivals. The SCPT data was processed by the CPT contractor to develop a single V_S profile at each site using the following procedure: (1) shear wave FA picks were made from the butterflied waveforms recorded every 0.5 m, (2) the forward modeling, downhole simplex method (Baziw 2002) was used to develop the V_S profile by comparing theoretical shear wave first arrival times calculated using a raytracing algorithm (Chandler 1977) to those experimentally measured in the field. The V_S profiles developed using the FBDSM raytracing algorithm are referred to as RT, for simplicity.

The authors were provided with the raw SCPT waveforms collected at each of the 31 sites. These waveforms were re-examined using the travel time evaluation methods (i.e., FA, PT, CO, and CC) and velocity analysis techniques (i.e., PI, TI, and SM) discussed above. The results from two sites are provided herein. The first site is located at the Avondale Playground (NZGD SCPT 57354, VSVP 57062, and BH 57217) and was chosen due to its relatively simple soil profile. The second site is located at St. Teresa's School (NZGD SCPT 57345, VSVP 57191, and BH 57241) and was chosen in contrast to the first site due to its complex interlayered profile. Each site is discussed in detail below and epistemic uncertainty in V_S is quantified. Additionally, discussions on epistemic

uncertainty are followed by an examination of the bias (inter-method variability) between V_S profiles determined at all 31 sites using two different direct-push testing methods, SCPT and DPCH.

3.3.1 Avondale Playground – Simple Soil Profile

The Avondale Playground dataset was used above in Figures 3.2-3.4 to illustrate some aspects of SCPT data reduction. The relatively simple soil profile is shown by the borehole log and CPT data in Figure 3.4. A two-meter thick silt layer is underlain by an 18-plus-meter thick poorly-graded sand deposit. The corrected cone tip resistance gradually increases from 2 to 25 MPa, with a significant decrease in cone tip resistance around 17 meters. Other small fluctuations and spikes in cone tip resistance may be indicative of thin soil layers (e.g., silt seams), but are difficult to resolve with the seismic measurements taken every half meter.

The stacked, butterflied SCPT waveform pairs are plotted in a waterfall-style plot in Figure 3.2. The FA, PT, and CO travel times are indicated directly on each waveform This SCPT dataset was collected using a true-interval cone, allowing the evaluation of both true- and pseudo-interval shear wave velocities. In this study, it is important to consider PI velocities because often cones used for SCPT only include a single set of transducers for seismic measurements. To best replicate PI conditions, the authors chose to use the waveforms measured by only the bottom crossline-horizontal geophone (i.e., the waveforms measured at 1 m and then every even meter after that down to 20 m). The CC time delays were obtained using both true-interval waveforms and pseudo-interval

waveforms (again, using only the bottom geophone). For the sloped-based velocity analysis method, the FA, PT, and CO travel times were each corrected to vertical travel times, as illustrated for the FA travel times shown in Figure 3.4. Informed by the borehole log and CPT q_C data, the vertical travel time values were broken into a series of horizontal layers. Three V_S profiles (i.e., one for each travel time) were developed by evaluating the S-wave velocity for each layer individually using the SM.

Eleven different profiles of V_S were developed, by the authors, from the various combinations travel time (FA, PT, CO, and CC) and velocity analysis methods (PI, TI, and SM). The V_S profiles determined from PI, TI, and SM analysis methods are shown in Figures 3.5a, 3.5b, and 3.5c, respectively. Profiles developed from FA picks, PT picks, CO picks, and CC time delays are indicated by solid, dashed, dotted, and dash-dotted lines, respectively. Note that the CC delay times are not compatible with the SM analysis. An additional RT V_S profile developed by the independent CPT contractor using FA travel times is shown in Figure 3.5d. As expected, all V_S profiles generally increase with depth through the thick sand layer as confinement increases. Additionally, all V_S profiles generally indicate a decrease, or leveling-off, in V_S between about 14 - 18.5 meters, where the cone tip resistance is also trending to lower values (see Figure 3.4b). However, some of the 1-m thick velocity layers associated with the PI and TI methods fluctuate significantly and often do not correlate well with each other, either within a given V_S analysis method based on different travel times, or between V_S analysis methods using the same travel times. The V_S profiles determined from the SM are remarkably similar over much of the depth range, regardless of the method used to obtain wave arrival times. The

single notable disagreement occurs in the depth range between 14.5 and 17 meters, where V_S from the FA travel times are ~50 m/s faster than those developed from the PT and CO travel times, most likely reflecting the difficulty of picking FA times over this depth interval. The overall stability of the SM analysis is attributed to two factors: (1) The layer boundaries were chosen using supporting geotechnical data collected at the site. (2) The layer velocities are obtained from the slope of the corrected vertical travel times, with each layer typically including more than two data points. The resulting velocities effectively average out errors associated with picking uncertainty and potential triggering errors that are more significant when using only two data points for an interval calculation. The layered profile used in RT analysis is constrained to a stack of half-meter thick horizontal layers and not informed by the additional geotechnical data at the site. Rather, each layer is assigned a single FA time to fit using the raytracing algorithm. The resulting V_S profile fluctuates, especially below 10 meters, to yield theoretical first arrival picks that match those experimentally measured which may include triggering, timing, and other sources of error. Similar fluctuations are observed in the interval-based velocity profiles, but are more pronounced in the RT profile due to thin layering. Regardless of the method used for velocity analysis, the PT and CO profiles are the most similar with depth, while the FA and CC profiles are more variable.

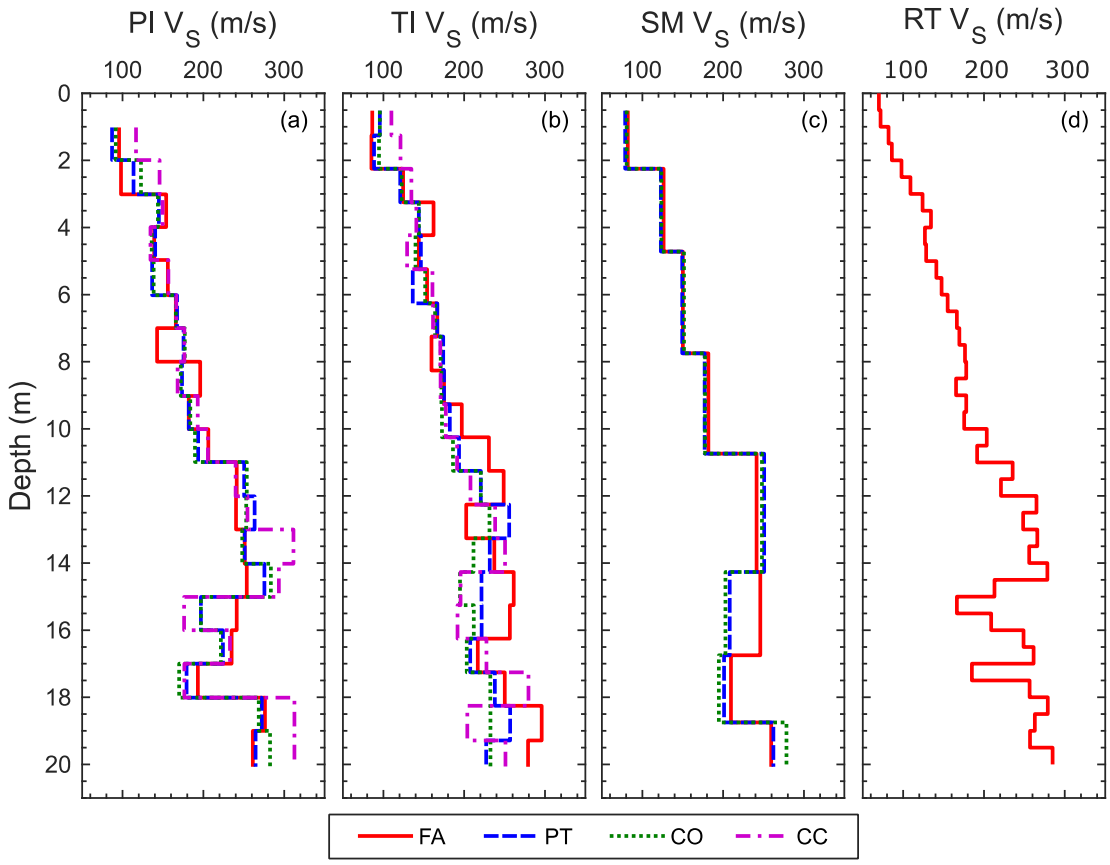

Figure 3.5: Comparison of SCPT V_S profiles developed for the Avondale Playground dataset: (a) pseudo-interval (PI), (b) true-interval (TI), slope-based method (SM), and (d) raytracing (RT) V_S profiles were developed for the first arrivals (FA), peak/trough (PT), crossovers (CO), and peak cross-correlation (CC) delay times.

It is useful to view the V_S profiles determined from different velocity analysis methods on top of one another and relative to the supporting geotechnical data at the site. This information is presented together for the Avondale Playground site in Figure 3.6. The V_S profiles shown in Figure 3.6b include: the PI, TI, and SM profiles determined from the PT arrival times (which generally yield stable V_S profiles, as compared FA picks), and the RT profile determined by the independent CPT contractor using FA times. Again, the SM

V_S profile is more stable with depth than the PI, TI, and RT profiles, each of which are comprised of relatively thin (i.e., one- or half-meter thick) layers with fluctuating velocities. However, each VS analysis method generally captures the trends in observed in the cone tip resistance, e.g. a gradual increase in stiffness with increasing confinement and localized decrease in stiffness at depths between 15 and 19 meters. Ideally, the near-surface velocity structure should be best captured using the raytracing algorithm which allows for refracted, slanted travel paths, while the PI, TI, and SM methods assume a straight-line travel path which is not reasonable in the near-surface. At a depth of ~2 meters, the PI, TI, and SM V_S profiles indicate a layer boundary with sharp increase in stiffness, whereas, the RT V_S profile indicates a more gradual increase in stiffness over the top 3 meters.

These four SCPT V_S profiles (and the others shown in Figure 3.5) are developed using widely-accepted data processing methods. Any of these profiles may be representative of "the" single V_S profile that might be provided by a SCPT contractor to an engineer. While it is not necessary to develop a full suite of V_S profiles using every conceivable analysis method, it is important to note that there is epistemic uncertainty associated with the development of SCPT V_S profiles.

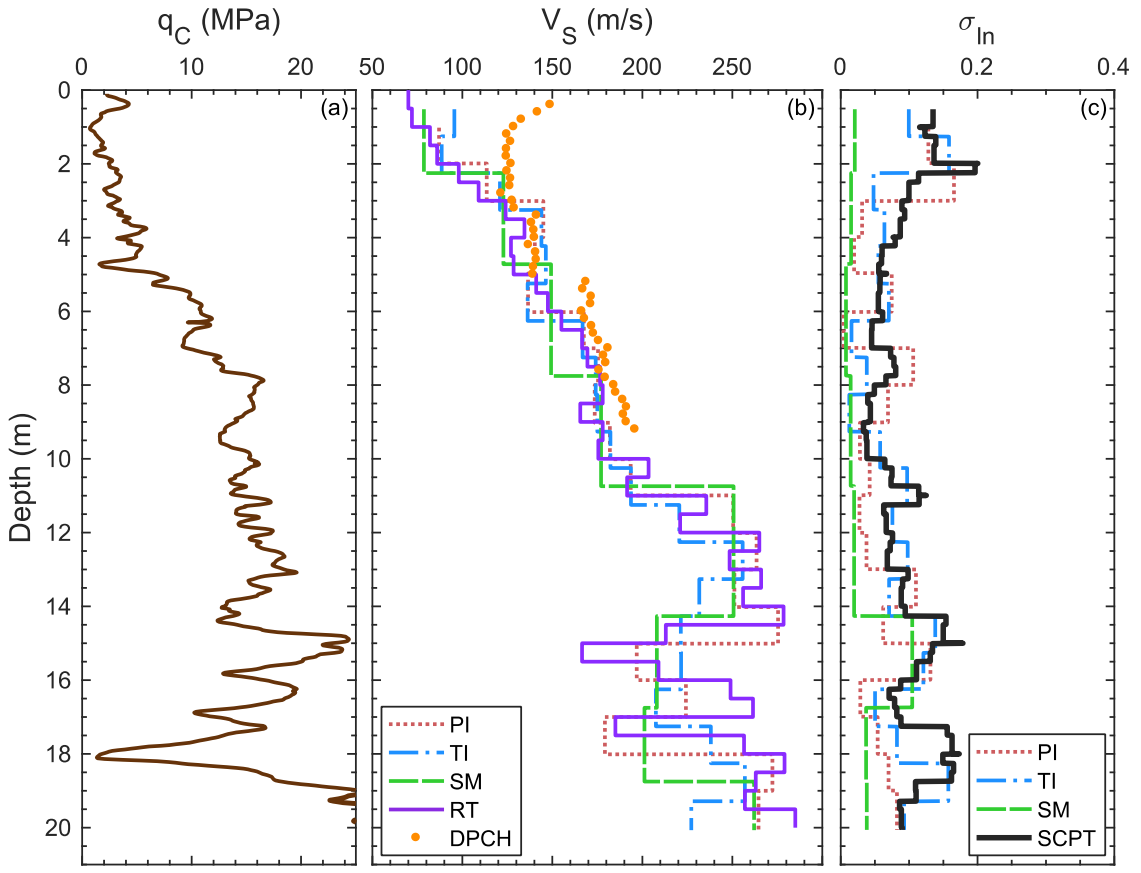

Figure 3.6: Summary of SCPT profiles for the Avondale Playground dataset: (a) Corrected cone tip resistance (q_C), (b) Comparison of shear wave velocity profiles, including pseudo-interval (PI), true-interval (TI), slope method (SM) developed from peak/trough picks (PT); raytracing (RT) developed from first arrival (FA) picks; and a Vs profile from another invasive seismic method, direct-push crosshole (DPCH) seismic testing, (c) The log-normal standard deviation of Vs (σ_{lnVs}) within each SCPT V_S analysis method (i.e., PI, TI, and SM) and between all SCPT methods.

The epistemic uncertainties associated with these V_S profiles are quantified in Figure 3.6c in terms of the log-normal standard deviation of V_S (σ_{lnVs}). The coefficient of variation (COV) and log-normal standard deviation (σ_{ln}) are directly related to each other through the mean and standard deviation of a given data set. When the COV is less than 0.3, the COV and σ_{ln} are approximately equal. However, σ_{ln} is more commonly used in

earthquake engineering, and V_S is often assumed to be log-normally distributed. Therefore, the intra-analysis-method σ_{lnVs} was evaluated as a function of depth for each of the three V_S analysis methods (PI, TI, and SM). For example, the σ_{lnVs} of the four PI V_S profiles shown in Figure 3.5a is indicated by the dotted line in Figure 3.6c. Additionally, σ_{lnVs} between all of the methods, including RT, was also calculated as a function of depth. While the number of velocity profiles included in the evaluation of σ_{lnVs} for each individual velocity analysis method is small (four or less), the values still provide a useful means of capturing the variability of the profiles with depth. Localized spikes in σ_{lnVs} are often an artifact of the different layer boundaries defined by each velocity analysis method and qualitatively reflect the uncertainty in the layer boundaries.

The lowest intra-analysis-method σ_{lnVs} is associated with the slope-based method, as expected given the consistency and stability of the SM V_S profiles with depth (refer to Figure 3.5c). The SM σ_{lnVs} only exceeds 0.05 in depth range between 14 and 16.5 meters, corresponding the localized high FA-pick V_S noted above. The σ_{lnVs} associated with either interval method is generally higher, but never exceeds 0.15. This reflects the increased uncertainty in interval V_S profiles, arising from both the fluctuating shear-wave velocity depth-to-depth and slight differences in interval travel times (i.e, FA, PT, CO, and CC) due to timing errors, changing frequency content, etc. The σ_{lnVs} associated with all twelve SCPT V_S profiles is highest: (1) at the near-surface (i.e., depths less than 2 m), where the straight travel path assumption is unreasonable, and (2) in the 14-19 meter depth range, where CPT q_C values indicate transitions from stiff sands to a thin, soft silt/clay layer and back to stiff sands again.

In practice, it is extremely common for engineers to account for epistemic uncertainty in seismic site response by creating upper- and lower-bound V_S profiles obtained by arbitrarily increasing and decreasing the reference V_S profile by a constant, depth-independent factor such as +/- 20% to 30% (Matasovic and Hashash 2012, Griffiths et al. 2016a). However, at the Avondale Playground, the σ_{lnVs} associated with the all twelve SCPT V_S profiles never exceeds 0.2 and is generally less than 0.1. While this quantification of epistemic uncertainty associated with SCPT V_S profiles does not directly consider other sources of uncertainty, such as noise in the signals (Styler and Weemees 2017), it represents a systematic, depth-dependent evaluation of the epistemic uncertainty associated with the use of different travel time and velocity analysis methods. At depths where the layering and V_S is well-constrained, the associated σ_{lnVs} is less than 0.10 representing a realistic reduction in the uncertainty, as compared to typically +/- 20% to 30%. Conversely, if the depth to a layer boundary is ill-defined or the V_S poorly-constrained, the associated epistemic uncertainty in V_S is reasonably increases, reflected by localized depth-dependent increases in σ_{lnVs}.

However, this only captures the epistemic uncertainty associated with V_S obtained via SCPT measurements. There is also epistemic uncertainty associated with the testing method selected to collect seismic merriments and develop V_S profiles. To illustrate this, a single V_S profile obtained via DPCH testing (this method is detailed in the SCPT and DPCH velocity bias section below) is shown in Figure 3.6b along with four of SCPT V_S profiles. While the DPCH V_S profile generally agrees with the SCPT profiles, there are notable differences. Specifically, at the near-surface (i.e. depth less than 2 meters) the

SCPT V_S ranges from 60 to 100 m/s, while the DPCH velocities from 120 to150 m/. Soils with V_S less than 100 m/s are very soft. At the ground surface it would be difficult to walk on these materials and more difficult to maneuver the CPT rig and vehicles. No such difficulties were observed during testing. This difference at near-surface V_S may be attributed to difficulty in defining downhole travel paths at shallow depths. This is explored in further detail below, in the SCPT and DPCH velocity bias section.

3.3.2 St. Teresa's School – Complex Interlayered Silty Soils

The second example dataset was collected at the St. Teresa's School. The borehole log, cone tip resistance, and normalized soil behavior type index profiles are shown in Figure 3.7 (panels a, b, and c, respectively). While all identified as low-plasticity silts, the borehole log indicates several, smaller interlayers with different soil descriptions and distinct soil properties. The boundaries of these interlayers are indicated by grey dashed lines on the borehole profile. Both the q_C and I_C profiles reflect the changing soil stiffness and material behavior across these interlayered soils. The borehole was terminated at 15.65 meters in a silty soil. The cone tip resistance rapidly increases below 17 meters corresponding to a transition from the silty material into a stiff gravelly soil below 17.5 meters, as indicated by I_C.

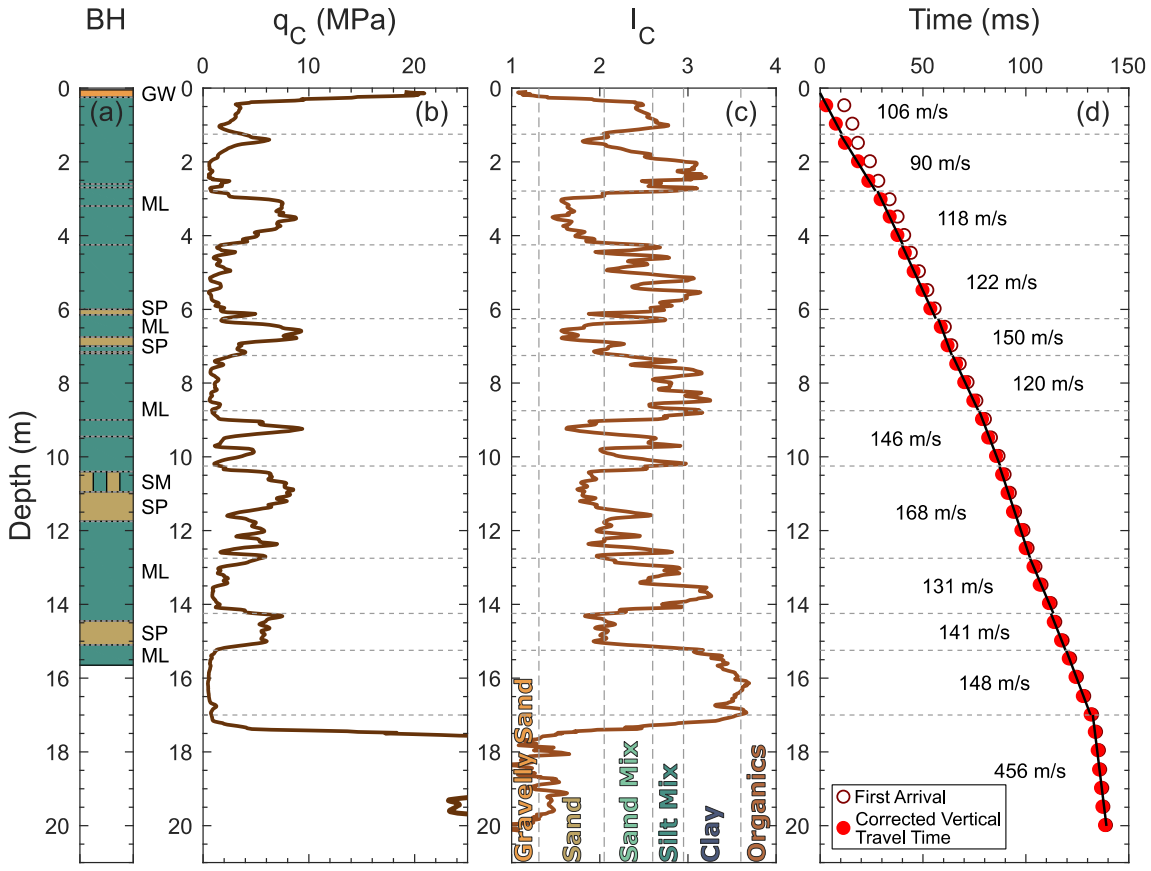

Figure 3.7: Slope-based SCPT V_S evaluation method for the St. Teresa's School dataset. Potential layer boundaries are defined based on supporting geotechnical data at the site including: (a) the continuous core sonic borehole log, (b) the raw cone tip resistance, q_C, and (c) the normalized soil behavior type, I_C. In panel (d), the shear wave first arrival (FA) times (hollow circular markers) have been corrected to vertical travel times (solid circular markers) using the SCPT testing geometry. Note that the correction is more pronounced in the near surface, with the apparent vertical travel time at the ground surface equal to zero. Linear slopes are fitted to vertical travel times to evaluate the associated V_S values of layers identified using the supporting geotechnical data.

The raw waveforms were processed and S-wave travel times (i.e., FA, PT, CO, and CC) were evaluated, as described above. Again, a true-interval cone was used testing and only the waveforms measured by the bottom geophone were used for PI velocity analysis. The layer boundaries for the SM were selected by identifying the trends in the cone data

and examining the fit slopes to the corrected vertical travel times, as shown in Figure 3.7d. In some cases, these layers are thin (i.e., 1.0 to 1.5 meters) relative to the half-meter spacing of the measured waveforms. In these layers, the slope velocities are evaluated using a linear fit to only two (or three) data points. If only two data points are used over a short distance, the slope of that line will be strongly influenced by any timing errors (e.g., measurement or picking errors) associated with either data point.

The PI, TI, and SM velocity analysis methods were used, by the authors, to develop a total of eleven V_S profiles, as shown in Figure 3.8 (panels a, b, and c, respectively). Additionally, the RT V_S profile developed by the independent CPT contractor from FA picks is shown in Figure 3.8d. Above 17 meters, the V_S of the interlayered silts and sands ranges between 80 and 150 m/s. However, the variability in any given set of V_S profiles is muted by the sharp increase in V_S at a depth of ~17 meters, associated with the transition into a gravel layer. The V_S of the gravel layer is not well constrained by the various velocity analyses, but typically ranges from 325 to 550 m/s.

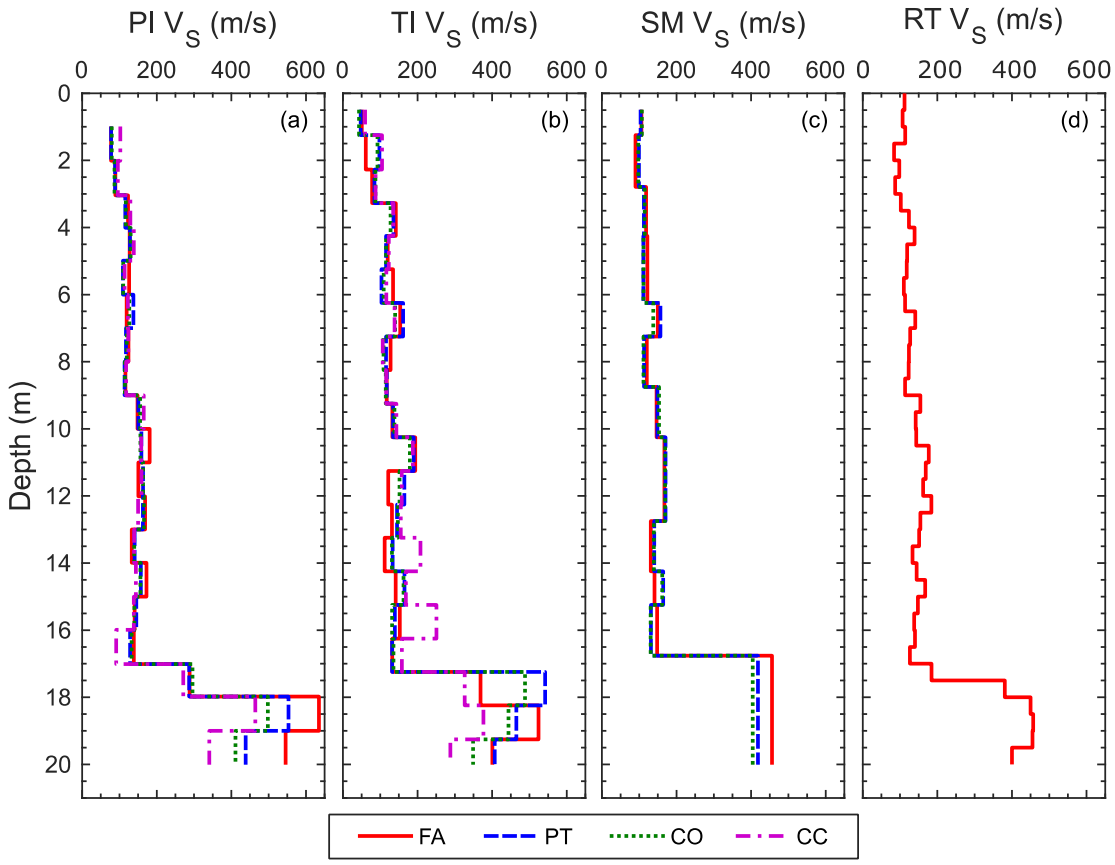

Figure 3.8: Comparison of SCPT V_S profiles developed for the St. Teresa's School dataset: (a) pseudo-interval (PI), (b) true-interval (TI), slope-based method (SM), and (d) raytracing (RT) V_S profiles were developed for the first arrivals (FA), peak/trough (PT), crossovers (CO), and peak cross-correlation (CC) delay times.

As observed at the previous site, the three SM profiles are generally stable with depth and velocity of individual layers are consistent, regardless of travel time (i.e., FA, PT, or CO). The V_S of the gravel layer is best constrained by the SM analysis, ranging from 400 to 450 m/s, as seven corrected vertical travel times are included in a single layer as defined by the q_C trend. At this site, many of the silts and sands layers above the gravel are thin, only two or three corrected travel times are included in the associated slope analysis.

The resulting SM V_S profiles moderately fluctuate layer-to-layer. However, as expected, the fluctuations in V_S are larger for the PI, TI, and RT VS profiles due the one- or half-meter thick layers. The V_S of the gravel layer is not well-constrained by the PI or TI analysis methods. Regardless of velocity analysis method, the PT and CO travel time VS profiles are generally consistent with each other, while the FA- and CC travel times occasionally result in localized outlier velocities.

As shown in Figure 3.9 for the St. Teresa's site, it is useful to view several V_S profiles developed using different velocity analysis methods plotted on top of each other and alongside supporting geotechnical data at the site (i.e., cone tip resistance in panel a). The V_S profiles shown in Figure 3.9b include: the PI, TI, and SM profiles determined from the PT arrival, and the RT profile developed by the independent CPT contractor using FA times. Viewed together, the V_S profiles capture the general trends in stiffness observed in the q_C profile. For example, local q_C peaks at approximately 7, 11, and 14.5 meters depth are reflected by slight increases in V_S. It bears repeating that any one of these V_S profiles (including those in Figure 3.8), may reasonably represent the single V_S profile provided by a SCPT contractor to an engineer. However, the epistemic uncertainty associated with the different travel time evaluation techniques and velocity analysis methods is rarely quantified or reported to the engineer.

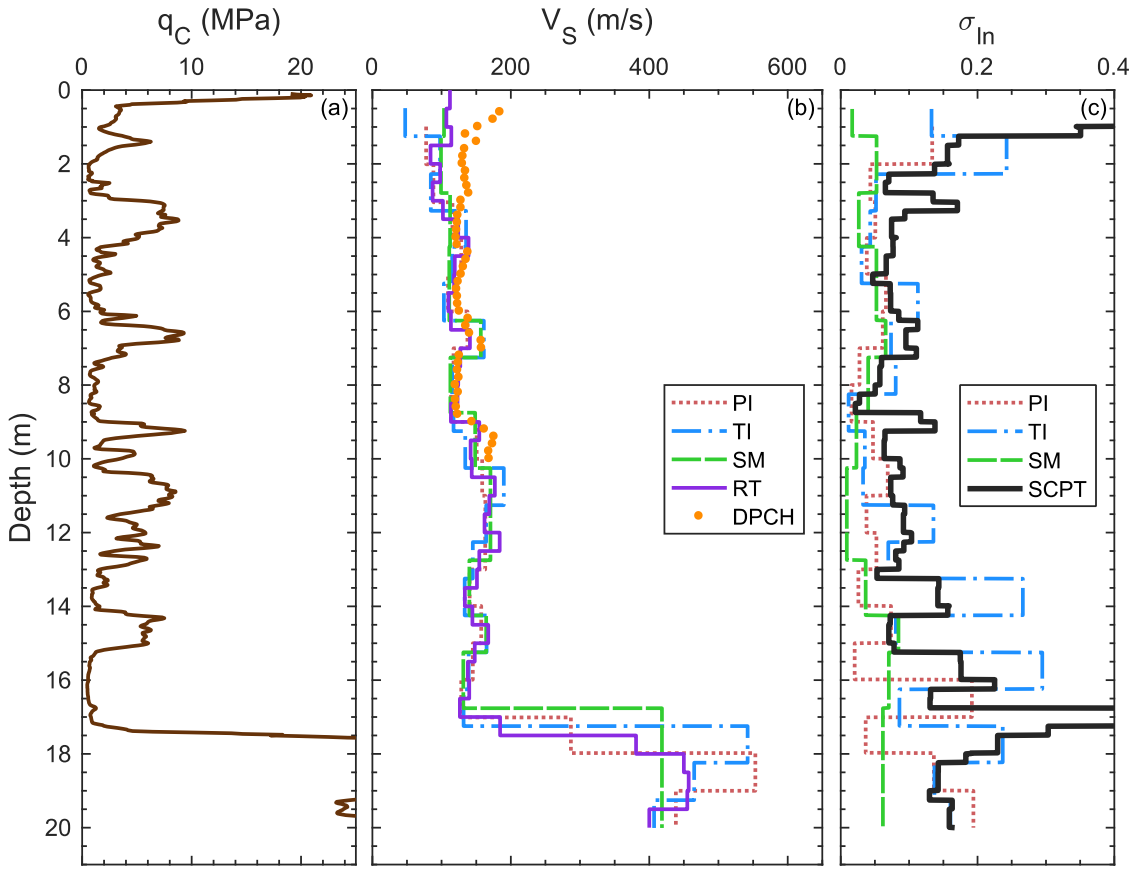

Figure 3.9: Summary of SCPT profiles for the St. Teresa's School dataset: (a) Corrected cone tip resistance (q_C), (b) Comparison of shear wave velocity profiles, including pseudo-interval (PI), true-interval (TI), slope method (SM) developed from peak/trough picks (PT); raytracing (RT) developed from first arrival (FA) picks; and a Vs profile from another invasive seismic method, direct-push crosshole (DPCH) seismic testing, (c) The log-normal standard deviation of Vs (σ_{lnVs}) within each SCPT V_S analysis method (i.e., PI, TI, and SM) and between all SCPT methods.

The epistemic uncertainties associated with all twelve of the St. Teresa's site SCPT V_S profiles are quantified in Figure 3.9c in terms of the log-normal standard deviation of V_S (σ_{lnVs}), as described above for the previous site. Also, the intra-analysis-method σ_{lnVs} was evaluated as a function of depth for each of the three V_S analysis methods (PI, TI, and

SM). For example, the σ_{lnVs} of the four PI V_S profiles shown in Figure 3.8a is indicated by the dotted line in Figure 3.9c.

The lowest intra-analysis-method σ_{lnVs} is again associated with the slope-based method, which is expected given the high level of consistency between each of the three SM V_S profiles layer-to-layer. The reduced consistency between individual PI or TI V_S profiles and the increased fluctuations in V_S layer-to-layer are reflected by elevated σ_{lnVs} values associated with the PI and TI analysis methods. Of three different intra-analysis-method σ_{lnVs} considered, the highest σ_{lnVs} values are those associated with four spikes in TI σ_{lnVs}. Each of these spikes is associated with a clear single outlier velocity in an individual layer. The outlier velocity is associated with either the CC or FA travel time.

At the St. Teresa's site, the σ_{lnVs} associated with all twelve SCPT V_S profiles is generally higher than those at the Avondale Playground site. This expected due to (1) the difficulty in resolving the boundaries between thin layers with seismic measurements taken once every half meter and (2) the fluctuating stiffness of these layers reflected in the q_C profile. The σ_{lnVs} typically ranges between 0.05 and 0.20 (i.e., less than a 20% COV). However, σ_{lnVs} exceeds 0.4, indicating a high level of epistemic uncertainty, at two depth ranges: (1) in the 1.5 meters of the profile, where straight-line travel path assumption breaks down and (2) from 17 to 17.5 meters, where the depth to the top of the gravel layer is uncertain and the associated V_S is not well constrained. Again, this analysis represents a realistic, quantitative, depth-dependent evaluation of the epistemic uncertainty associated with SCPT V_S profiles developed at this site.

To qualitatively highlight the epistemic uncertainty associated with use of two different direct-push, invasive seismic methods, a single V_S profile obtained via DPCH testing is shown Figure 3.9b with four of the SCPT V_S profiles. At depths greater than 3 meters, the DPCH and SCPT velocity profiles agree remarkably well, capturing the same localized changes in V_S across the interlayered soils. However, at the near-surface (depth less than 3 meters), the DPCH velocities are 30 to 60 m/s faster than the associated SCPT velocities. This is consistent with the near-surface velocity bias observed at the Avondale Playground site and is discussed in further detail in the following section.

3.3.3 SCPT and DPCH Velocity Bias

The Avondale Playground and St. Teresa's School are two of the 31 sites in Christchurch with complete sonic borehole logs, SCPT soundings, and DPCH tests with data typically collected down to 10 meters. The SCPT data at the 31 sites was collected and analyzed by the CPT contractor, producing a V_S profile developed using the FMDSM raytracing algorithm. As shown in Figures. 3.6 and 3.9, despite velocity fluctuations associated with the relatively thin layering, the RT V_S profiles agree well with the other SCPT V_S profiles and therefore may be used as a representative SCPT V_S profile for comparison purposes instead of reprocessing the entire SCPT dataset.

The DPCH testing method is the direct-push equivalent of conventional, borehole-based crosshole seismic testing (ASTM D4428/D4428M-14) and is well-documented in Chapter 2. Testing is conducted by advancing a pair of instrumented cone directly into the ground to common measurement depths, using CPT-type rigs and push rods. At each

measurement depth, seismic waves are propagated from one cone (the source) to the other (the receiver) along a horizontal travel path. The travel time of the S- and/or P-waves and the distance between the cones (as determined by a tilt measurements) are used to evaluate the V_S and/or V_P at each measurement depth.

The SCPT RT and DPCH V_S profiles were compared to evaluate any potential bias associated with the use of either method. The percent difference between the two V_S profiles for each of the 31 sites, indicated by the cloud of thin grey lines in Figure 3.10. The median percent difference (bold black line) is greater than 60% at depths less than 1 meter below the ground surface. Over the 1 to 3 meter depth range, the median percent difference decreases and remains stable at approximately 15% at depths below the ground surface greater than 3 meters. This general trend is consistent with observations at the two example sites, where the DPCH V_S is 50 to 100 m/s greater than the SCPT velocities at the near-surface.

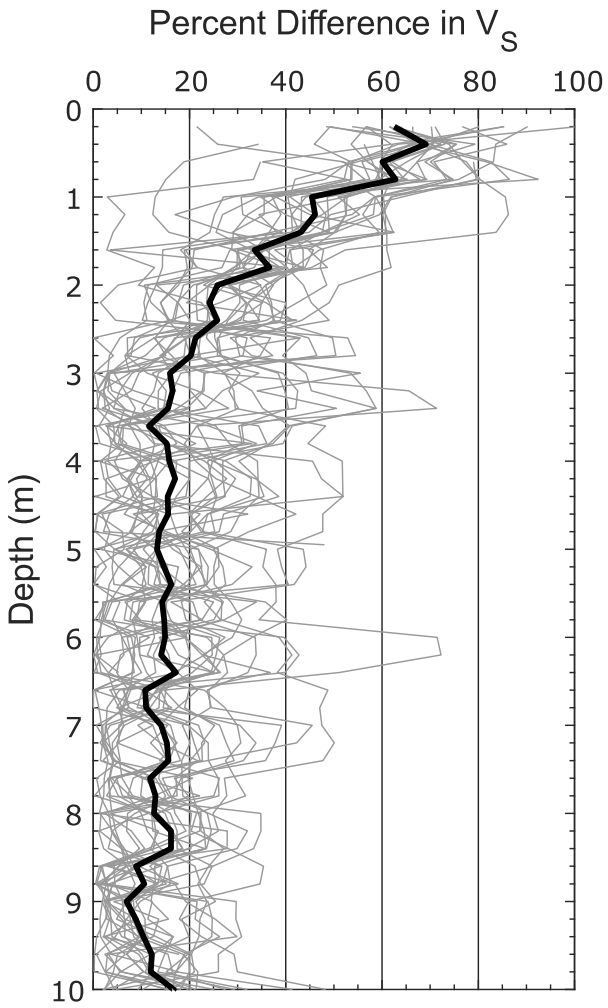

Figure 3.10: Percent difference in V_S as determined from SCPT raytracing and DPCH at 31 sites across Christchurch, New Zealand. The 31 percent difference profiles are indicated by the thin, grey lines and the median percent difference is indicated by the bold, black line.

3.4 CONCLUSIONS

A dataset was developed consisting of 31 soil liquefaction case history sites in Christchurch, New Zealand. At each site, the geotechnical site investigation included the following: (1) continuous disturbed soil sampling from sonic-drilling, (2) a SCPT sounding

collected and initially processed by a well-regarded, independent CPT contractor, and (3) DPCH testing conducted by the authors. At two of the thirty-one sites, the SCPT data was reprocessed using analysis methods representative of those commonly used in geotechnical practice. The travel time techniques considered include the first arrival, peak/trough, and crossover picks and the time delay associated with the peak response of the cross correlation function between pairs of waveforms. The velocity analysis methods include pseudo-interval, true-interval, and corrected vertical travel time slope-based method. Using all possible combinations of travel time and velocity analysis methods, eleven SCPT V_S profiles have been developed for each site. An additional twelfth V_S profile was developed by the independent CPT contractor using first arrival picks and a raytracing algorithm.

The epistemic uncertainty associated with the different travel time and velocity analysis methods has been quantified through the evaluation of the log-normal standard deviation of V_S for (a) each of the velocity analysis methods (i.e., PI, TI, and SM) to capture the intra-velocity-analysis-method uncertainty associated with consideration of different travel times (i.e., FA, PT, CO, and CC) and (b) all twelve of the SCPT V_S profiles together. At the first site, with a relatively simple near-surface soil profile, the σ_{lnVs} never exceeds 0.2 and is typically less than 0.1. The soil profile at the second site consists of interlayered sands and silts. The thin layering and the corresponding fluctuations in soil stiffness results in increased uncertainty in the SCPT profiles, reflected by a corresponding increase in $\sigma_{lnVs.}$ At his second site, the σ_{lnVs} typically ranges between 0.05 and 0.2, with σ_{lnVs} values above 0.4 at depths where layer boundaries and the associated shear-wave velocities are poorly constrained. At both of these sites, the σ_{lnVs} represent a realistic, depth-dependent

quantification of the epistemic uncertainty associated with V_S profiles obtained via SCPT testing.

Furthermore, the epistemic uncertainty associated with the use of different invasive seismic testing methods has been examined through a comparison of the SCPT raytracing and DPCH VS profiles developed at each of the 31 case history sites. At the near-surface (i.e., depth < 3 m), the SCP_T VS profiles are biased towards lower velocities and the median percent difference between the SCPT RT and DPCH V_S profiles is 60%. Below 3 meters, the two sets of V_S profiles generally agree with percent differences, on average, less than 15%.

Given these results and those presented in the literature (Garofalo et al. 2016, Styler, M.A. and Weemees 2017), it is important to note that there is epistemic uncertainty associated with the development V_S profiles from SCPT testing, indeed from any invasive seismic testing method. In practice, it is common for an SCPT contractor to provide a single V_S profile to the engineer, with no indication of the associated uncertainty. While in many cases this single V_S profile may be sufficient for engineering purposes, the engineer should always be informed of the assumptions and analysis methods used in the development of this profile. Furthermore, the SCPT picked travel times should be indicated directly on the measured waveforms in a waterfall style plot and provided in a table, such that the engineer could reprocess the data, as needed, using other analysis methods, such as the corrected-vertical travel time slope-based method.

As engineering practice moves from deterministic to probabilistic analyses, a meaningful, realistic assessment of the uncertainty with seismic measurements is needed.

The process developed in this paper, through the consideration of several analysis methods to evaluate V_S obtained via SCPT, profiles a suitable means to quantify the epistemic uncertainty associated with these V_S profiles. Even at a complex, interlayered soil site (e.g., the St. Teresa's site) the depth-dependent σ_{lnVs} typically ranges between 0.05 and 0.20. At depths where layer boundaries are poorly resolved and/or V_S is poorly constrained by the analysis methods, the uncertainty is realistically captured by a corresponding increase in σ_{lnVs}. This process provides: (1) several "real" V_S profiles, developed from measurements in situ, which can be used directly in the engineering analysis, and (2) a realistic assessment of epistemic uncertainty that varies with depth and better reflects the uncertainty in the measurements than the commonly assumed depth-independent constant coefficient of variations.

3.5 ACKNOWLEDGEMENTS

This work was partially supported by U.S. National Science Foundation (NSF) grant CMMI-1547777. However, any opinions, findings, conclusions, or recommendations expressed in this material are those of the authors and do not necessarily reflect the views of NSF.

Financial support was also provided by the New Zealand Earthquake Commission (EQC) under the Capability Building Fund at the University of Auckland and QuakeCoRE through Technology Platform 2.

Chapter 4: Feasibility of in-situ evaluation of soil void ratio using high resolution measurements of V_S and V_P from DPCH testing

Andrew C. Stolte and Brady R. Cox

This chapter contains a journal article that is in preparation. The full citation is listed below:

Stolte, A. C., and Cox, B. R, (2018). "Feasibility of in-situ evaluation of soil void ratio using high resolution measurements of V_S and V_P from DPCH testing". Manuscript in preparation.

As first author, I was responsible for approximately 50% of the concept development, 100% of the data processing, and 50% of the results interpretation.

ABSTRACT

The density (i.e., compactness) of the solid soil particles is often expressed in terms of void ratio or porosity and through critical state soil mechanics is important to the understanding of behavior, e.g., soil compressibility, permeability, shear strength. Typically, the in-situ void ratio is evaluated based on laboratory measurements on high-quality, "undisturbed" samples of soil. While "undisturbed" sampling of clayey soils is commonplace in geotechnical practice, high-quality samples of granular soils are difficult and expensive to obtain. Hence, in-situ void ratio is typically estimated using relative density empirical relationships to in-situ measurements from penetration testing (e.g., CPT) and laboratory measurements of the minimum and maximum void ratio. CPT-based relationships are typically developed based on calibration chamber testing on reconstituted clean sands. Void ratios relationships with strong theoretical underpinnings are needed for application to a wider range of soils. The theory of linear poroelasticity (Biot 1956a and

1956b) describes the propagation of seismic waves (i.e., P- and S-waves) through fluid-saturated porous materials (e.g., fully-saturated soils). Foti et al. (2002) used this theoretical framework to develop a relationship to evaluate soil porosity (i.e., void ratio) from seismic wave propagation velocities (i.e., V_P and V_S). Soil porosity is evaluated as a function of V_P, V_S, and four additional parameters describing the physical properties of the soil (i.e., the Poisson's ratio of the soil skeleton, the bulk modulus and mass density of water, and the mass density of the solid soil particles). V_S and V_P are measured in situ using seismic testing methods. Specifically, invasive techniques (e.g., crosshole seismic testing) are well-suited to the development of V_P and V_S profiles for porosity estimates. In this study, the effectiveness and feasibility of using high-resolution V_S and V_P measurements from direct-push crosshole (DPCH) testing to estimate in-situ void ratios is investigated at ten, predominantly clean sand case history sites in Christchurch, New Zealand.

4.1 INTRODUCTION

The evaluation of in-situ soil volumetric state (e.g., density) is fundamental to understanding the compressibility, permeability, and shear strength of soils. The volumetric state of soil is often expressed in terms of parameters such as porosity (n), void ratio (e), or relative density (D_r). These parameters are employed as a means to describe the density or compactness of the soil, and are often used directly in engineering analyses. For example, porosity is used to estimate the flow of water through soil and rock, void ratio is used in consolidation settlement analyses and critical state soil mechanics, and relative density is a key parameter in soil liquefaction analyses.

Volumetric state parameters are defined by considering that soil is a multi-phase porous material consisting of solid particles and void space, which is filled with fluid and/or gas. Soil porosity is defined as the ratio of the volume of the void space relative to the total volume of the soil mass (void space plus solid particles), and theoretically ranges between zero and one. Soil void ratio is defined as the volume of the void space relative to the volume of the solid particles, and theoretically ranges between zero and infinity. The porosity and void ratio may be used interchangeably and are directly related through the following equation:

$$e = \frac{n}{1-n} \tag{4.1}$$

Despite having simple definitions, n and e are difficult to evaluate in situ. Typically, in-situ void ratio is evaluated from high-quality, "undisturbed" soil samples collected in the field and carefully transported to the laboratory. High-quality sampling of most clayey soils is achievable and relatively inexpensive for use in geotechnical engineering practice. Hence, it is reasonable to develop good estimates of in-situ void ratio by carefully sampling the soil and obtaining weight-volume measurements in the lab. On the other hand, undisturbed sampling of granular materials, like clean sands and non-plastic silts, are extremely difficult and expensive, as these soils easily densify or completely lose their structure during sampling. Complex sampling techniques (e.g., soil freezing and gel-push sampling) can be used to obtain high-quality samples in some granular soils, but require a level of expertise and attention to detail that is beyond standard geotechnical practice. These methods are typically reserved for high-end, critical facilities or research purposes.

As it is difficult to obtain sufficiently high-quality samples of granular materials, evaluation of in-situ void ratio from laboratory measurements is rare. However, laboratory testing is commonly performed on reconstituted/prepared granular soil samples. While the important effects of aging, cementation, fabric, etc. are lost in the disturbed sampling and specimen preparation process, laboratory tests on reconstituted samples provide insight into the strength and compressibility of these soils relative to their volumetric state. The relative density (D_r) parameter is used to describe of the compactness of a soil sample relative to its "loosest" (e_{max}) and "densest" (e_{min}) possible void ratios, as defined in the following equation:

$$D_r = \frac{e_{max} - e}{e_{max} - e_{min}} \tag{4.2}$$

Both e_{min} and e_{max} are evaluated from laboratory weight-volume measurements of carefully prepared granular soil samples using a variety of techniques, including ASTM Standards D4254-16 and D4253-16. However, it is inherently difficult to consistently achieve either state. Any vibration or perturbation serves to collapse soils arranged in a loose state, hence making evaluation of e_{max} difficult. Conversely, friction between solid soil particles coupled with variable particle shapes and local particle gradations make determination of "maximum" soil densification and e_{min} challenging. Therefore, achieving consistent estimates of e_{min} and e_{max} for a given granular soil is inherently difficult and strongly dependent on the care and abilities of the technician. These challenges are carried through to any evaluation of relative density.

Given these difficulties, in-situ relative density is often estimated using empirical relationships to measurements from field penetration testing methods, such as the standard

penetration test (SPT, ASTM D1586-11) and cone penetration test (CPT, ASTM D5778-12). Since its introduction in 1902, the SPT method has been widely used to investigate in-situ properties of soils for geotechnical engineering purposes. The primary result of SPT testing is N, the number of blows required to advance a split-spoon sampler a foot into soil. The blow count, N, requires subsequent correction for hammer energy and overburden pressure, among other things. Kulhawy and Mayne (1990) provide an overview of various correlations of D_r to both uncorrected and corrected SPT blow counts. First introduced in 1932, the CPT has been used more frequently for geotechnical engineering purposes over the past three decades (Robertson and Cabal 2015). The cone tip resistance (q_C), sleeve friction (f_S), and pore water pressure developed at the u_2 location are measured nearly continuously (less than every 20 mm) as the cone is advanced into the ground. Various empirical relationships have also been developed to evaluate the relative density of granular soils (typically, clean sands) based on CPT measurements (Baldi et al. 1986, Kulhawy and Mayne 1990, Salgado et al. 1997, Jamiolkowski et al. 2001, and Salgado and Prezzi 2007). While these relative density empirical relationships are limited to specific soil types (e.g., quartz-based clean sands for many CPT relationships), they provide a means to evaluate the compactness of soils in situ. Furthermore, if consistent values of e_{min} and e_{max} are available from laboratory testing, these relative density empirical relationships may be used to estimate in-situ void ratio of granular soils, according to Equation 4.2.

Empirical relationships between in-situ penetration testing measurements and relative density provide a means to estimate in-situ porosity and void ratio. However,

alternative relationships based on in-situ seismic wave velocity measurements have also been developed. Invasive seismic techniques such as crosshole (CH) seismic testing (ASTM D4428/D4428M-14) are well-suited to develop high-quality measurements of constrained compression wave (i.e., P-wave) and shear wave (i.e., S-wave) propagation velocities (V_P and V_S, respectively). The use of V_P and V_S measurements to evaluate in-situ porosity was first considered in the petroleum industry, focusing on porous rock (e.g., sandstone) and very-dense or cemented granular soils. Wyllie et al. (1956) conducted laboratory testing on various fluid-saturated, porous-media with measured porosities. They developed the concept of a time-averaged velocity based on the V_P of the solid grains (e.g., soil particles) and the V_P of the fluid in the voids (e.g., water or oil). This time-averaged velocity provides a lower-limit bound on the P-wave velocity of the composite, porous material. As field data acquisition systems improved and seismic testing methods were more widely adopted in practice, researchers in the 1980's developed empirical relationships to evaluate the porosity of rock and dense granular soil based on laboratory measurements of V_S and V_P (Raymer et al. 1980 and Domenico 1984). Later, empirical relationships considered the effects of clay content in the voids (Castagna et al. 1985 and Han et al. 1986) and the effects of confining pressure (Ederhart-Phillips et al. 1989). Using the theory of linear poroelasticty (Biot 1956a and 1956b) as a theoretical underpinning, coupled with the Raymer et al. 1980 empirical relationship, Krief et al. (1990) developed a semi-empirical relationship for porosity that better fit experimental measurements.

The theory of linear poroelasticity provides a framework to describe the propagation of small-strain stress waves through fluid-saturated, porous materials (e.g.,

soils) at low (Biot 1956a) and high (Biot 1956b) excitation frequencies. These materials are modeled by the super-positon of the fluid and solid phases occupying the same physical space. The propagation of three different stress waves (two dilatational and one rotational) were described based on the physical properties of both the porous material and the saturating fluid. The dilatational (i.e., compression) wave of the first kind and rotational (i.e., shear) wave are P- and S-waves, respectively, commonly measured using seismic testing methods. The dilatational wave of the second kind arrives after the P-wave and is difficult to observe experimentally. Biot made the following assumptions in the development of this framework: (1) The material consists of an isotropic, linear elastic, porous solid saturated by a non-dissipative, compressible fluid. (2) The stress waves are propagated through the material in undrained conditions with no relative movement between the fluid and solid phase. Miura et al. (2001) have shown this assumption is valid a low frequencies, with an upper limit at the characteristic frequency (ω_C) of the soil, as defined by the following equation:

$$\omega_C = \frac{ng}{k} \tag{4.3}$$

where g is the acceleration due to gravity and k is the hydraulic conductivity of the material. The characteristic frequency of a clean, loose sand is approximately 7 kHz, which is well above the frequencies excited during most in-situ seismic testing used for geotechnical purposes. (3) The dilatational and rotational motions induced by stress waves are uncoupled, allowing the derivation of independent wave equations describing the propagation of P- and S-waves. (4) The saturating fluid is unable to sustain shear, therefore,

the small-strain shear modulus of the fluid-saturated, porous material is simply that of the porous solid.

Using Biot's low-frequency framework, Foti et al. (2002) derived a relationship that can be used to estimate soil porosity based on experimentally measured stress wave propagation velocities (i.e., V_P and V_S) and the physical properties of the soil, including the mass density (ρ_W) and bulk modulus (K_W) of water, the mass density (ρ_S) and bulk modulus (K_S) of the solid soil particles, and the Poisson's ratio of the soil skeleton (v_{SK}). By using typical values for many of the parameters, which can be reasonably assumed in most cases, the relationship may be iteratively solved to evaluate porosity using measurements of V_S and V_P. If the soil particles are assumed to be incompressible (i.e., K_S approaches infinity), which is a reasonable assumption, then the relationship simplifies to a closed-form quadratic equation. By constraining porosity to realistic values (i.e., $0 \leq n \leq 1$) the quadratic equation may be solved to directly evaluate porosity:

$$n = \frac{\rho_S - \sqrt{(\rho_S)^2 - \frac{4(\rho_S - \rho_W)K_W}{V_P^2 - 2\left(\frac{1-v_{SK}}{1-2v_{SK}}\right)V_S^2}}}{2(\rho_S - \rho_W)} \tag{4.4}$$

The Foti et al. (2002) relationship has been used to estimate in-situ porosity (and void ratio) at several case history sites with mixed levels of success, as evaluated through comparisons to laboratory porosity measurements on high-quality soil samples. Foti and Lancellota (2004) considered seven case histories at sites with high-quality sampling of clays. Laboratory measurements were compared to seismic-based porosity estimates from downhole (DH) testing at six of the sites and crosshole (CH) testing at the other. On average, the percent difference in porosity was less than 10% across all seven sites, with

some percent differences as large as 30%. Lai and Crempien (2012) numerically examined the validity of the relationship over wide ranges of V_P, V_S, and ν_{SK} values and found that the relationship produces non-real valued porosity estimates when V_P is less than ~1,450 m/s. They also developed porosity estimates for a single case history site using CH testing and high-quality sampling of silty sands with moderate clay content. They qualitatively described the porosity comparison as satisfactory, however, the seismic-based estimates generally under predicted the laboratory measurements. Foti and Passeri (2016) used a numerical sensitivity study to examine how errors in seismic measurements and parameter assumptions affect the porosity estimates. Errors in the measurement of V_P were found to produce the largest errors in the porosity estimates. Jamilkowski (2012) considered five case history sites with high-quality, undisturbed samples of a variety soils, including clays, sands, silty sands, and mine tailings. At each of these sites, CH measurements of V_S and V_P were used to develop profiles of in-situ porosity. The seismic-based estimates of porosity/void ratio generally ranged from 10 to 15% different than the lab measurements, and at one clay site the seismic estimates under predicted porosity/void ratio consistently by 30 to 50%. Jamilkowski (2012) concludes that in-situ evaluation of porosity via seismic measurements shows promise, but that obtaining realistic results depends on the ability to make very accurate measurements of V_S and V_P. He further notes that CH seismic measurements are best suited for this purpose, however, improvements are needed in order to more precisely determine wave travel time and evaluate wave travel path before seismic-based estimates of porosity/void ratio can be used in advanced geotechnical analyses.

The greatest advantages of CH seismic testing are: (1) maintaining a relatively consistent and short wave travel path, (2) preserving a strong signal-to-noise ratio as a function of depth, and (3) predominantly propagating waves through a single layer at each measurement depth. However, conventional CH testing requires drilling and casing two or three boreholes in close proximity to each other, an expense not justifiable for many geotechnical site characterization efforts. Furthermore, the soil can be disturbed significantly by drilling the boreholes and grouting the casings in place. To overcome both of these challenges, a direct-push crosshole (DPCH) testing method has been developed which combines the desirable aspects of CH testing (i.e., the high-quality measurements of V_S and V_P) with the benefits of direct-push testing methods, such as cone penetration testing as detailed in Chapter 2. DPCH testing is conducted by pushing instrumented cones into the ground using two CPT-type rigs spaced 1.5 to 2.5 m apart. Typically, seismic measurements are taken every 0.2 to 0.5 m, resulting in V_S and V_P profiles with high-spatial resolution. The direct advancement of seismic instrumentation into the ground causes less disturbance and provides excellent coupling, ensuring the best possible measurement of seismic waves. Furthermore, the deviation/position of each instrumented cone may be tracked during testing, increasing confidence in the evaluation of the length of the wave travel path between cones. DPCH testing is significantly less expensive than traditional CH testing and is well suited for soft, near-surface (top 20 to 30 m) soils.

The use of DPCH testing accelerated greatly in the aftermath of the 2010-2011 Canterbury Earthquake Sequence, which caused unprecedented soil liquefaction damage to the city of Christchurch, New Zealand. Following these earthquakes, an extensive study

was initiated to investigate the effectiveness of various shallow ground improvement methods at mitigating soil liquefaction damage to residential structures (Van Ballegooy et al. 2015, Wentz et al. 2015). DPCH testing played a key role in these ground improvement trails (Stokoe et al. 2014, Wotherspoon et al. 2015, Stokoe et al. 2016, Wotherspoon et al. 2017, Hwang et al. 2017), allowing for measurements of V_P and V_S at high spatial resolution in the unimproved soils, in the zones of improved soil between ground improvements, and directly across ground improvement elements. Following the ground improvement trials, DPCH testing was conducted at 31 additional sites in Christchurch to contribute high-resolution profiles of V_P and V_S at key liquefaction/no-liquefaction case history sites (McLaughlin 2017). Both the V_P and the V_S profiles played important roles in attempting to rectify a number of false-positive liquefaction case histories predicted by CPT-based simplified liquefaction triggering analyses (Cox et al. 2017). Some of these 31 DPCH case history sites are considered herein for estimating in-situ void ratio.

The effectiveness and limitations of using high-quality in-situ measurements of V_S and V_P from DPCH testing to evaluate in-situ void ratio are critically examined in this paper. First, the sensitivity of the Foti et al. (2002) relationship to measured and assumed input parameters (e.g., V_P, V_S, ρ_W, K_W ρ_S, K_S, and v_{SK}) is evaluated through a simple parametric study applicable to soft, near-surface (top 20-30 m) soils. Then, the in-situ evaluation of void ratio of granular soils is further examined through consideration of case history sites in Christchurch, New Zealand, including ten of the 31 sites with DPCH testing mentioned above. A comparison of in-situ granular soil void ratios is developed from the following: (1) laboratory void ratio measurements on high-quality samples, (2) in-situ void

ratio estimates from several CPT-based relative density empirical relationships and laboratory measurements of e_{min} and e_{max}, and (3) seismic-based estimates of in-situ void ratio using high-quality, high-resolution profiles of V_P and V_S from DPCH testing in conjunction with the Foti et al. (2002) relationship.

4.2 PARAMETRIC STUDY

The Foti et al. (2002) porosity relationship (see Equation 4.4) is a function of six parameters: V_P, V_S, v_{SK}, ρ_W, K_W, and ρ_S. In soft soils, the measured V_P is a function of the solid soil particle skeleton stiffness and the compressional stiffness of the pore fluid. At low degrees of saturation (e.g., less than ~98%), gas in the pore spaces limits the transmission of P-waves, such that the measured V_P is largely controlled by the compressional stiffness of, and the contacts between, the solid soil particles. As the soil transitions from nearly- to fully-saturated (~98% to 100%), the V_P steadily increases to, and ultimately exceeds, the P-wave velocity of water, approximately 1,500 m/s (Tamura et al. 2002, Valle-Molina 2006, Valle-Molina and Stokoe 2012). P-wave velocities exceeding 1,500 m/s are used as a screening tool to identify fully-saturated soils both in the laboratory and field. This is quite useful, as the theory of linear poroelasticity, and thus the Foti et al. (2002) porosity relationship, was derived for fully-saturated soils. On the other hand, the V_S of soils is only dependent on the shear stiffness of, and interactions between, the solid soil particles, because water cannot sustain shear stress. Based on a large number of DPCH case histories in the soft, near-surface soils of Christchurch, we have found that V_P for fully saturated soils typically ranges from 1,500 to 2,000 m/s (increasing with soil skeleton

compressional stiffness) and V_S typically ranges from 100 to 300 m/s (increasing with soil skeleton shear stiffness). These typical ranges are used in the void ratio parametric study developed below.

It is also important to consider typical ranges for each of the other parameters (i.e., v_{SK}, ρ_W, K_W, and ρ_S) and understand how assumed values may influence the evaluation of soil void ratio/porosity. The mass density and bulk modulus of fresh water are directly related to water temperature (T_W). Therefore, our void ratio sensitivity analysis will focus on only three additional parameters: (a) v_{SK}, (b) T_W, and (c) ρ_S.

The Poisson's ratio of the evacuated soil skeleton (i.e., the drained Poisson's ratio) has been studied in the laboratory using granular soil specimens prepared and tested under varying conditions (e.g., ranges of confining pressures, relative densities, and grain size distributions). As confining pressure on the soil increases, the v_{SK} has been shown to decrease. (Bates 1989, Nakagawa et al. 1997). Kumar and Madhusudhan (2010) found that v_{SK} decreases with increasing relative density (i.e., decreasing void ratio). Wichtmann and Triantafyllidis (2010) noted that the Poisson's ratio of the soil skeleton is dependent on the grain size distribution of the soil, specifically v_{SK} decreases as the coefficient of uniformity increases. Given the range of soils and testing conditions considered in the literature, v_{SK} typically ranges from 0.15 to 0.35 for granular soils.

The properties of the saturating fluid (i.e., water) are represented by two parameters, the mass density and the bulk modulus. For simple purposes, typical values may be assumed for both parameters: approximately 1,000 kg/m^3 for ρ_W and 2.15 GPa for K_W. However, ρ_W and K_W are both a function of both temperature and pressure (Wagner

and Pruß 2002). The temperature of the earth is relatively stable beneath the immediate ground surface. A study considering data at 63 stations across the continental USA found that, at depths between 1 and 3 meters, the temperature of the ground typically ranges between 10 and 18 °C (Kusuda and Achenbach 1965). During field testing, a thermometer lowered down a borehole or CPT sounding hole may be used to directly measure the ground water temperature. This is recommended to limit one source of uncertainty when estimating porosity. At atmospheric pressure, Kell (1975) developed a relationship between water temperature and mass density. Using this relationship the density of water ranges from 999.7 to 998.6 kg/m^3 (i.e., 0.1% change) over the 10-18 °C temperature range for near-surface soils. The effects of temperature on the compressibility of water should also be considered. The constrained-compression modulus (M_W) and the bulk modulus (K_W) of water are equal, because water cannot sustain shear. At small-strains, the bulk modulus may be expressed as a function of the acoustic wave (i.e., P-wave) velocity of water:

$$K_W = M_W = \rho_W \left(V_{P,W}\right)^2 \tag{4.5}$$

The P-wave velocity of water also varies with temperature (Lubbers and Graaff 1998). Over the typical ground temperature range (i.e., 10-18 °C), the P-wave velocity of water increases from 1447.4 m/s to 1475.9 m/s, corresponding to an increase in bulk modulus from 2.09 to 2.17 GPa (a 3.8% difference). Both the bulk modulus and density of fresh water are directly related to the temperature of water. To simplify parametric study, the sensitivity of void ratio estimates to K_W and ρ_W will be considered together by changing only the single parameter, T_W, over the range from 10 to 18 °C.

The last parameter to consider is the mass density of solid soil particles, which is typically expressed relative to the mass density of water using specific gravity, G_S. While the G_S of soil particles is relatively simple to evaluate in the laboratory, it typically takes on a narrow range of values that is dependent on mineralogy. The specific gravity of granular soils is typically assumed to be 2.65 (i.e., the G_S of quartz/silica), but may vary between 2.6 and 2.75 depending on the specific mineralogy of the soil particles. The specific gravity of clay minerals is higher, ranging between 2.65 and 2.85 (Lambe and Whitman, 1967). To capture the range of G_S for granular soils (e.g., sand and silts) and allow the inclusion of some clay minerals, a range of G_S between 2.6 and 2.8 should be considered. Thus, if ρ_W is approximately 1,000 kg/m^3, the corresponding ρ_S varies between 2,600 and 2,800 kg/m^3.

The sensitivity of the Foti et al. (2002) porosity relationship to v_{SK}, T_W, and ρ_S is evaluated over the reasonable range of values developed above: (a) $v_{SK} = 0.25 \pm 0.10$, (b) $T_W = 14 \pm 4$ °C, and (c) $\rho_S = 2{,}700 \pm 100$ kg/m^3. For each analysis, one parameter is varied and the other two are held constant at the median value. Figure 4.1 shows the void ratio as evaluated over the typical range of S-wave velocities for soft soils (e.g., Vs = 100 to 300 m/s), while P-wave velocity is held constant at one of six values ranging from 1500 to 2000 m/s, as indicated by line type. The sensitivity of the void ratio relationship to the parameter of interest (e.g., v_{SK} in Figure 4.1a) is indicated by the line (i.e., the median value) and the associated shaded area (i.e., the range of values considered).

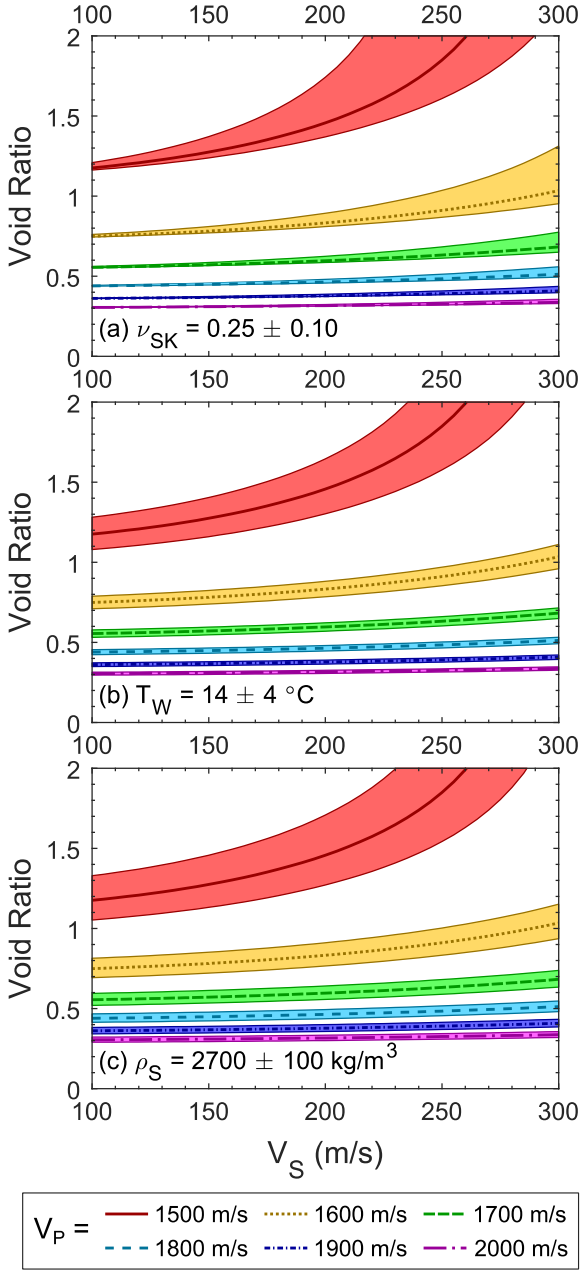

Figure 4.1: Sensitivity analysis of void ratio estimates based on typical values of V_S and V_P for soils relative to typical ranges in: (a) Poisson's ratio of the soil skeleton [ν_{sk}], 0.25 ± 0.15, (b) pore-water temperature [T_w], 14 ± 4 °C, and (c) mass density of the solid soil particles [ρ_s], 2,700 ± 100 kg/m^3. Each line and shaded area indicate the median value and bound limits, respectively, of the parameter varied in the sensitivity analysis. The void ratio is evaluated for six constant values of V_P, as indicated by line type.

The following may be observed from Figure 4.1: (1) Void ratio is most strongly controlled by P-wave velocity. As V_P increases, the void ratio decreases and the influence of other parameters is significantly reduced, as expressed by the decreasing width of the void ratio ranges. This is best visualized in Figure 4.1 by observing how the ranges in void ratio collapse together for V_P values greater than 1,700 m/s. (2) The sensitivity of void ratio to changes in the Poisson's ratio of the soil skeleton is dependent on V_S (refer to Figure 4.1a). At low V_S values the range of void ratios is narrow, while the range in void ratio values broadens at higher V_S values. In Equation 4.4, the v_{SK} term acts as a scaling factor for the square of V_S, explaining this behavior. (3) The void ratio is less sensitive to changes in either water temperature or solid soil particle density. However, care must be taken when assuming typical values. At V_P greater than or equal to 1,600 m/s, simply assuming the median water temperature (i.e., 14 °C) yields up to an 8% error in void ratio if the in-situ T_W is at the edge of the typical range. Similarly, assuming the median solid soil grain density (i.e., 2,700 kg/m^3) may result in an error of up to 10%, if the true ρ_S is at the extreme of the typical range. At lower P-wave velocities, the errors in any of the other parameters may significantly change the void ratio estimate, but the magnitudes of these errors are strongly tied to V_P and V_S.

In summary, the Foti et al. (2002) relationship for porosity based on the theory of linear poroelasticity is most sensitive to changes in V_P, followed by V_S, v_{SK}, ρ_S, and T_W (in order of decreasing sensitivity). The particular sensitivity of void ratio to V_P has also been noted by (Lai and Crempien 2012, Jamiolkowski 2012, Foti and Passeri 2016). As suggested in the literature, typical values may be assumed for v_{SK}, ρ_S, and T_W (i.e., ρ_W and

K_W). However, a poor assumption (even within the range of typical values) for any parameter may produce errors as large as 10% in void ratio, underscoring the importance of using site and soil specific values whenever possible (e.g., measure the ground water temperature and evaluate the specific gravity of the soil).

4.3 DATASETS

Ideally, the seismic-based estimates of in-situ void ratio from DPCH testing should be directly compared to void ratio measurements from laboratory testing on high-quality granular soil samples. At seven sites with DPCH testing in Christchurch, several high-quality samples of predominantly silts, sandy silts, and silty sands were collected to study their cyclic stress-strain behavior (Beyzaei 2017, Beyzaei et al. 2017). However, most of the corresponding DPCH measurements at these sites indicate that these silty soils were not fully saturated in situ (i.e., V_P < 1,500 m/s). Hence, the Foti et al. (2002) porosity relationship could not be used at these sites. Many of the DPCH datasets in Christchurch indicate that sandy soils typically do not become fully saturated for 1 – 2 m below hydrostatic ground water level (GWL). This unsaturated transition zone is even more significant for silty soils, with some silty soils not reaching full saturation for 5 – 6 m below the GWL. Since fully saturated conditions are needed to estimates void ratio, we chose to focus on sandy-soil (ideally, clean sand) sites.

Ten predominantly sand case history sites with both DPCH and CPT testing were identified from the 31 DPCH case history sites in Christchurch. However, high-quality granular soil samples were not collected at any of these sites. So, seismic-based estimates

of void ratio at these ten DPCH sites cannot be directly compared to those obtained from high-quality samples. Nonetheless, high-quality samples of sand obtained from gel-push sampling were available in the same geologic formations at two other sites in Christchurch (Taylor 2015). As CPT soundings are available for both sets of case histories, an examination of the effectiveness of using DPCH seismic-measurements to estimate in-situ void ratio is developed below in two parts: (1) The laboratory measurements of void ratio on high-quality gel-push specimens at two sites, including statistical ranges for e_{min} and e_{max}, are used to "calibrate" the CPT-based estimates of void ratio. (2) Using insight gained from this comparison, the CPT-based estimates of in-situ void ratio are directly compared to the seismic-based estimates of void ratio at the ten predominantly sand DPCH case history sites.

4.3.1 Sand Sites with High-quality Soil Sampling

At two sites located in the central business district (CBD) of Christchurch, several high-quality sand samples s were collected using a gel-push sampler in an effort to characterize the behavior of typical Christchurch sandy soils under cyclic loading conditions (Taylor 2015). These sites were targeted due to the manifestation of liquefaction following the 2010-2011 Canterbury Earthquake Sequence and availability of CPT data nearby (Bray et al. 2014). Figures 4.2 and 4.3 show the: (a) cone tip resistance (q_C) and (b) normalized soil behavior type index (I_C) from CPT soundings located at the Kilmore Street and Madras-Armagh sites, respectively. The near-surface soil profile at the Kilmore St. site consists of a 2-m thick man-made gravel layer, a 6-m thick layer of silty sand of the

Springston Formation, and a clean medium-grained sand layer of the Christchurch Formation. The gel-push sampling targeted both the silty sand and clean sand layers (Figure 4.2c). The silty sand samples from the Springston Formation, obtained at depths between 2.5 - 6.5 m, had fines contents (FC) ranging from 20% to 50%, while the clean sands from the Christchurch Formation had FC ≤ 5%, based on sampling between 11 and 13 m. At the Madras-Armagh site, another silty sand of the Springston Formation (20% ≤ FC ≤ 50%) was targeted for sampling at 2 m, 3.5 to 4.5 m, and 5.5 to 7 m, as indicated in Figure 4.3c. The suite of laboratory tests on specimens obtained via gel-push sampling included measurement of, presumably, in-situ void ratio as individual specimens were consolidated and prepared for subsequent monotonic- and cyclic-strength testing, and the evaluation of e_{min} and e_{max} on reconstituted specimens. In Figures 4.2c and 4.3c, the laboratory void ratio measurements, indicated by circular markers, are compared with CPT-based estimates of in-situ void ratio.

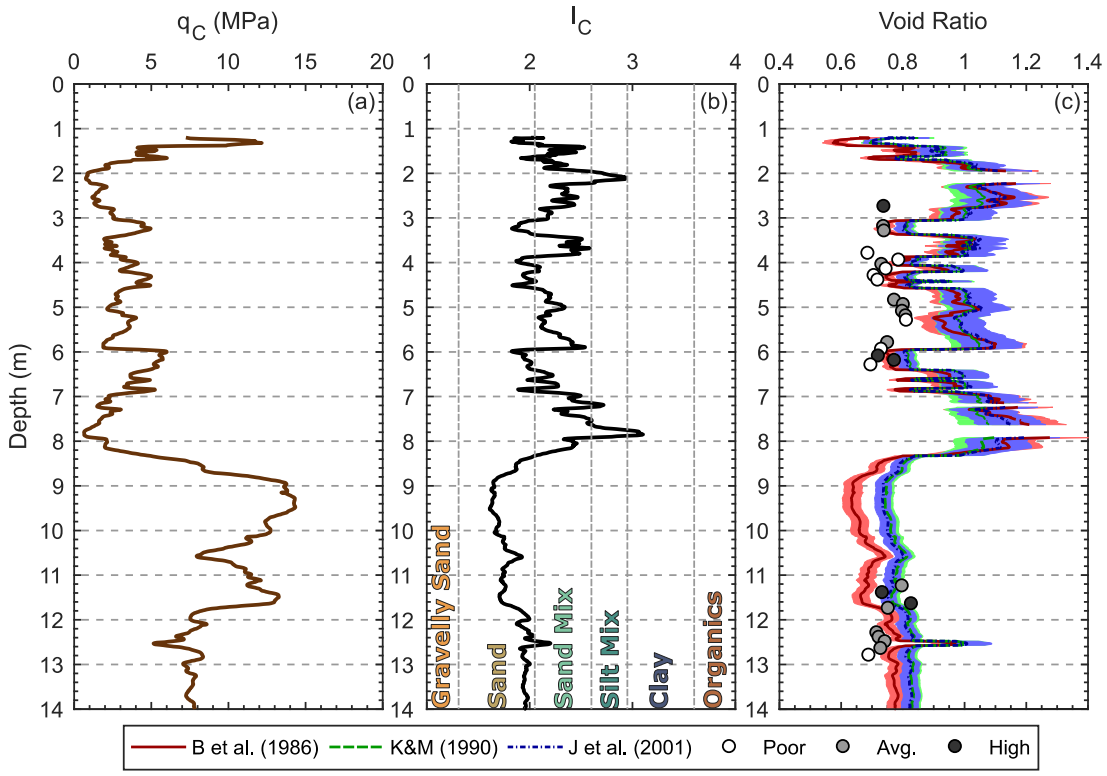

Figure 4.2: Comparison of site investigation data at the Kilmore Street site: (a) CPT cone tip resistance [q_C], (b) normalized soil behavior type index [I_C], and (c) void ratio measurements from gel-push samples of varying quality (poor, average, and high) in comparison to in situ estimates obtained from three CPT-based relative density [D_r] empirical relationships (i.e. Baldi et al. 1986, Kulhawy and Mayne 1990, and Jamiolkowski et al. 2001) and representative ranges of e_{min} and e_{max} from laboratory testing. The mean void ratio profile is indicated by the solid, dashed, and dot-dashed line, respectively, for each D_r empirical relationship. The associated ±1 standard deviation bounds are indicated by the shaded areas.

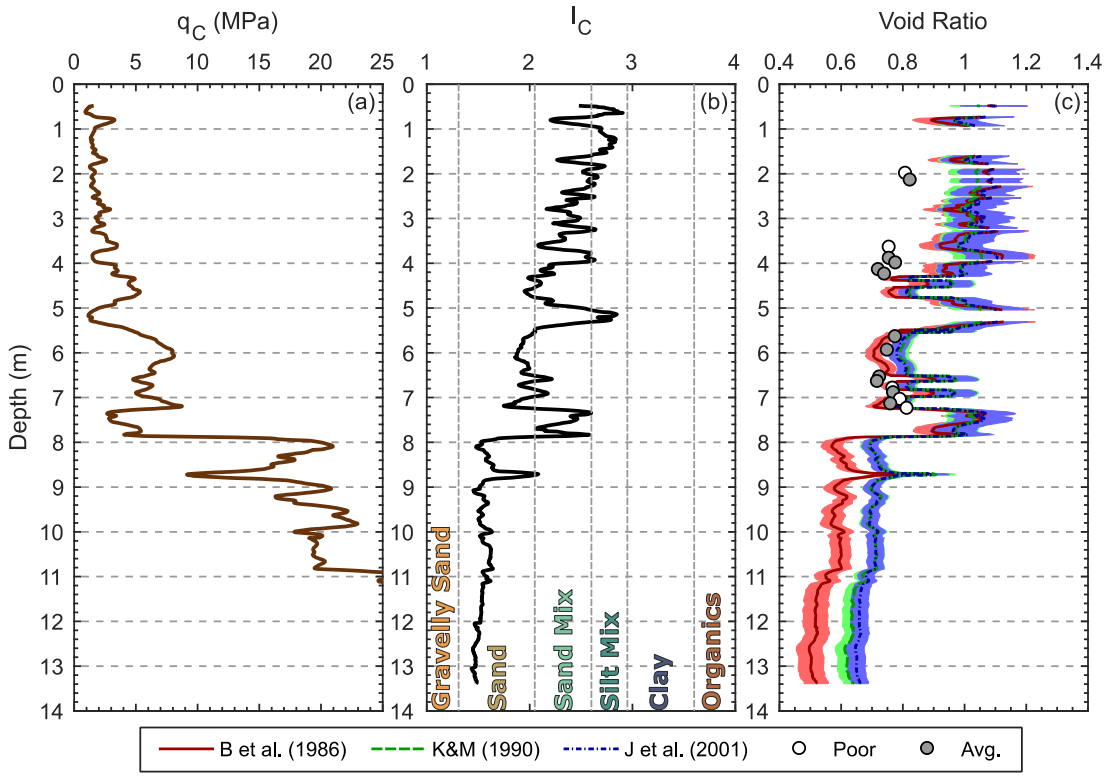

Figure 4.3: Comparison of site investigation data at the Madras-Armagh site: (a) CPT cone tip resistance [q_C], (b) normalized soil behavior type index [I_C], and (c) void ratio measurements from gel-push samples of varying quality (poor and average) in comparison to in situ estimates obtained from three CPT-based relative density [D_r] empirical relationships (i.e. Baldi et al. 1986, Kulhawy and Mayne 1990, and Jamiolkowski et al. 2001) and representative ranges of e_{min} and e_{max} from laboratory testing. The mean void ratio profile is indicated by the solid, dashed, and dot-dashed line, respectively, for each D_r empirical relationship. The associated ±1 standard deviation bounds are indicated by the shaded areas.

CPT measurements are correlated to relative density, rather than directly to void ratio or porosity. These empirical relationships have been developed primarily from laboratory calibration chamber testing on various clean sands. Thus, the CPT-based relationships for relative density are less reliable with increasing fines content. In this study, three CPT-based relative density empirical relationships are considered: Baldi et al.

(1986), Kulhawy and Mayne (1990), and Jamiolkowski et al. (2001). Thus, three D_r estimates are obtained for each CPT measurement. Using these D_r estimates and appropriate values of e_{min} and e_{max}, in-situ void ratio can be evaluated by re-arranging Equation 4.2 into the following form:

$$e = D_r \cdot e_{min} + (1 - D_r) \cdot e_{max} \tag{4.6}$$

As noted above, the laboratory characterization of both e_{min} and e_{max} are inherently difficult and subjective. Rather than develop single representative values of e_{min} or e_{max}, reasonable ranges have been developed from the Taylor (2015) dataset. The soils and associated testing results were bundled into two groups: (1) clean sands of the Christchurch Formation from the Kilmore St. site and (2) silty sands of the Springston Formation, including samples from both sites. The laboratory measurements of e_{min} and e_{max} were separated by group and assumed to be normally distributed to develop representative mean and standard deviation values (summarized in Table 4.1). As fines content measurements are not always available, these e_{min} and e_{max} values are assigned to each individual CPT measurement based on the normalized soil behavior type index (I_C), as follows: (1) If I_C is less than 2.05, the clean sand e_{min} and e_{max} values are assigned. (2) If I_C ranges between 2.05 and 2.60, the silty sand e_{min} and e_{max} values are assigned. (3) If I_C exceeds 2.6, the soil is considered predominantly fine-grained (silty), the associated CPT-based D_r estimates are unreasonable, and e_{min} and e_{max} values are not assigned.

Table 4.1: Mean and standard deviation values of minimum and maximum void ratio for clean sand (Christchurch Formation) and silty sand (Springston Formation) soil groups

		e_{min}		e_{max}		Number of Specimens
Soil Type	I_C Range	μ	σ	μ	σ	
Clean Sand	$I_C \leq 2.05$	0.598	0.032	0.991	0.041	9
Silty Sand	$2.05 \leq I_C \leq 2.6$	0.603	0.037	1.260	0.120	33

However, the uncertainties associated with e_{min} and e_{max} also need to be addressed. The relative contribution of uncertainty to the void ratio estimates from either e_{min} or e_{max} changes with relative density, according to Equation 4.6. For example, as relative density increases, the uncertainty contribution from e_{min} increases and the uncertainty contribution from e_{max} is diminished. Thus, the uncertainty in an individual CPT-based void ratio estimate needs to consider the relative uncertainty contribution from both e_{min} and e_{max} as a function of each individual D_r estimate. In order to account for this, a series of Monte Carlo simulations was used to develop 100,000 different realizations of void ratio for each individual D_r estimate. For each realization, independent random values of e_{min} and e_{max} are generated based on the associated mean and standard deviation values (refer to Table 4.1) for the appropriate soil type. As e_{min} and e_{max} are both assumed to be normally distributed, the associated void ratio estimate will also be normally distributed, following the Central Limit Theorem. The mean and standard deviation of the 100,000 void ratio realizations are then used to establish the mean and the ±1 standard deviation bounds for each individual CPT-based estimate of in-situ void ratio.

The CPT-based in-situ void ratio estimates developed from three D_r empirical relationships (Baldi et al. 1986, Kulhawy and Mayne 1990, and Jamiolkowski et al. 2001) are shown in Figures 4.2c and 4.3c. The associated mean in-situ void ratio estimates are indicated by solid, dashed, and dot-dashed lines for each CPT-D_r relationship, respectively. The ±1 standard deviation bounds for the void ratio estimates are indicated by the shaded areas. The Baldi et al. (1986) relationship consistently yields lower void ratio estimates compared to the other two relationships, which provide similar estimates of void ratio over the range of soil types. Specifically, in clean sands (e.g., below 8.5 m in Figure 4.2c and below 8 m in Figure 4.3c) the Baldi et al. (1986) void ratio estimates are on average 15% lower and as q_C increases, the more the estimates separate. These CPT-based void ratio estimates are directly compared with the laboratory void ratio measurements, which are indicated by circular markers in Figures 4.2c and 4.3c; the relative sample quality descriptions (e.g., poor, average, or high), are indicated by the circular marker fill (e.g., white, light-grey, or dark-grey).

First, consider the clean sands samples from Kilmore St., which occur at depths between 11-13m (see Figure 4.2c). The CPT-based estimates of in-situ void ratio compare favorably with the laboratory values. This is expected as the CPT-D_r empirical relationships were developed based on laboratory testing in clean sands. In contrast, the in-situ void ratios of the silty sands, sampled at depths between 2.5 and 6.5 meters, were estimated with mixed levels of success. The measured fines contents in these soil specimens were quite variable, generally ranging between 20% and 50%. However, a few silty-soil specimens had fines contents as high as 80%. This fines content variability is

reflected in the measured cone tip resistance, the normalized soil behavior type index, and the resulting void ratio estimates. In general, the CPT-based void ratio estimates are greater than the measured values in the silty sands, especially estimates based on lower cone tip resistances. Given that many of these specimens were also of average to poor quality, it is hard to say if the CPT estimates are "wrong" or if the specimen measurements are "wrong". More than likely it is a combination of both factors.

Additional comparisons of measured and estimated void ratio for the silty sand at the Madras-Armagh site are shown in Figure 4.3c. These samples are, in general, higher quality than those obtained in the silty sand at Kilmore St. At this site, the silty sands can be separated into two distinct groups based on cone tip resistance. Above 5.5 m, the q_C is less than 5 MPa and the corresponding CPT-based void ratio estimates are consistently greater than the laboratory measurements. On the other hand, when q_C exceeds 5 MPa, the associated I_C values are below 2.05 (indicating a sand normalized soil behavior type) and the measured and estimated void ratios agree quite well.

In summary, this dataset provides valuable insight into the performance of CPT-based relative density relationships in sandy-soils of the Springston and Christchurch Formations. The CPT-based estimates of void ratio are best in sands with relatively low fines contents, when I_C is less than 2.05, and cone tip resistances are greater than about 5MPa. The CPT-based estimates apparently over predict void ratio for silty sands with higher fines content, when Ic exceeds 2.05, and q_C is less than 5MPa. This qualitative calibration of the CPT-based D_r relationships for the sandy-soils in Christchurch, coupled with the representative e_{min} and e_{max} ranges, allows meaningful comparisons of CPT-based

empirical estimates of void ratio with those obtained from DPCH seismic measurements at other site sites in Christchurch with similar soils.

4.3.2 Sand Sites with DPCH Testing

As noted above, ten sites with DPCH measurements of V_P and V_S were selected for seismic-based estimation of in-situ void ratio based on the following criteria: (1) the sonic borehole logs, I_C profiles, and geology indicated that the soils were predominately sandy and similar to those studied in the Taylor (2015) case histories, (2) the DPCH data was of the highest quality, with the best possible cone deviation and waveform measurements, and (3) the sandy-soils were saturated over most of the depth range, as indicated by V_P measurements greater than 1,500 m/s. The geotechnical site investigation data (e.g., sonic borehole log, CPT sounding, and DPCH V_S/V_P profiles) at each of these sites may be found in the New Zealand Geotechnical Database (https://www.nzgd.org.nz). The ten site names and NZGD DPCH testing reference numbers are summarized in Table 4.2. The CPT and DPCH measurements have been used in the development and comparison of in-situ void ratio estimates, as described below.

Table 4.2: Sandy-soil sites with DPCH testing used to estimate in-situ void ratio

Site Name	NZGD VSVP Reference Number	Site Name	NZGD VSVP Reference Number
Avondale Playground	57062	Carisbrooke Playground	57193
Cresselly Place	57183	Corhampton Street	57194
Palinurus Road	57185	Charles Street	57196
Ti Rakau Reserve	57186	North New Brighton School	57198
Rawhiti Domain	57188	Normans Road/Papanui Road	57200

The Baldi et al. (1986), Kulhawy and Mayne (1990), and Jamiolkowski et al. (2001) CPT-based relative density empirical relationships have been used to estimate in-situ void ratios at each of the ten sites. The CPT-based estimates of void ratio are compared with those obtained from the DPCH V_S and V_P measurements using the Foti et al. (2002) porosity relationship developed from the theory of linear poroelasticity. As noted in the parametric study, this relationship requires the evaluation or assumption of several other parameters (i.e., ν_{SK}, ρ_W, K_W, and ρ_S). After V_P and V_S, the void ratio is most sensitive to ν_{SK}. Hence, the seismic-based void ratio estimates are evaluated at ν_{SK} equal to 0.15 and 0.35, capturing the typical range of values. The density and bulk modulus of water have been shown to vary with water temperature. The temperature of the ground water is assumed to be 14 °C, the median of near-surface ground temperatures discussed above. Given laboratory testing results on similar soils, the density of the solid soil grains is assumed to be 2,700 kg/m^3.

To highlight the varying levels of agreement between the CPT-based and seismic-based void ratio estimates, four of the ten sites are discussed in detail below: (1) Rawhiti Domain, (2) Charles Street, (3) Palinurus Road, and (4) Carisbrooke Playground. Figures

4.4 through 4.7 present the void ratio estimates and supporting geotechnical data at each of these sites in a five-panel format: (a) sonic borehole log with USCS soil classifications, (b) CPT cone tip resistance, (c) V_S, (d) V_P, and (e) void ratio estimates.

The Rawhiti Domain dataset (see Figure 4.4) represents the highest level of agreement between the seismic- and CPT-based in-situ void ratio estimates. The near-surface soil profile is solely comprised of clean sands of the Christchurch Formation. Limited specimens tested from disturbed sonic sampling at this site indicate fines contents lower than 5%. The q_C values generally range between 10-20 MPa, while the Vs values range from about 140-240 m/s. Even though the hydrostatic water table is located just below 1 m, the V_P values do not indicate that the soil is saturated until near 2.5 m. Below 3 m, the seismic-based void ratio estimates agree well with the CPT-based Baldi et al. (1986) estimates, with both ν_{SK} markers falling in or near the $\pm 1\sigma$ bounds. A few important observations should be highlighted: (1) As noted in the parametric study (refer to Figure 4.1), the Foti et al. (2002) relationship is very sensitive to slight changes in V_P. The void ratio estimates are unstable from 2.6 to 3 meters as the soil is just reaching full saturation and V_P increases from 1,500 to 1,700 m/s. At four meters, a small (3%) decrease in V_P results in a 12% jump in the void ratio estimate. (2) The seismic-based estimates are relatively insensitive to the assumed ν_{SK} value until V_S exceeds about 200 m/s at depths greater than 7 m. This effect was also noted in the parametric study (refer to Figure 4.1a). (3) In general, there is excellent agreement between in-situ void ratio estimates developed from DPCH measurements and the Baldi et al. (1986) CPT relationship. When differences do exist, it is impossible to say which method is "better", particularly since fairly

significant differences in-void ratio exist between Baldi et al. (1986) and the other two CPT-based relationships.

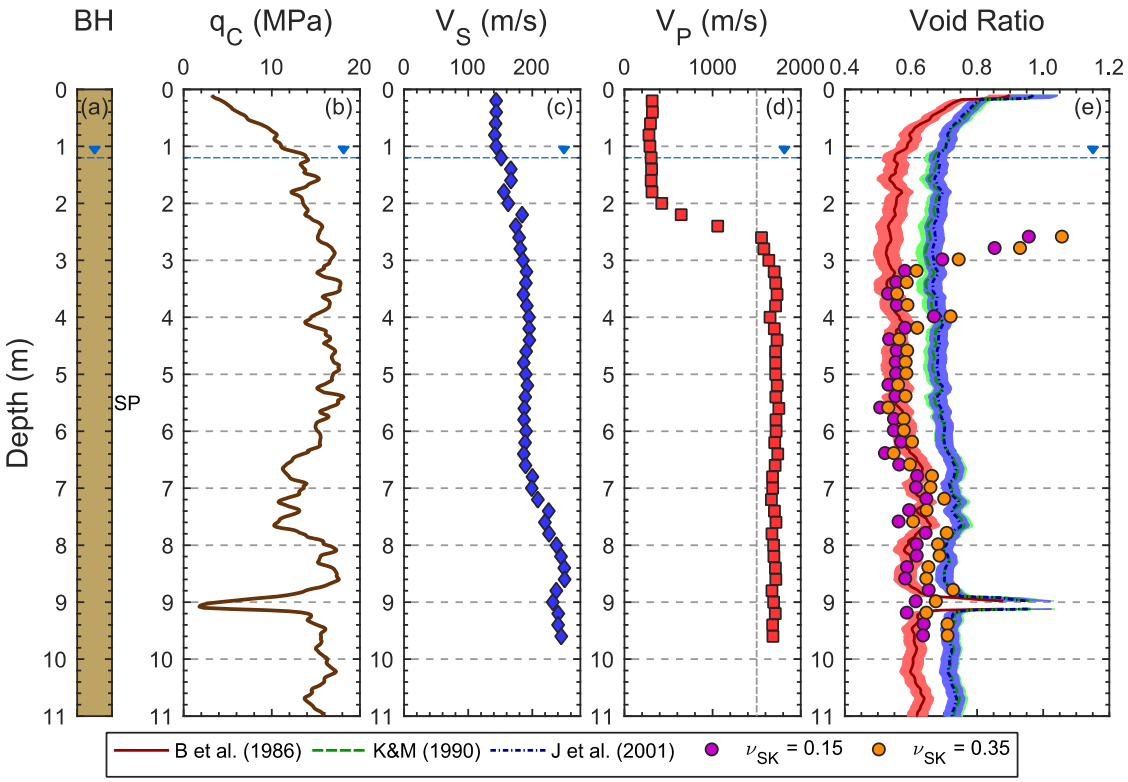

Figure 4.4: Comparison of site investigation data at the Rawhiti Domain (NZGD VSVP 57188) site: (a) soil classification from continuous sonic borehole samples, (b) CPT cone tip resistance [q_C], (c) V_S from DPCH testing, (d) V_P from DPCH testing, and (e) in situ estimates of void ratio, developed from CPT-based and seismic-based relationships. Three CPT-based relative density (D_r) empirical relationships (i.e. Baldi et al. 1986, Kulhawy and Mayne 1990, and Jamiolkowski et al. 2001) and representative ranges of e_{min} and e_{max} from laboratory testing were used to estimate in situ void ratio. The mean void ratio profile is indicated by the solid, dashed, and dot-dashed line, respectively, for each D_r empirical relationship. The associated ±1 standard deviation bounds are indicated by the shaded areas. Seismic-based estimates of in situ void ratio are indicated by circular markers at two assumed values for Poisson's ratio of the soil skeleton (ν_{SK}), with ν_{SK} = 0.15 always yielding lower void ratio estimates than ν_{SK} = 0.35.

The Charles Street dataset, as shown in Figure 4.5, illustrates the impact of increased fines content and reflects greater disagreements in the void ratio estimates. A 3-m thick deposit of low plasticity silt of the Springston Formation overlies clean sands of the Christchurch Formation. The silt-to-sand transition is marked by a sharp increase in soil stiffness, as indicated by an increase in q_C from 0.5 to 10 MPa and a jump in V_S from 100 to 155 m/s. The observed GWL at 1.1 m is marked by a sharp increase in P-wave velocity from 700 to 1,350 m/s. The soil remains *nearly* saturated in the silt layer. At the silt-to-sand transition, the P-wave velocity increases to 1,600 m/s, reflecting both the increase in soil skeleton stiffness and full saturation of the soil. In the silty-soil deposit, high fines contents and I_C greater than 2.6 prohibit reasonable evaluation of the CPT-based void ratio, except at two localized measurement depths, 2.4 and 2.8 m, where Ic < 2.6. The seismic-based void ratio estimates at these two depths fall within the ±1σ bounds of the CPT-based estimates, showing a high-level of agreement despite the silty soil conditions. The void ratio comparisons in the clean sand should be considered in three distinct depth ranges: (1) 3.2 to 5 m, (2) 5 to 7.2 m, and (3) 7.4 to 9.8 m. From 3.2 to 5 m, the measured V_P reaches 1,750 m/s as the q_C approaches 15 MPa. The associated seismic-based void ratio estimates agree best with the Baldi et al. (1986) estimates over most of this range. However, as the q_C starts to drop near 5 m, V_P also drops, causing the seismic-based void ratios to jump across the range of all three CPT-based estimates. At measurement depths between 5 and 7.2 m, the V_P profile stabilizes at ~1,650 m/s, resulting in consistent void ratio estimates of approximately 0.65 to 0.73, depending on v_{SK}. The associated CPT-based estimates of void ratio gradually change with cone tip resistance, however, the

seismic-based estimates generally fall within the Baldi et al. (1986) bounds. Below 7.4 meters, the q_C values gradually decrease and similar trends are observed in the V_S and V_P profiles. Specially, V_P decreases from about 1,650 to 1,550 m/s, corresponding to an increase in void ratio of about 0.30 (from about 0.7 to about 1.0). Over the same depth range, each of the three CPT-based estimates increase by only 0.05. The void ratio estimates over all three depth ranges underscore the sensitivity of the seismic-based void ratios to changes in V_P. While there is remarkable agreement in the trends between q_C and V_P, it appears that the seismic-based void ratio estimates are changing too much as a function of V_P.

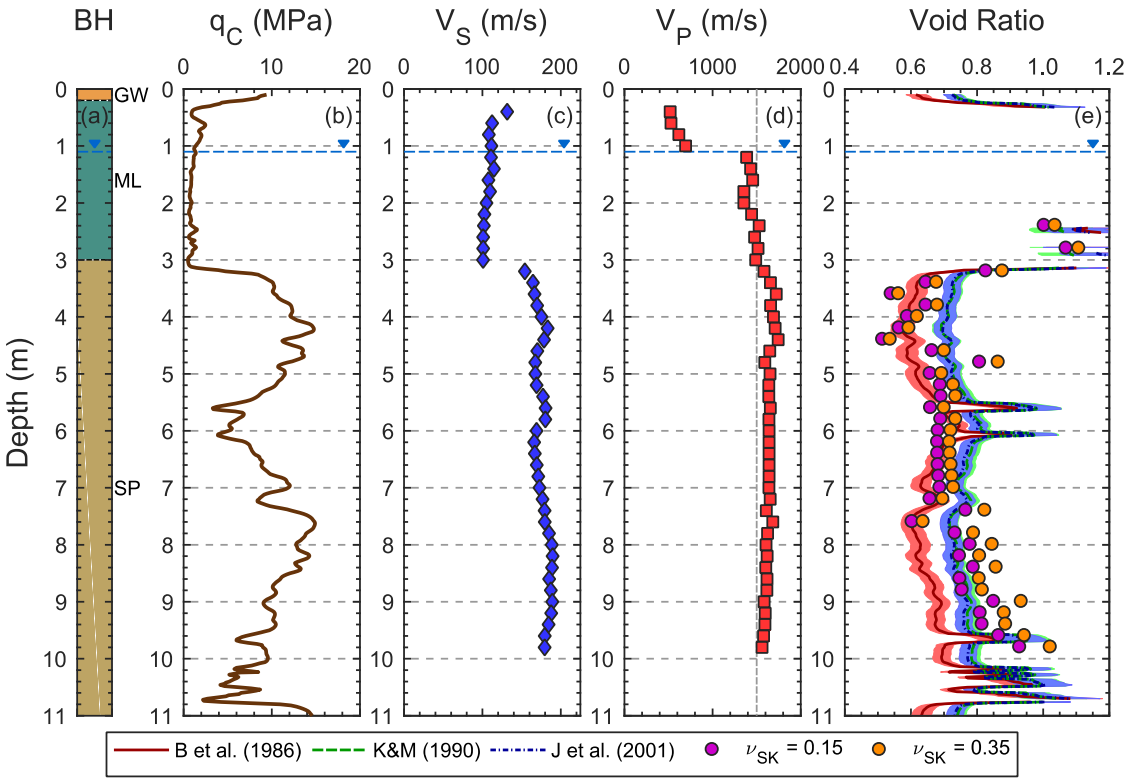

Figure 4.5: Comparison of site investigation data at the Charles Street (NZGD VSVP 57196) site: (a) soil classification from continuous sonic borehole samples, (b) CPT cone tip resistance [q_C], (c) V_S from DPCH testing, (d) V_P from DPCH testing, and (e) in situ estimates of void ratio, developed from CPT-based and seismic-based relationships. Three CPT-based relative density (D_r) empirical relationships (i.e. Baldi et al. 1986, Kulhawy and Mayne 1990, and Jamiolkowski et al. 2001) and representative ranges of e_{min} and e_{max} from laboratory testing were used to estimate in situ void ratio. The mean void ratio profile is indicated by the solid, dashed, and dot-dashed line, respectively, for each D_r empirical relationship. The associated ±1 standard deviation bounds are indicated by the shaded areas. Seismic-based estimates of in situ void ratio are indicated by circular markers at two assumed values for Poisson's ratio of the soil skeleton (ν_{SK}), with ν_{SK} = 0.15 always yielding lower void ratio estimates than ν_{SK} = 0.35.

The Palinurus Road dataset (see Figure 4.6) highlights disagreement between seismic- and CPT-based void ratio estimates in soils with increased fines content. At this

site, a 3-m thick deposit of silts and silty sands of the Springston Formation overlies clean sands of the Christchurch Formation. The transitions between these soils are clearly reflected in the cone tip resistance, which exceeds 10 MPa in the clean sands and is lower than 3 MPa in the silty sands and silts. In the clean sands, the seismic-based void ratios are slightly lower than the Baldi et al. (1986) -1σ bound. Given better agreement in clean sands at the two previous sites, low void ratios may indicate slightly high/inaccurate V_P measurements at this site. The seismic-based void ratio estimates in the silty sands are substantially lower than those obtained from the CPT relationships over the depth range of 6.0 - 9.5 m. As noted above, the CPT-based estimates are not very reliable in silty sands, and likely too high. While the Foti et al. (2002) porosity relationship should be valid for these silty sands, the void ratio estimates from seismic DPCH testing are suspected to be too low, and likely caused by slightly high V_P values. However, the seismic-based void ratio estimates cannot be quantitatively evaluated in the silty sands given the limitations of the CPT-based relationships.

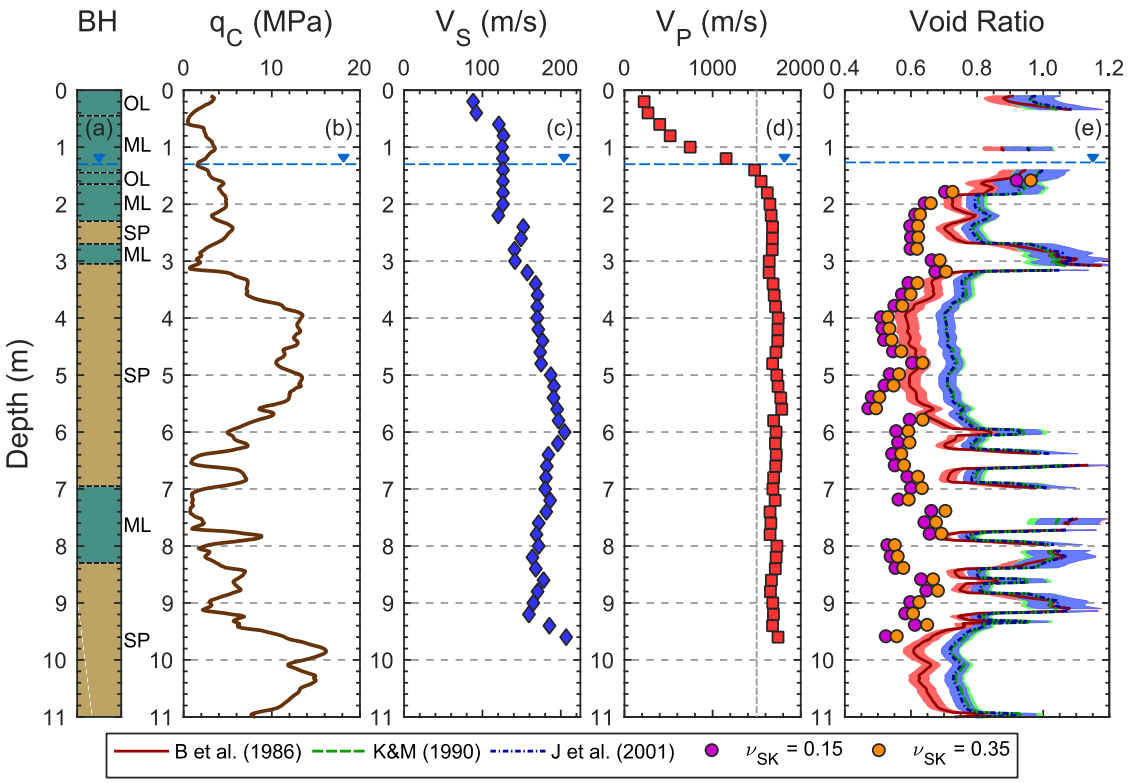

Figure 4.6: Comparison of site investigation data at the Palinurus Road (NZGD VSVP 57185) site: (a) soil classification from continuous sonic borehole samples, (b) CPT cone tip resistance [q_C], (c) V_S from DPCH testing, (d) V_P from DPCH testing, and (e) in situ estimates of void ratio, developed from CPT-based and seismic-based relationships. Three CPT-based relative density (D_r) empirical relationships (i.e. Baldi et al. 1986, Kulhawy and Mayne 1990, and Jamiolkowski et al. 2001) and representative ranges of e_{min} and e_{max} from laboratory testing were used to estimate in situ void ratio. The mean void ratio profile is indicated by the solid, dashed, and dot-dashed line, respectively, for each D_r empirical relationship. The associated ±1 standard deviation bounds are indicated by the shaded areas. Seismic-based estimates of in situ void ratio are indicated by circular markers at two assumed values for Poisson's ratio of the soil skeleton (ν_{SK}), with ν_{SK} = 0.15 always yielding lower void ratio estimates than ν_{SK} = 0.35.

The last of the four selected sites, Carisbrooke Playground (see Figure 4.7), represents the greatest level of disagreement between seismic- and CPT-bases estimates of void ratio at all ten sites considered. Here, a thin, silt surface layer overlies a thick deposit of clean sands of the Christchurch Formation. Generally, the stiffness of the clean sands steadily increases below the observed GWL, as indicated by several measurements: q_C increases from 10 to 18 MPa, V_S increases from 170 to 270 m/s, and V_P increases from 1,650 to 2,050 m/s. While the P-wave velocities are high, the relatively high q_C and S-wave velocities lend some confidence to these measurements. Given the predominantly clean sand profile, a high level of agreement between the seismic- and CPT-based estimates of void ratio is anticipated. However, the seismic-based estimates range between 0.33 and 0.45, significantly lower than those developed from any of the three CPT-based D_r empirical relationships and lower than one would expect (significantly lower than the e_{min} values indicated in Table 4.1). Even relative to the lowest CPT-based estimates of Baldi et al. (1986), the seismic-based estimates are 55 to 70% lower.

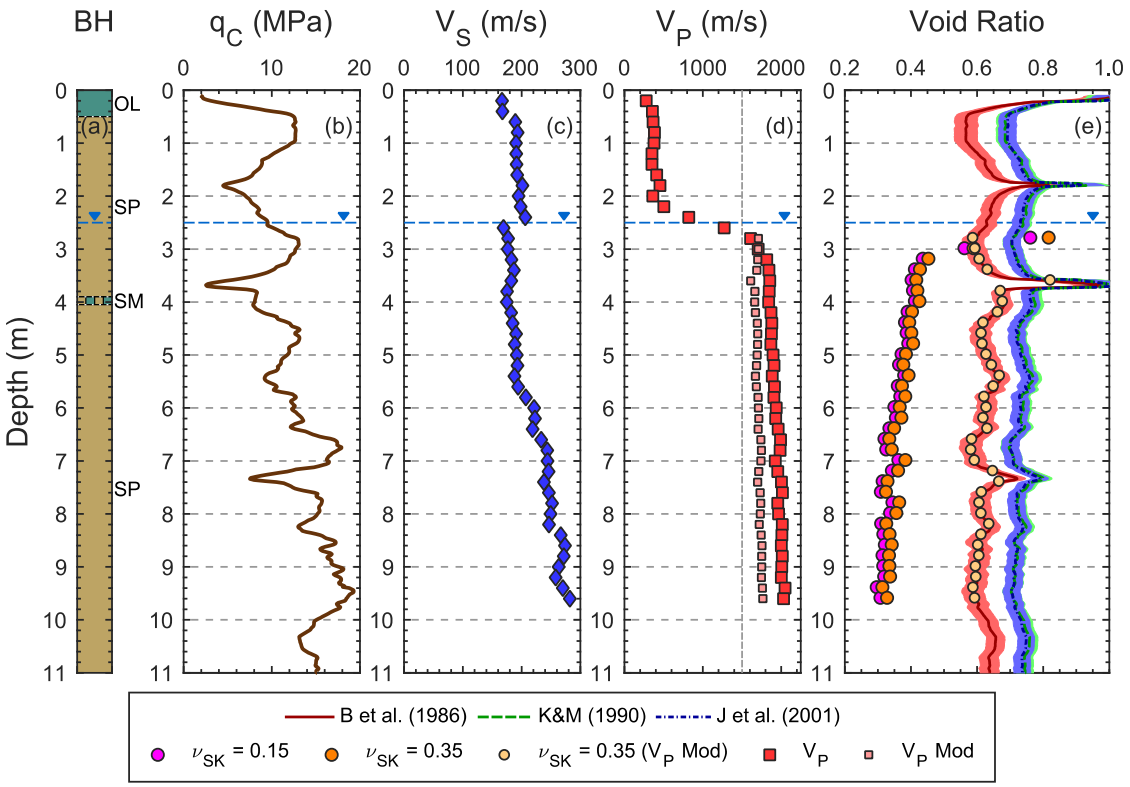

Figure 4.7: Comparison of site investigation data at the Carisbrooke Playground (NZGD VSVP 57193) site: (a) soil classification from continuous sonic borehole samples, (b) CPT cone tip resistance [q_C], (c) V_S from DPCH testing, (d) V_P from DPCH testing, and (e) in situ estimates of void ratio, developed from CPT-based and seismic-based relationships. Three CPT-based relative density (D_r) empirical relationships (i.e. Baldi et al. 1986, Kulhawy and Mayne 1990, and Jamiolkowski et al. 2001) and representative ranges of e_{min} and e_{max} from laboratory testing were used to estimate in situ void ratio. The mean void ratio profile is indicated by the solid, dashed, and dot-dashed line, respectively, for each D_r empirical relationship. The associated ±1 standard deviation bounds are indicated by the shaded areas. Seismic-based estimates of in situ void ratio are indicated by circular markers at two assumed values for Poisson's ratio of the soil skeleton (ν_{SK}), with ν_{SK} = 0.15 always yielding lower void ratio estimates than ν_{SK} = 0.35. As indicated by small square markers, individual V_P measurements were modified such that the corresponding ν_{SK} = 0.35 void ratio estimate (small circular markers) agrees with the mean Baldi et al. (1986) estimate at the same testing depth.

Given the better agreement between seismic- and CPT-based estimates of in-situ void ratio at the other example sties, it is important to investigate potential causes for this disagreement. At the Carisbrooke Playground, V_P measurements exceed 1,800 m/s in the fully-saturated soils. According to the results of the sensitivity study shown in Figure 4.1, these high P-wave velocities essentially limit the effect that V_S (or any other parameter) has on the void ratio. Specifically, when V_P is equal to 1,800 m/s the seismic-based void ratio estimates are restricted to values of about 0.4 - 0.5, irrespective of V_S changing over 200% from 100 to 300 m/s. So, it is clear that the high V_P values at this site are governing the apparently low seismic-based estimates of void ratio. Assuming the mean Baldi et al. (1986) void ratio profile reasonably reflects the in-situ conditions, and ν_{SK} is equal to 0.35, the percent decrease in V_P required to make the seismic- and CPT-based void ratios match was investigated. It was determined that the original V_P measurements (ranging from 1,700 to 2,050 m/s) only needed to be reduced by 9 to 16% percent (refer to the V_P Mod symbols in Figure 4.7d) in order to match the Baldi et al. (1986) void ratio estimates (refer to the ν_{sk} = 0.35 (V_P Mod symbols) in Figure 4.7e). The modified P-wave velocity profile ranges from 1,625 to 1,775 m/s. A slightly, larger reduction (up to 18%) in V_P is necessary to match the other CPT relationships.

4.4 DISCUSSION

To understand potential sources of error in these V_P measurements, consider the evaluation of V_P (and V_S) from DPCH testing. Seismic waves are assumed to directly travel along a horizontal path from the source to the receiver. At each measurement depth, the

seismic wave velocities (i.e. distance per unit time) are evaluated by dividing the length of the travel path by the associated wave travel time. Measurement errors in travel path length and/or time are carried into the velocity evaluation. In the fully-saturated Christchurch sands, V_P generally ranges from 1,500 to 1,850 m/s and V_S generally ranges from 80 to 300 m/s, depending on the density, state of stress, and soil skeleton stiffness. Assuming the P- and S-waves travel along the same travel path from source to receiver, a 10% measurement error in the travel path length results in a 10% error in both V_P and V_S. However, in fully-saturated soils the P-wave travel time is an order of magnitude smaller than the S-wave travel time. A 10% error in the travel path may change the V_S by 8 to 30 m/s, while the corresponding V_P may be off by 150 to 185 m/s. As noted in the parametric study, the void ratio estimates would minimally change due to this error in V_S (see Figure 4.1), but would be greatly altered by the corresponding error in V_P. At the Carrisbrooke Playground and Charles Street sites, the V_P profiles appear to gradually drift. In part, this may be due to the gradual changes in the stiffness of the soil skeleton, as observed in cone tip resistance. However, this drift may also reflect a systematic, cumulative error in determining the travel path distance. In DPCH testing, the distance between the cones is evaluated based on the cone positions, which are updated based on changes in the tilt angles and push distance between each seismic measurement. Thus any measurement errors are carried through each successive testing depth. Another potential source of error in V_P (and V_S) is the evaluation of the direct wave travel times. As noted in Chapter 2, timing errors in DPCH testing may arise from several sources: the misidentification of the direct arrivals, improper consideration/calibration of data acquisition triggering, and noise in the recorded

waveforms. While P-wave arrivals in saturated soils are high-frequency and relatively easy to identify, noise and poor triggering may obscure the arrival. At typical sampling rates (~20 kHz) and travel path lengths (1 to 3 m, depending on cone deviation), picking a trigger time or wave arrival time that is in error by only a single time sample may result in a V_P error as large as ~5%. As the waveforms are independently generated and measured at each testing depth, the minor timing errors are likely isolated to individual or small subsets of velocity measurements. For example, the slightly decreased P-wave velocity at a depth of 4 meters at the Rawhiti Reserve (see Figure 4.4) may be caused by such a timing error.

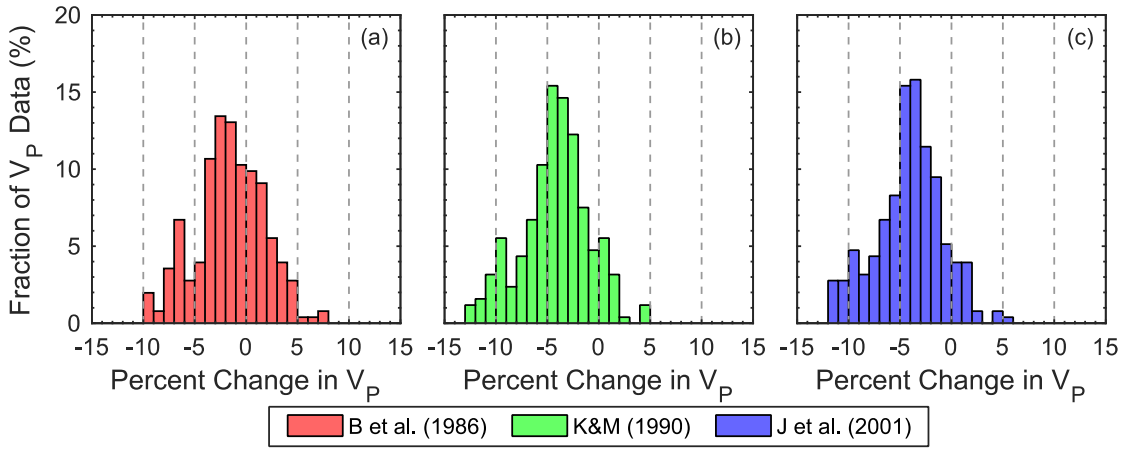

Figure 4.8: Histograms of the percent change in VP required to adjust seismic-based in situ void ratio estimates to match the corresponding mean estimate from each CPT-based empirical relationship: (a) Baldi et al. (1986), (b) Kulhawy and Mayne (1990), and (c) Jamiolkowski et al. (2001). The histograms are based on 253 void ratio estimates in clean sands across nine sites in Christchurch, New Zealand.

Given that undisturbed soil samples have not been obtained at the case history sites where high-resolution DPCH V_S and V_P data are available, it is impossible to know what the "true" void ratios at these sites are. However, across all ten of the predominantly sand

sites discussed in this paper, the following trends have been observed: (1) the CPT-based void ratio estimates vary from one another, with those from Baldi et al. (1986) being on average 10% - 15% less than the others, (2) the seismic-based void ratio estimates tend to agree best with the CPT-based estimates of Baldi et al. (1986), and (3) in some cases it appears that the seismic-based void ratio estimates may be too low due to suspected small errors in measuring V_P (potentially caused by errors in the tilt/distance calculations). The impact of potential small errors in V_P is investigated further by considering the percent change in V_P needed in order to make the seismic-based void ratio estimates match those of the CPT-based estimates. This exercise is similar to what was performed above at the Carrisbrooke Playground site. However, it is now expanded to consider the nine other sand sites in our database. Note that the Carrisbrooke Playground site is not considered further below since the seismic-based void ratio estimates have already been shown to be suspiciously low.

Neglecting measurements made in silty sands with I_C greater than 2.05, 253 distinct V_S and V_P seismic measurements were made in soils consisting of clean sands, across nine sites. The void ratio estimates from these 253 seismic measurements have been statistically compared to the median values of the CPT-based void ratio estimates by computing the percent change in V_P required to bring these estimates into agreement with one another. To simplify these comparisons, the seismic-based void ratio estimates were evaluated using a single ν_{SK} value of 0.25. In Figure 4.8, the distributions of required percent changes in V_P are presented in three histograms, one for each CPT relationship: (a) Baldi et al. (1986), (b) Kulhawy and Mayne (1990), and (c) Jamiolkowski et al. (2001). The width of each

histogram bin represents a 1% change in V_P. Each of these histograms are approximately bell-shaped. The peak of the bell is centered at approximately -2%, -4%, and -4% change in V_P for the Baldi et al. (1986), Kulhawy and Mayne (1990), and Jamiolkowski et al. (2001) relationships, respectively. Meaning, on average, only a slight decrease in V_P is needed to bring the seismic-based void ratio estimates into agreement with the CPT-based estimates. These small changes in V_P are within the range of potential measurement errors in DPCH testing. Hence, improvements need to be made to seismic testing methods such that V_P can be evaluated within 1% - 2% in order to have confidence in the void ratio estimates.

It is also important to quantify the difference between seismic-based and CPT-based void ratio estimates beyond qualitative observations. To this end, the percent difference between the seismic-based void ratio estimates (with $\nu_{SK} = 0.25$) and each of the three CPT-based estimates were evaluated for the 253 clean sand data points. In addition, the percent difference between the Baldi et al. (1986) and the Kulhawy and Mayne (1990) CPT-based void ratio estimates was also evaluated for the same 253 clean sand data points. The empirical cumulative distribution functions (CDF) for each set of percent differences in estimated void ratio are shown together in Figure 4.9. First, consider the percentage of DPCH seismic-based void ratio estimates that are within 10% of the CPT-based estimates: approximately 43% relative to Baldi et al. (1986) and approximately 19% relative to the other two CPT relationships. While these numbers may not seem great, it should be noted that only about 9% of the void ratio estimates of Baldi et al. (1986) and Kulhawy and Mayne (1990) agree within 10% of one another. In fact, for more than 65% of the data

points considered, the Baldi et al. (1986) CPT-based estimates agree better with the seismic-based estimates than with the other CPT-based estimates. However, for the remaining 35% of the data points, the maximum percent difference between the CPT-based estimates is no more than 20%, while the maximum percent difference between the seismic- and CPT-based estimates ranges from about 45% to 55%. These large differences are most likely attributed to small errors in determining V_P, which result in large underestimation of void ratio. Statistically, the DPCH V_S and V_P measurements coupled with the Foti et al. (2002) theoretical relationship proved to be relatively effective at evaluating the in-situ void ratio of clean sands relative to the CPT-based relationships.

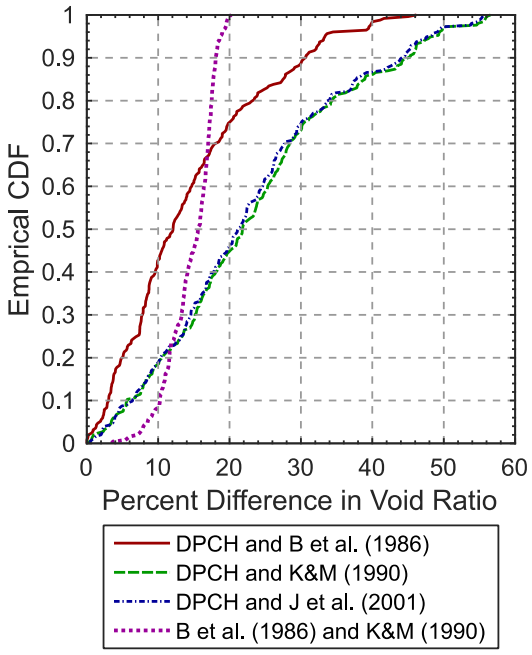

Figure 4.9: Comparison of empirical cumulative distribution functions showing the percent difference between DPCH seismic-based in situ void ratio estimates and those obtained from three CPT-based estimates [e.g. Baldi et al. (1986), Kulhawy and Mayne (1990), and Jamiolkowski et al. (2001)], and the percent difference between the Baldi et al. (1986) and the Kulhawy and Mayne (1990) CPT-based void ratio estimates.

4.5 CONCLUSIONS

A relationship to evaluate soil porosity (i.e., void ratio) in fully-saturated soils from seismic wave propagation velocities (i.e., V_P and V_S) was developed by Foti et al. (2002) using the theory of linear poroelasticity (Biot 1956a) as an underlying framework. Soil porosity is evaluated as a function of V_P, V_S and four additional parameters describing the physical properties of the soil (i.e., ν_{SK}, ρ_S, ρ_W, and K_W). In this study, the effectiveness and feasibility of using high-resolution V_S and V_P measurements from DPCH testing to estimate in-situ void ratios was investigated at ten, predominantly clean sand case history sites in Christchurch, New Zealand. As high-quality, "undisturbed" samples were not available at these ten sites, absolute comparisons of in-situ void ratio estimates could not be made. Hence, only relative comparisons could be made between CPT-based estimates of in-situ void ratio and those obtained from seismic measurements. Nonetheless, the CPT-based estimates of in-situ void ratio were "calibrated" using soil-specific e_{min} and e_{max} values, including associated uncertainties, and were demonstrated to yield fairly consistent agreement with void ratio measurements obtained from gel-push samples of sand at two other sites in Christchurch.

Detailed comparisons between seismic- and CPT-based void ratio estimates have been shown at four sites, where agreement between estimates ranges from excellent to poor. From a statistical analysis of 253 seismic-based void ratio estimates across nine of the ten sites considered in this study, it was found that approximately 43% of the in-situ void ratio estimates for the clean sand data points fell within 10% of the Baldi et al. (1986) CPT-based estimates. While this agreement may not seem amazing, it should be noted that

only about 9% of the CPT-based void ratio estimates of Baldi et al. (1986) agree within 10% of the CPT-based estimates of Kulhawy and Mayne (1990) and Jamiolkowski et al. (2001). In fact, for more than 65% of the data points considered, the Baldi et al. (1986) CPT-based estimates agree better with the seismic-based estimates than with the other CPT-based estimates. However, for the remaining 35% of the data points, the maximum percent difference between the CPT-based void ratios is no more than 20%, while the maximum percent difference between the seismic- and CPT-based void ratios ranges from about 45% to 55%. These large differences are attributed to small errors in determining V_P, which result in significant underestimation of void ratio. While the "true" void ratios in this study are not known, when very poor agreement between seismic- and CPT-based estimates of void ratio are observed in clean sands, we believe the seismic-based estimates are most likely in error. However, it has been demonstrated that only moderate adjustments to V_P are required to bring the seismic- and CPT-based void ratio estimates into agreement with one another. Specifically, it has been demonstrated that V_P only needs to be adjusted by 2 to 4%, on average, in order to bring the seismic- and CPT-based estimates into agreement with one another. This finding is both encouraging and discouraging; encouraging because estimating void ratio based on in-situ measurements of V_S and V_P seems attainable, and discouraging because it is extremely difficult to measure any parameter in situ within 2%.

We believe that DPCH testing has the potential to enable very high-resolution measurements of V_P and V_S. With slight improvements to the equipment and testing procedures we hope to be able to track cone deviations and resolve P-wave travels times

even more accurately. If this can be done, more consistent and reliable estimates of in-situ void ratio can be obtained from linear poroelasticity theory, which is valid for all fluid-saturated porous materials (e.g., sands, silts, and clays). Estimating void ratio in this way is much more satisfying than continuing to rely on empirical correlations to penetration resistance that also show significant scatter and, at best, are currently only appropriate for use in clean sands. Additional case histories are needed to increase confidence in void ratio estimates made via DPCH seismic measurements through direct comparisons with laboratory measured void ratios on high-quality samples of both granular and cohesive soils.

4.6 ACKNOWLEDGEMENTS

This work was partially supported by U.S. National Science Foundation (NSF) grant CMMI-1547777. However, any opinions, findings, conclusions, or recommendations expressed in this material are those of the authors and do not necessarily reflect the views of NSF.

Financial support was also provided by the New Zealand Earthquake Commission (EQC) under the Capability Building Fund at the University of Auckland and QuakeCoRE through Technology Platform 2.

Chapter 5: Conclusions

5.1 Major Findings, Recommendations, and Future Work

Chapters 2, 3, and 4 represent three self-contained journal articles, each with fully developed conclusions, recommendations, and proposals for future work. These conclusions are reproduced below to conclude this work in developed in three parts.

5.1.1 A Direct-Push Crosshole (DPCH) Test Method for the In-Situ Evaluation of High-Resolution P- and S-wave Velocities

A new, invasive seismic testing method called direct-push crosshole (DPCH) testing has been developed. DPCH combines the technical benefits of crosshole seismic testing with the ease and speed of direct-push downhole/SCPT methods. DPCH testing uses a pair of instrumented seismic cones pushed into the ground with two closely-spaced CPT rigs. Pushing the cones into the ground provides excellent coupling with the soil and eliminates the need for expensive cased boreholes. The relative position of each cone is tracked using tilt angles obtained from MEMS accelerometers, thus allowing for accurate calculations of the distance between cones at each measurement depth. The seismic energy required for testing is easily generated by tapping a hammer on top of the CPT push rod connected to the source cone. In this manner, both P-waves and S-waves are propagated from one cone (the source) to the other (the receiver). A significant advantage of DPCH testing is the ability to maintain a consistent wave travel path and strong signal-to-noise ratio as a function of depth. These two factors allow for consistent resolution of V_P and V_S

as a function of depth, resulting in detailed wave velocity profiles with the potential to detect thin layers.

Using the methodology detailed in this paper, DPCH field data can be collected at a rate of approximately 1.0 to 1.5 minutes per test depth. Thus, using a depth increment of 20 cm, it is possible to simultaneously collect V_P and V_S data down to a depth of 10 m in 50 to 75 minutes. The maximum DPCH testing depth to date is just over 20 m, but it is possible to go deeper. In order to avoid potential problems with non-direct wave paths, the cones should be placed no more than 1.5 to 2.5 meters apart and friction reducers should be used on the cone rods. Other strategies for dealing with complicated wave arrivals in interlayered soil deposits have been discussed.

DPCH testing has thus far been used for in-situ evaluation of various ground improvement methods, allowing for measurements of V_P and V_S directly across/through vertical elements such as stone columns, which cannot be achieved with any other in-situ testing methodology (Stokoe et al. 2014, Wotherspoon et al. 2015, Stokoe et al. 2016, Hwang et al. 2017, Wotherspoon et al. 2017). DPCH has also been used in soil liquefaction studies to account for the beneficial effects of partial saturation, which can be inferred from high quality measurements of V_P, and soil microstructure, which can be inferred from high quality measurements of V_S (Cox et al. 2017, McLaughlin 2017). An area of ongoing research is the in-situ evaluation of soil porosity and void ratio, which requires extremely precise values of V_S and V_P (Foti et al. 2002, Foti and Lancellota 2004). It is anticipated that DPCH testing will play a key role in eventually being able to measure soil void ratio in situ, which is currently obtained only by correlations to penetration test results. These

applications, and no doubt others yet to be discovered, make DPCH testing an important in-situ site characterization tool for geotechnical engineering in the future.

5.1.2 Epistemic uncertainty in shear wave velocity measurements obtained via SCPT

A dataset was developed consisting of 31 soil liquefaction case history sites in Christchurch, New Zealand. At each site, the geotechnical site investigation included the following: (1) continuous disturbed soil sampling from sonic-drilling, (2) a SCPT sounding collected and initially processed by a well-regarded, independent CPT contractor, and (3) DPCH testing conducted by the authors. At two of the thirty-one sites, the SCPT data was reprocessed using analysis methods representative of those commonly used in geotechnical practice. The travel time techniques considered include the first arrival, peak/trough, and crossover picks and the time delay associated with the peak response of the cross correlation function between pairs of waveforms. The velocity analysis methods include pseudo-interval, true-interval, and corrected vertical travel time slope-based method. Using all possible combinations of travel time and velocity analysis methods, eleven SCPT V_S profiles have been developed for each site. An additional twelfth V_S profile was developed by the independent CPT contractor using first arrival picks and a raytracing algorithm.

The epistemic uncertainty associated with the different travel time and velocity analysis methods has been quantified through the evaluation of the log-normal standard deviation of V_S for (a) each of the velocity analysis methods (i.e., PI, TI, and SM) to capture the intra-velocity-analysis-method uncertainty associated with consideration of different travel times (i.e., FA, PT, CO, and CC) and (b) all twelve of the SCPT V_S profiles together.

At the first site, with a relatively simple near-surface soil profile, the σ_{lnVs} never exceeds 0.2 and is typically less than 0.1. The soil profile at the second site consists of interlayered sands and silts. The thin layering and the corresponding fluctuations in soil stiffness results in increased uncertainty in the SCPT profiles, reflected by a corresponding increase in $\sigma_{lnVs.}$ At his second site, the σ_{lnVs} typically ranges between 0.05 and 0.2, with σ_{lnVs} values above 0.4 at depths where layer boundaries and the associated shear-wave velocities are poorly constrained. At both of these sites, the σ_{lnVs} represent a realistic, depth-dependent quantification of the epistemic uncertainty associated with V_S profiles obtained via SCPT testing.

Furthermore, the epistemic uncertainty associated with the use of different invasive seismic testing methods has been examined through a comparison of the SCPT raytracing and DPCH VS profiles developed at each of the 31 case history sites. At the near-surface (i.e., depth < 3 m), the SCP_T VS profiles are biased towards lower velocities and the median percent difference between the SCPT RT and DPCH V_S profiles is 60%. Below 3 meters, the two sets of V_S profiles generally agree with percent differences, on average, less than 15%.

Given these results and those presented in the literature (Garofalo et al. 2016, Styler, M.A. and Weemees 2017), it is important to note that there is epistemic uncertainty associated with the development V_S profiles from SCPT testing, indeed from any invasive seismic testing method. In practice, it is common for an SCPT contractor to provide a single V_S profile to the engineer, with no indication of the associated uncertainty. While in many cases this single V_S profile may be sufficient for engineering purposes, the engineer should

always be informed of the assumptions and analysis methods used in the development of this profile. Furthermore, the SCPT picked travel times should be indicated directly on the measured waveforms in a waterfall style plot and provided in a table, such that the engineer could reprocess the data, as needed, using other analysis methods, such as the corrected-vertical travel time slope-based method.

As engineering practice moves from deterministic to probabilistic analyses, a meaningful, realistic assessment of the uncertainty with seismic measurements is needed. The process developed in this paper, through the consideration of several analysis methods to evaluate V_S obtained via SCPT, profiles a suitable means to quantify the epistemic uncertainty associated with these V_S profiles. Even at a complex, interlayered soil site (e.g., the St. Teresa's site) the depth-dependent σ_{lnVs} typically ranges between 0.05 and 0.20. At depths where layer boundaries are poorly resolved and/or V_S is poorly constrained by the analysis methods, the uncertainty is realistically captured by a corresponding increase in σ_{lnVs}. This process provides: (1) several "real" V_S profiles, developed from measurements in situ, which can be used directly in the engineering analysis, and (2) a realistic assessment of epistemic uncertainty that varies with depth and better reflects the uncertainty in the measurements than the commonly assumed depth-independent constant coefficient of variations.

5.1.3 Feasibility of in-situ evaluation of soil void ratio using high resolution measurements of V_S and V_P from DPCH testing

A relationship to evaluate soil porosity (i.e., void ratio) in fully-saturated soils from seismic wave propagation velocities (i.e., V_P and V_S) was developed by Foti et al. (2002) using the theory of linear poroelasticity (Biot 1956a) as an underlying framework. Soil porosity is evaluated as a function of V_P, V_S and four additional parameters describing the physical properties of the soil (i.e., ν_{SK}, ρ_S, ρ_W, and K_W). In this study, the effectiveness and feasibility of using high-resolution V_S and V_P measurements from DPCH testing to estimate in-situ void ratios was investigated at ten, predominantly clean sand case history sites in Christchurch, New Zealand. As high-quality, "undisturbed" samples were not available at these ten sites, absolute comparisons of in-situ void ratio estimates could not be made. Hence, only relative comparisons could be made between CPT-based estimates of in-situ void ratio and those obtained from seismic measurements. Nonetheless, the CPT-based estimates of in-situ void ratio were "calibrated" using soil-specific e_{min} and e_{max} values, including associated uncertainties, and were demonstrated to yield fairly consistent agreement with void ratio measurements obtained from gel-push samples of sand at two other sites in Christchurch.

Detailed comparisons between seismic- and CPT-based void ratio estimates have been shown at four sites, where agreement between estimates ranges from excellent to poor. From a statistical analysis of 253 seismic-based void ratio estimates across nine of the ten sites considered in this study, it was found that approximately 43% of the in-situ void ratio estimates for the clean sand data points fell within 10% of the Baldi et al. (1986)

CPT-based estimates. While this agreement may not seem amazing, it should be noted that only about 9% of the CPT-based void ratio estimates of Baldi et al. (1986) agree within 10% of the CPT-based estimates of Kulhawy and Mayne (1990) and Jamiolkowski et al. (2001). In fact, for more than 65% of the data points considered, the Baldi et al. (1986) CPT-based estimates agree better with the seismic-based estimates than with the other CPT-based estimates. However, for the remaining 35% of the data points, the maximum percent difference between the CPT-based void ratios is no more than 20%, while the maximum percent difference between the seismic- and CPT-based void ratios ranges from about 45% to 55%. These large differences are attributed to small errors in determining V_P, which result in significant underestimation of void ratio. While the "true" void ratios in this study are not known, when very poor agreement between seismic- and CPT-based estimates of void ratio are observed in clean sands, we believe the seismic-based estimates are most likely in error. However, it has been demonstrated that only moderate adjustments to V_P are required to bring the seismic- and CPT-based void ratio estimates into agreement with one another. Specifically, it has been demonstrated that V_P only needs to be adjusted by 2 to 4%, on average, in order to bring the seismic- and CPT-based estimates into agreement with one another. This finding is both encouraging and discouraging; encouraging because estimating void ratio based on in-situ measurements of V_S and V_P seems attainable, and discouraging because it is extremely difficult to measure any parameter in situ within 2%.

We believe that DPCH testing has the potential to enable very high-resolution measurements of V_P and V_S. With slight improvements to the equipment and testing

procedures we hope to be able to track cone deviations and resolve P-wave travels times even more accurately. If this can be done, more consistent and reliable estimates of in-situ void ratio can be obtained from linear poroelasticity theory, which is valid for all fluid-saturated porous materials (e.g., sands, silts, and clays). Estimating void ratio in this way is much more satisfying than continuing to rely on empirical correlations to penetration resistance that also show significant scatter and, at best, are currently only appropriate for use in clean sands. Additional case histories are needed to increase confidence in void ratio estimates made via DPCH seismic measurements through direct comparisons with laboratory measured void ratios on high-quality samples of both granular and cohesive soils.

Appendix: Improvements to DPCH Instrumentation

This appendix documents the development and refinement of the instrumented cones used for direct-push crosshole testing (as described in Chapter 2), including the development and testing of a pushable in-ground seismic source cone.

A1.1 Refinement of the DPCH receiver cones

A1.1.1 Early DPCH Cones

As described in Chapter 2, early DPCH testing was conducted in support of in-situ liquefaction testing described in Cox 2006 and Cox et al. 2008. The seismic source for the DPCH testing was a hammer tap on an un-instrumented cone pushed to the same elevation as the in-situ liquefaction seismic cones. The hammer was instrumented with a shock accelerometer to trigger data acquisition and calibrations were performed to remove the travel time of the P-waves down the steel cone push rod. The in-site liquefaction cones were instrumented with 3D-MEMS accelerometers to measure vibrations (primarily to evaluate shear-strain induced during testing) and to measure tilt as the cones were embedded into the ground to form a trapezoidal array. They also included a pore pressure transducer (PPT) to measure pore pressure build-up during liquefaction testing, but the PPT was not used for DPCH testing. The instrumentation was encased in an acrylic cone housing, as shown in Figure A.1. The cones were designed to be pushed into the ground using a metal collar slip-fitted into a CPT cone rod adaptor and retrieved using a metal pull cable. The MEMS accelerometer was well suited to measure P- and S-waves for DPCH

testing, and it was possible to track the tilt of the receiver cone during testing. However, the tilt of the un-instrumented source cone was not tracked. However, these MEMS accelerometers were expensive and not robust enough to withstand repeated testing. The acrylic housing of the cone and the metal cable were not suited to repeated testing cycles of cone advancement into the ground and subsequent retrieval.

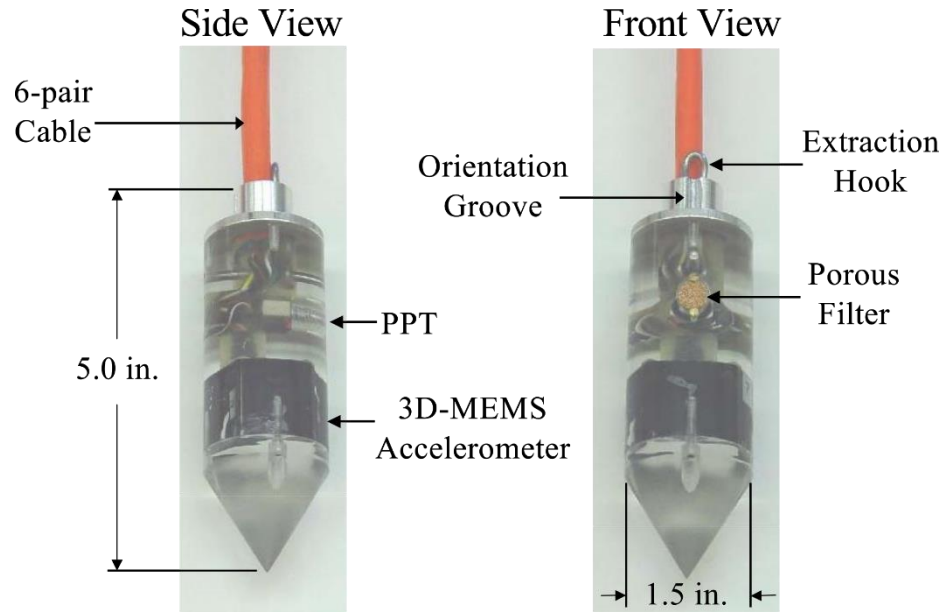

Figure A.1: In-site liquefaction testing instrumented cones adapted for use in early DPCH testing. Note the 3D-MEMS accelerometer, the acrylic cone body, and the extraction hook and collar (from Cox 2006).

Next, DPCH testing was conducted as a part of the Christchurch ground improvement trials in 2014. Three-component DPCH cones (shown in Figure A.2) were designed for this project, based on the in-situ liquefaction dynamic measurement cones. The fragile MEMS accelerometer was replaced with vertical, in-line horizontal, and crossline horizontal geophones. The three-geophones were housed in a machined polycarbonate housing and epoxied in place. A steel pull cable was attached to the metal

top cap of the cone body and used for cone extraction after testing. These cones were not capable of tracking tilt, but they were only used to test at shallow depths (i.e., less than 5 m). These instrumented cones were only used as receivers. As with the WLA testing, a dummy steel cone was advanced into the ground and used as the seismic source by tapping the top of the push rod with a hammer.

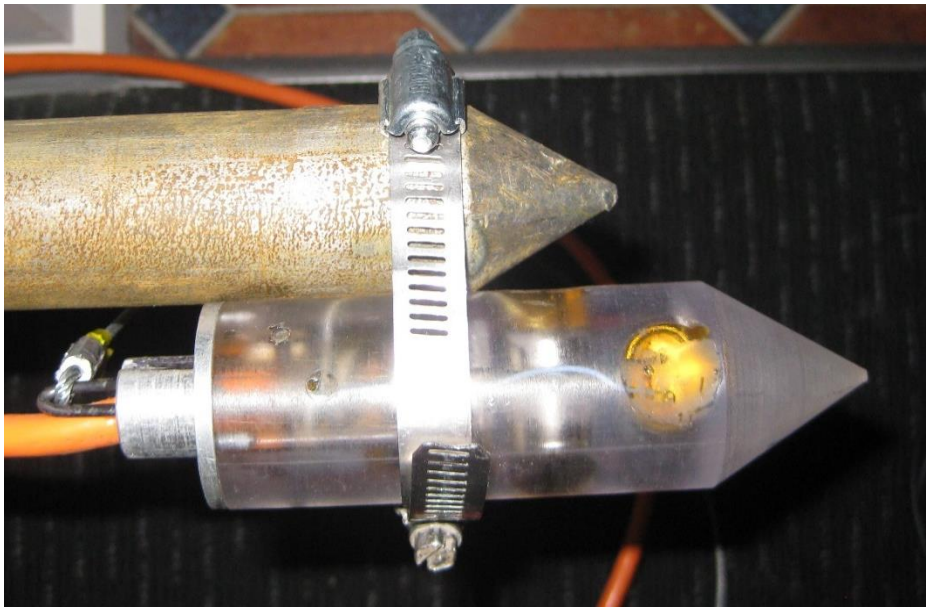

Figure A.2: A three-component polycarbonate DPCH instrumented cone. The cone is attached to a dummy cone for trigger calibration, prior to testing in the field.

During the second portion of the ground improvement trials, new three-component DPCH cones were fabricated from steel (shown in Figure A.3). The wiring and geophones were epoxied into place, inside of the steel cone housing. The epoxy was exposed to the ground during testing and was subject to pitting. The steel retrieval cable was replaced by threading at the top of the cone, allowing firm attachment to the cone push rods for advancement and simplified retrieval.

Figure A.3: The first DPCH instrumented cone fabricated from steel. Note the threading at the top and the exposed, epoxied geophone wells.

A1.1.2 Two-Component Cones with Tilt Measurement

After the Christchurch ground improvement trials in 2014, new two-component (i.e., in-line horizontal and vertical geophones) DPCH specific cones were designed and constructed at the University of Texas, as shown in Figure A.4. This design incorporated improvements based on field experience with prior cone iterations. The fabrication of these were first involvement of the author in the development of instrumented cones. These DPCH cones were the first to incorporate a removable hardened steel jacket to protect the instrumentation and provide the robustness needed to withstand many cycles of cone advancement and retrieval. An inexpensive, low power, 3D-MEMS accelerometer was re-introduced in this design to track tilt and allow for the evaluation of the true distance between the cones, which is a concern as testing depths increased to 10 meters and beyond.

The exterior of the cone housing is marked with a vertical groove to indicate the positive in-line horizontal direction and the orientation of the horizontal geophone.

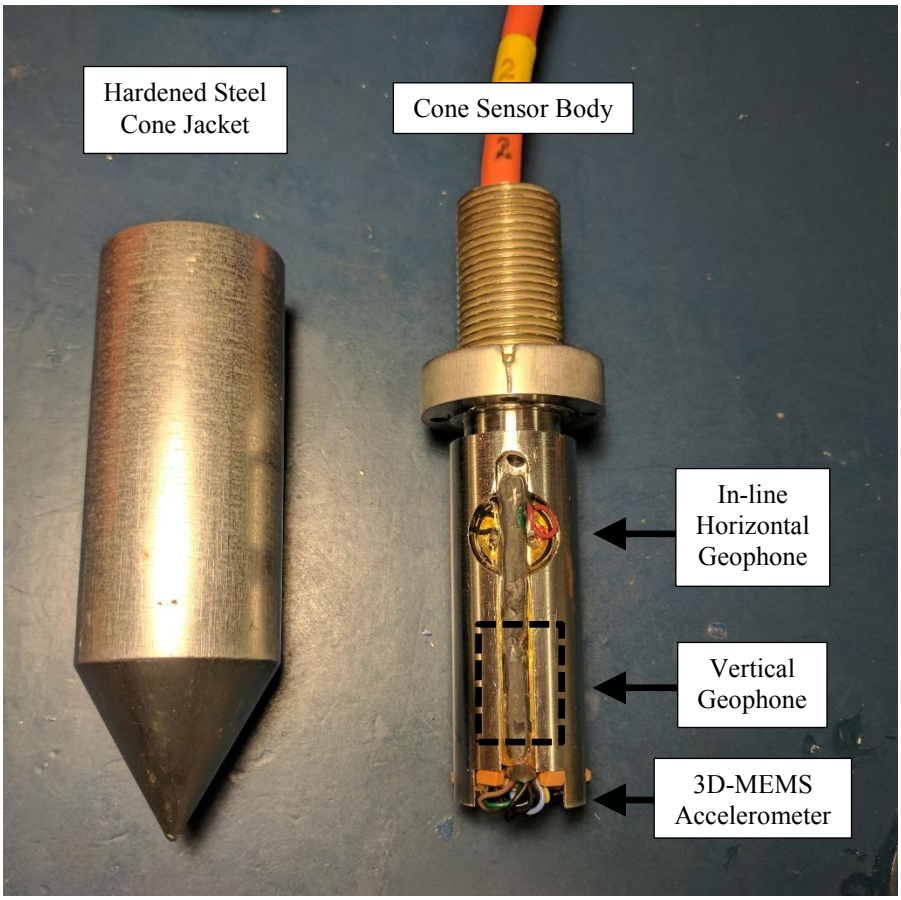

Figure A.4: Two Component DPCH Instrumented Cone. Note the removable hardened steel cone jacket, the threaded collar, the 28 Hz Geophones, and the 3D-MEMS Accelerometer

A1.1.3 Three-Component Cones with Tilt Measurement

The most recent iteration of the DPCH instrumented receiver cone is simple refinement of the two-component cones with tilt measurement shown above. These cones were designed and built by the author. A third geophone oriented in the in the cross-line horizontal direction was added to the cones to measure S_{HH}-waves generated using the in-

ground source cone discussed below. The exterior of the hardened steel jacket was engraved with markings to indicate the orientation and location of the components inside the cone housing to simplify placement and orientation of the cones during testing. A picture and sketch of the three-component cone with tilt measurement is shown in Figure A.5.

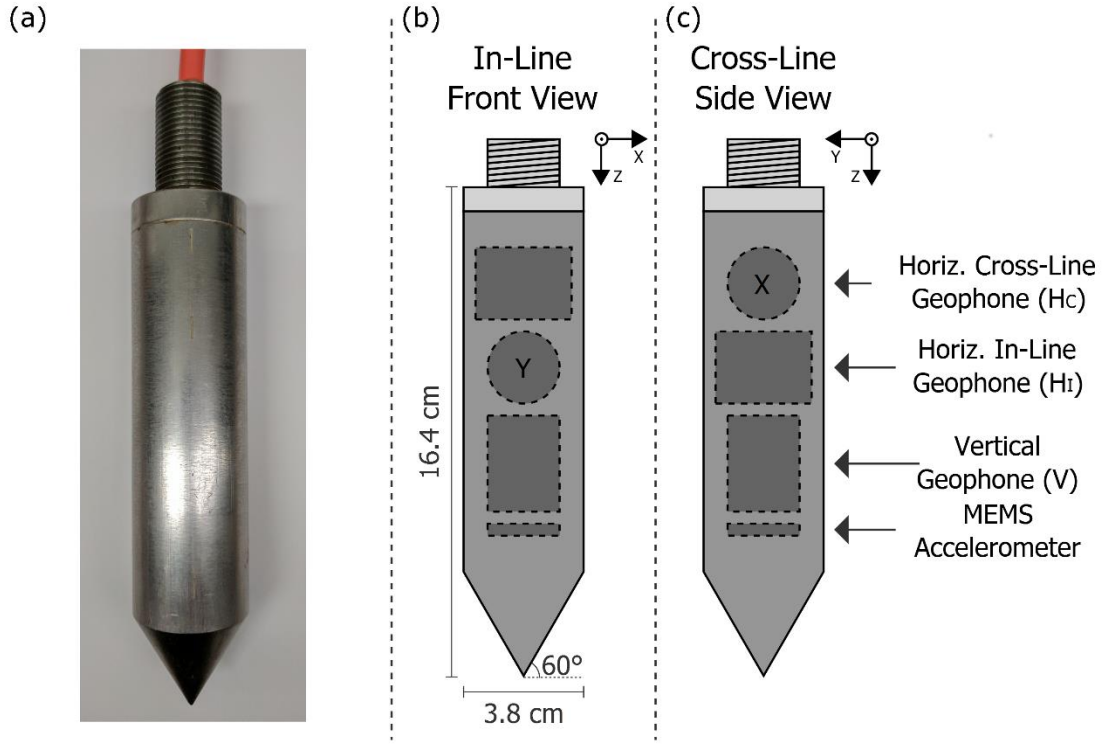

Figure A.5: Three-component instrumented cone used for DPCH testing. (a) Photograph of instrumented cone showing the exterior hardened steel jacket, the threaded connection to the rod adaptor, and the orange 6-pair cable. The positive horizontal in-line and cross-line directions are indicated by capital Y and X markings, respectively. Schematic of geophone and accelerometer orientation inside the instrumented cone as viewed from the positive horizontal (b) in-line, and (c) cross-line directions.

A1.2 IN-GROUND SOURCE CONE

A pushable in-ground seismic source cone was designed and built by the author. The source cone is 30.5 cm (12 in) long, excluding threading, and 5.3 cm (2.1 in) in diameter, as shown in Figure A.6 with a three-component receiver for comparison. The increased size is needed to accommodate six solenoids, the three orthogonally-oriented geophones and the 3D-MEMS accelerometer. The solenoids are individually controlled using a breakout/control box. When current is applied to an individual solenoid coil circuit, the solenoid retracts a spring loaded plunger into the solenoid. When the current is cut, the "cocked" spring is released to propel the plunger to strike against the hardened cone jacket or sensor body. The solenoids are oriented in pairs to strike the cone with positive or negative polarity in the vertical, in-line horizontal, and cross-line horizontal directions, generating repeatable S_{HV}-, P_H-, and S_{HH}-waves, respectively. In contrast, hammer taps on the push rod is generate P_H-waves and S_{HV}-waves with an initial downward particle motion.

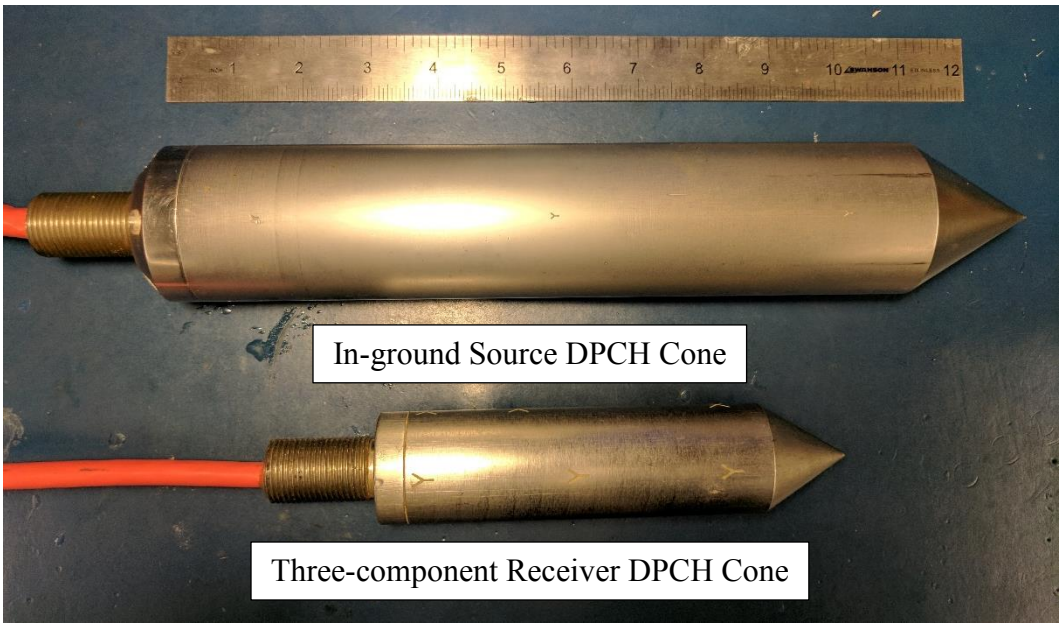

Figure A.6: In-ground source DPCH cone and three-component receiver DPCH cone

The in-ground source cone has been successfully used at two sites in Christchurch, NZ to aid in the identification of direct S_{HV}-wave arrivals. Previous site characterization at the Cashmere Rd. site indicated significant interlayering of sands and silts, overlying a stiff gravel layer. The interlayering is characterized by alternating changes in stiffness (i.e., V_S) over the near-surface soil profile. As discussed in Chapter 2, there is difficulty identifying the direct arrival of S-waves through thin, soft layers in-between stiffer layers, especially near the layer boundaries. Profiles of V_S from the in-ground source cone dataset collected in at the 200 Cashmere Rd. site in Christchurch, NZ are shown in Figure A.7 along with the associated waveforms and picks in waterfall format. The cone tip resistance is plotted beside the S-wave velocity profiles for comparison. In general, the hammer and source generated S_{HV}-waves agree well over the entire depth range, while the S_{HH}-waves differ slightly, possibly indicating structural or stress anisotropy in the soil.

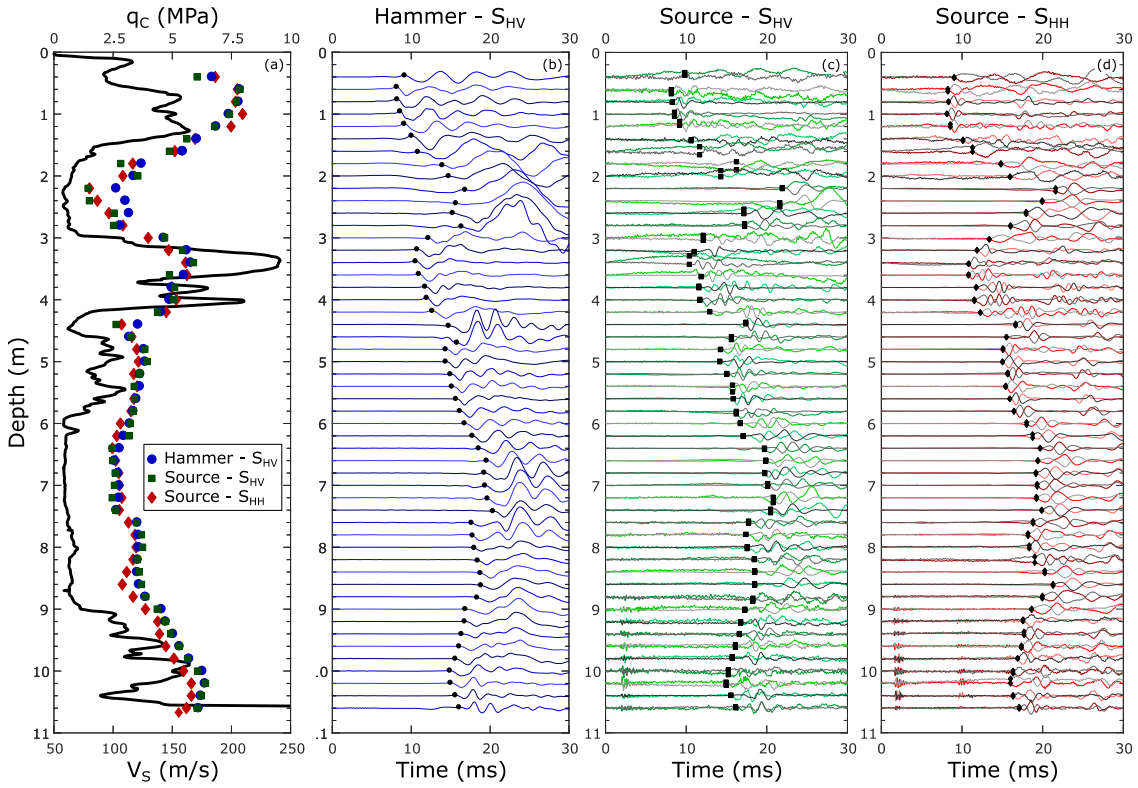

Figure A.7: In-ground source cone DPCH Cashmere Rd. dataset: (a) Comparison of CPT cone tip resistance with three V_S profiles obtained via DPCH testing, i.e., hammer tap $V_{S,HV}$, in-ground source cone $V_{S,HV}$, and in-ground source cone $V_{S,HH}$. In panels (b), (c), and (d), the associated S_{HV} (hammer tap), S_{HV} (source cone), and S_{HH} (source cone) waveforms are shown in waterfall format with associated S-wave direct arrival picks, indicated by circle, square, and diamond markers, respectively.

References

Andrus, D.R. and Stokoe, K. H., II., (2000). "Liquefaction Resistance of Soils from Shear-Wave Velocity," ASCE, *Journal of Geotechnical and Geoenvironmental Engineering*, Vol. 126, No. 11, pp 1015-1025.

ASTM International, (2001). ASTM D5777-00(2011)e1 Standard Guide for Using the Seismic Refraction Method for Subsurface Investigation, West Conshohocken, PA, www.astm.org.

ASTM International, (2011). ASTM D1586-11 Standard Test Method for Standard Penetration Test (SPT) and Split-Barrel Sampling of Soils, West Conshohocken, PA, www.astm.org.

ASTM International, (2012). ASTM D5778-12 Standard Test Method for Electronic Friction Cone and Piezocone Penetration Testing of Soils, West Conshohocken, PA, www.astm.org.

ASTM International, (2012). ASTM D5778-12 Standard Test Method for Electronic Friction Cone and Piezocone Penetration Testing of Soils, West Conshohocken, PA, www.astm.org

ASTM International, (2014). ASTM D4428/D4428M-14 Standard Test Methods for Crosshole Seismic Testing.

ASTM International, (2014). .ASTM D7400-14 Standard Test Methods for Downhole Seismic Testing, West Conshohocken, PA, www.astm.org

ASTM International, (2016). ASTM D4253-16 Standard Test Methods for Maximum Index Density and Unit Weight of Soils Using a Vibratory Table, West Conshohocken, PA, www.astm.org.

ASTM International, (2016). ASTM D4254-16 Standard Test Methods for Minimum Index Density and Unit Weight of Soils and Calculation of Relative Density, West Conshohocken, PA, www.astm.org.

Backus, G. E., (1962) "Long-wave elastic anisotropy produced by horizontal layering," *Journal of Geophysical Research*, 67(11), 4427-4440.

Baldi, G., Bellotti, R., Ghionna, V.N., Jamiolkowski, M., and Lo Presti, D.F.C. (1989). Modulus of sands from CPTs and DMTs. *In Proceedings of the 12th International Conference on Soil Mechanics and Foundation Engineering*. Rio de Janeiro. Balkema Pub., Rotterdam, Vol.1, pp. 165-170.

Bang, E. S., Cho, S. J., & Kim, D. S. (2014). “Mean refracted ray path method for reliable downhole seismic data interpretations”. *Soil Dynamics and Earthquake Engineering*, 65, 214-223.

Bates, C. R. (1989). Dynamic soil property measurements during triaxial testing. *Géotechnique* 39(4): 721-726.

Baziw, E., (1993). “Digital Filtering Techniques for Interpreting Seismic Cone Data,” *ASCE J. Geotech. Eng.*, Vol. 119, No. 6, pp. 998–1018.

Baziw, E., (2002). “Derivation of Seismic Cone Interval Velocities Utilizing Forward Modeling and the Downhill Simplex Method,” *Can. Geotech. J.,* Vol. 39, pp. 1–12.

Beyzaei, C.Z., Bray, J.D., Cubrinovski, M., Riemer, M., Stringer, M.E. (2017a). “Laboratory-Based Characterization of Shallow Silty Soils in Southwest Christchurch.” *Soil Dyn. Earthquake Eng.*, submitted January 2017.

Biot, M. A., (1956a). “Theory of propagation of elastic waves in a fluid-saturated porous solid. I. Lower frequency range,” *J. Acoust. Soc. Am.* 28, pp. 168–178.

Biot, M. A., (1956b) “Theory of propagation of elastic waves in a fluid-saturated porous solid. II. Higher frequency range,” *J. Acoust. Soc. Am.* 28, pp. 179–191.

Boore, D. M., and Thompson, E. M., (2007). "On using surface-source downhole-receiver logging to determine seismic slowness," *Soil Dynamics and Earthquake Engineering*, 27, 971-985.

Bray, J.D., Cubrinovski, M., Zupan, J., and Taylor, M. (2014) Liquefaction Effects on Buildings in the Central Business District of Christchurch. *Earthquake Spectra J.*, Earthquake Engineering Research Institute, Vol. 30(1), 85-109, DOI: 10.1193/022113EQS043M

Castagna, J. P., Batzle, M. L. & Eastwood, R. L. (1985). Relationship between compressional-wave and shear-wave velocities in clastic silicate rocks. *Geophysics* 50, 571–581.

Chander, R., (1977). "On tracing seismic rays with specified end points in layers of constant velocity and plane interfaces," *Geophysical Prospecting*, 25: 120–124.

Cox, B. R., 2006, *Development of a Direct Test Method for Dynamically Assessing the Liquefaction Resistance of Soils In Situ*, Ph.D. Dissertation, The University of Texas, Austin, TX, 498 pp.

Cox, B.R., McLaughlin, K.A., van Ballegooy, S., Cubrinovski, M., Boulanger, R., Wotherspoon, L., (2017). “In-Situ Investigation of False-Positive Liquefaction Sites in Christchurch, New Zealand: St. Teresa’s School Case History," presented at *3rd International Conference on Performance-based Design in Earthquake Geotechnical Engineering*, Vancouver, Canada, 16-19 July 2017.

Cox, B. R., Stokoe, K. H., and Rathje, E. M., (2009). "An In Situ Test Method for Evaluating the Coupled Pore Pressure Generation and Nonlinear Shear Modulus Behavior of Liquefiable Soils," *Geotechnical Testing Journal*, Vol. 32, No. 1, pp. 11-21, https://doi.org/10.1520/GTJ101484.

Cubrinovski, M., Rhodes, A., Ntritsos, N., van Ballegooy, S., (2017). “System response of liquefiable deposits," presented at *3rd International Conference on Performance-based Design in Earthquake Geotechnical Engineering*, Vancouver, Canada, 16-19 July 2017.

Cubrinovski, M., & Robinson, K., (2016). “Lateral spreading: Evidence and interpretation from the 2010-2011 Christchurch Earthquakes,” *Soil Dynamics and Earthquake Engineering*, 91, pp. 187-201.

Dix, C. H. (1939). Interpretation of well-shot data. *Geophysics* 4(1), 24-32.

Domenico, S. N. (1984). Rock lithology and porosity determination from shear and compressional wave velocity. *Geophysics*, 49(8), 1188-1195. https://doi.org/10.1190/1.1441748

Ederhart-Phillips, D., Han, D.-H. & Zoback, M. D. (1989). Empirical relationships among seismic velocities, effective pressure, porosity, and clay content in sandstones. *Geophysics,* 54, 82–89.

Electric Power Research Institute (EPRI), (2012). "Seismic Evaluation Guidance: Screening, Prioritization and Implementation Details (SPID) for the Resolution of Fukushima Near-Term Task Force Recommendation 2.1: Seismic", Palo Alto, CA, Report 1025287, pp. 206.

Foti, S., Comina, C., Boiero, D., & Socco, L. V. (2009). Non-uniqueness in surface-wave inversion and consequences on seismic site response analyses. *Soil Dynamics and Earthquake Engineering*, 29(6), 982-993.

Foti, S., Lai, C. G., & Lancellotta, R., (2002). "Porosity of fluid-saturated porous media from measured seismic wave velocities," *Géotechnique*, 52, pp. 359-373.

Foti, S. and Lancellotta, R., (2004). "Soil porosity from seismic velocities," *Géotechnique*, 54, pp. 551-554.

Foti, S., & Passeri, F. (2016). Reliability of soil porosity estimation from seismic wave velocities. *In Isc5-International Conference on Geotechnical and Geophysical Soil Characterisation*, Gold Coast, Australia (Vol. 1, pp. 425–430).

Garofalo, F., Foti, S., Hollender, F., Bard, P.-Y., Cornou, C., Cox, B.R., Ohrnberger, M., Sicilia, D., Asten, M., Di Giulio, G., Forbriger, T., Guiller, B., Hayashi, K., Martin, A., Matsushima, S., Mercerat, D., Poggi, V., Yamanaka, H., (2016), "InterPACIFIC Project: Comparison of Invasive and Non-Invasive Methods for Seismic Site Characterization Part I: Intra-Comparison of Surface Wave Methods," *Soil Dynamics and Earthquake Engineering*, 82(1), pp. 222-240, http://dx.doi.org/10.1016/j.soildyn.2015.12.010

Garofalo, F., Foti, S., Hollender, F., Bard, P.-Y., Cornou, C., Cox, B.R., Dechamp, A., Ohrnberger, M., Sicilia, D., D. Teague, Vergniault, C., (2016). "InterPACIFIC Project: Comparison of Invasive and Non-Invasive Methods for Seismic Site Characterization Part II: Inter-Comparison Between Surface Wave and Borehole Methods," *Soil Dynamics and Earthquake Engineering*, 82(1), pp. 241-254, http://dx.doi.org/10.1016/j.soildyn.2015.12.009

Griffiths, S.C., Cox, B.R., Rathje, E.M., Teague, D.P. (2016a). "Surface Wave Dispersion Approach for Evaluating Statistical Models That Account for Shear-Wave Velocity

Uncertainty," *Journal of Geotechnical and Geoenvironmental Engineering*, 142(11), 04016061. (http://dx.doi.org/10.1061/(ASCE)GT.1943-5606.0001552).

Griffiths, S.C., Cox, B.R., Rathje, E.M., Teague, D.P. (2016b). "Mapping Dispersion Misfit and Uncertainty in Vs Profiles to Variability in Site Response Estimates," *Journal of Geotechnical and Geoenvironmental Engineering*, 142(11), 04016062. (http://dx.doi.org/10.1061/(ASCE)GT.1943-5606.0001553).

Gu, X., Yang, J., & Huang, M. (2013). Laboratory measurements of small strain properties of dry sands by bender element. *Soils and Foundations*, 53(5), 735-745.

Han, D.-H., Nur, A. & Morgan, D. (1986). Effects of porosity and clay content on wave velocity in sandstones. *Geophysics* 51, 2093–2107.

Hossain, A. M., Andrus, R. D., & Camp III, W. M., 2012, "Correcting liquefaction resistance of unsaturated soil using wave velocity," *Journal of Geotechnical and Geoenvironmental Engineering*, 139(2), pp. 277-287.

Hunter, J. A. (2003). Some observations of Vp, Vs, depth and porosity from boreholes in water-saturated unconsolidated sediments. *Proc. SAGEEP 2003*, San Antonio, 650–661.

Hwang, S., Roberts, J. N., Stokoe, K. H., II, Cox, B. R., van Ballegooy, S., & Soutar, C., (2017). "Utilizing Direct-Push Crosshole Seismic Testing to Verify the Effectiveness of Shallow Ground Improvements: A Case Study Involving Low-Mobility Grout Columns in Christchurch, New Zealand." presented in *Grouting 2017*, pp. 415-424.

Ishihara, K., & Tsukamoto, Y., (2004). "Cyclic strength of imperfectly saturated sands and analysis of liquefaction," *Proceedings of the Japan Academy, Series B*, 80(8), pp. 372-39.

Jamiolkowski, M. (2012). Role of Geophysical Testing in Geotechnical Site Characterization. *Soils and Rocks.* 35(2): 117-137.

Jamiolkowski, M., Lancellotta, R., Lo Presti, D., & Pallara, O. (1994). Stiffness of Toyoura sand at small and intermediate strain. *In XIII ICSMFE*, New Delhi (Vol. 1, pp. 169-172). Oxford & IBH Publishing Co. PVT. LTD.

Jamiolkowski, M., LoPresti, D.C.F., and Manassero, M. (2001). Evaluation of relative density and shear strength of sands from cone penetration test and flat dilatometer test. *Soil Behavior and Soft Ground Construction* (GSP 119), ASCE, Reston, VA: 201-238.

Kayen R., Moss R., Thompson E., Seed R., Cetin K., Der Kiureghian A., Tanaka Y., Tokimatsu, K., 2013. “Shear Wave velocity–based probabilistic and deterministic assessment of seismic soil liquefaction potential,” *J. Geotech. Geoenviron. Eng.*, 139(3), pp. 407–419.

Kell, G. S. (1975). Density, thermal expansivity, and compressibility of liquid water from 0. deg. to 150. deg.. Correlations and tables for atmospheric pressure and saturation reviewed and expressed on 1968 temperature scale. *Journal of Chemical and Engineering Data*, 20(1), 97-105

Kim, Dong-Soo, Eun-Seok Bang, and Won-Chul Kim. "Evaluation of various downhole data reduction methods for obtaining reliable Vs profiles." *Geotechnical Testing Journa,l* 27.6 (2004): 585-597.

Kokusho, T., (2000). “Correlation of pore-pressure B-value with P-wave velocity and Poisson's ratio for imperfectly saturated sand or gravel,” *Soils and Foundations, 40*(4), pp. 95-102.

Krief, M., Garat, J., Stellingwerff, J. & Ventre, J. (1990). A petrophysical interpretation using the velocities of P and S waves. *The Log Analyst* 31, 355–369.

Kulhawy, F.H. and Mayne, P.W. (1990). Estimating Soil Properties for Foundation Design. *EPRI Report EL-6800*, Electric Power Research Institute, Palo Alto: 306 p. www.epri.com

Kumar, J., & Madhusudhan, B. N. (2010). Effect of relative density and confining pressure on Poisson ratio from bender and extender elements tests. Géotechnique, 60(7), 561-567.

Kusuda, T. and Achenbach, P.R. (1965) Earth temperature and thermal diffusivity at selected stations in the United States, *ASHRAE Transactions*, 71 (1), pp. 61-75.

Lambe, T.W. and Whitman, R.V. (1967). *Soil Mechanics*. John Wiley & Sons.

Lai, C. G. & Crempien de la Carrera, J. G. F. (2012). Stable inversion of measured VP and VS to estimate porosity in fluid-saturated soils. *Géotechnique* 62(4): 359-364.

Lubbers, J., & Graaff, R. (1998). A simple and accurate formula for the sound velocity in water. *Ultrasound in medicine and biology*, 24(7), 1065-1068.

Marosi, K. T., & Hiltunen, D. R. (2004). Characterization of spectral analysis of surface waves shear wave velocity measurement uncertainty. *Journal of geotechnical and geoenvironmental engineering*, *130*(10), 1034-1041.

Matasovic, N., and Hashash, Y. (2012) "NCHRP Synthesis 428: Practices and Procedures for Site-Specific Evaluations of Earthquake Ground Motions, A Synthesis of Highway Practice." *National Cooperative Highway Research Program of the Transportation Research Board*, Washington, D.C.

McCollum, B., & LaRue, W. W. (1931). Utilization of existing wells in seismograph work. *AAPG Bulletin*, 15(12), 1409-1417.

McLaughlin, K., (2017). *Investigation of false-positive liquefaction case history sites in Christchurch, New Zealand*. M.S. Thesis. The University of Texas at Austin.

Miura, K., Yoshida, N. & Kim, Y. S. (2001). FreSquency dependent property of waves in saturated soil. *Soils and Foundations*, 41, No. 2, 1–19.

Nakagawa, K., Soga, K., & Mitchell, J. K. (1997). Observation of Biot compressional wave of the second kind in granular soils. *Géotechnique*, 47(1), 133-147.

Nigbor, R L., and Imai, T., (1994). "The suspension PS velocity logging method." *Proc. XIII International Conference on Soil Mechanics and Foundation Engineering*.

Raymer, L. L., Hunt, E. R. & Gardner, J. S. (1980). An improved sonic transit time-to-porosity transform. *presented in Trans. Soc. Prof. Well Log Analysts*, 21st Annual Logging Symposium, Paper P.

Ohya, S., K. Ogura, and T. Imai., (1984). "The suspension PS velocity logging system," *Offshore Technology Conference*

Redpath, B.B., (2007). "Downhole Measurements of Shear- and Compression-Wave Velocities in Boreholes C4993, C4996, C4997, and C4998 at the Waste treatment Plant DOE Hanford Site". www.pnl.gov/main/publications/external/technical_reports/PNNL-16559.pdf

Richart, F. E., Hall, J. R., & Woods, R. D., (1970). *Vibrations of soils and foundations*. Prentice-Hall, Inc.

Robertson, P.K., (2015) "Comparing CPT and V_S liquefaction triggering methods," *Journal of Geotechnical and Geoenvironmental Engineering*, ASCE, 141(9), 04015037, 10.1061/(ASCE)GT.1943-5606.0001338.

Robertson, P. K., Campanella, R. G., Gillespie, D., & Rice, A. (1986). "Seismic CPT to measure in situ shear wave velocity". *Journal of Geotechnical Engineering*, 112(8), 791-803.

Salgado, R., Mitchell, J. K., & Jamiolkowski, M. (1997). Cavity expansion and penetration resistance in sand. Journal of Geotechnical and Geoenvironmental Engineering, 123(4), 344-354.

Spetzler, J. and Snieder, R., (2004). "The Fresnel volume and transmitted waves." *Geophysics*, 69(3), 653-663. https://doi.org/10.1190/1.1759451

Stokoe, Kenneth H., II, (1972). "Dynamic Response of Embedded Foundations," Ph.D. Dissertation, University of Michigan, Michigan, 251 pp.

Stokoe, Kenneth H., II, and Hoar, Richard, (1978). "Variables Affecting In Situ Seismic Measurements", *Proceedings of Earthquake Engineering and Soil Dynamics, ASCE Geotechnical Engineering Specialty Conference*, Pasadena, California, Vol. I, June 1978, pp. 919-939.

Stokoe, K. H., II, Roberts, J. N., Hwang, S., Cox, B.R., Menq, F.Y., and van Ballegooy, S., (2016). "Effectiveness of Effectiveness of Inhibiting Liquefaction Triggering by Shallow Ground Improvement Methods: Field Shaking Trials with T-Rex at One Area in Christchurch, New Zealand," *24th Geotechnical Conference of Torino, Design; Construction & Controls of Soil Improvement Systems* 25-26 February 2016, Turin, Italy, pp. 1-20.

Stokoe, K. H., II, Roberts, J.N., Hwang, S., Cox, B. R., Menq, F.Y., and van Ballegooy, S., (2014). "Effectiveness of Inhibiting Liquefaction Triggering by Shallow Ground Improvement Methods: Initial Field Shaking Trials with T-Rex at One Site in Christchurch, New Zealand," *Soil Liquefaction during Recent Large-Scale Earthquakes,* Orense, Towhata & Chouw (Eds.)

Stokoe, Kenneth H., II, Woods, Richard D., (1972). "In Situ Shear Wave Velocity by Cross-Hole Method", *Journal of Soil Mechanics and Foundation Division*, Proceedings of ASCE, Vol. 98, No. SM5, May, 1972, pp. 443-460.

Styler, M.A. and Weemees, I. (2017). "Evaluating and reporting uncertainty in downhole shear wave velocities," presented in *3rd International Conference on Performance-based Design in Earthquake Geotechnical Engineering*, Vancouver, Canada, 16-19 July 2017.

Tamura, S., Tokimatsu, K., Abe, A., and Sato, M. (2002). Effects of the air bubbles on B value and P wave velocity of a partially saturated sand. *Soils and Foundations*, 42(1): 121–129.

Taylor, M. (2015). *The Geotechnical Characterisation of Christchurch Sands for Advanced Soil Modelling.* Ph.D. Thesis. The University of Canterbury.

Teague, D.P., Cox, B.R. (2016). "Site Response Implications Associated with using Non-Unique Vs Profiles from Surface Wave Inversion in Comparison with Other Commonly Used Methods of Accounting for Vs Uncertainty," *Soil Dynamics and Earthquake Engineering* 91(1), 87-103. (https://doi.org/10.1016/j.soildyn.2016.07.028).

Teague, D.P., Cox, B.R., Bradley, B., Wotherspoon, L. (2018). "Development of Deep Shear Wave Velocity Profiles with Estimates of Uncertainty in the Complex Inter-Bedded Geology of Christchurch, New Zealand," *Earthquake Spectra*, (https://doi.org/10.1193/041117EQS069M)

Tsukamoto, Y., Ishihara, K., Nakazawa, H., Kamada, K., & Huang, Y., (2002). "Resistance of partly saturated sand to liquefaction with reference to longitudinal and shear wave velocities," *Soils and Foundations*, *42*(6), pp. 93-104

Valle-Molina, Celestino, (2006). *Measurements of V_P and V_S in dry, unsaturated and saturated sand specimens with piezoelectric transducers*, Ph.D. Dissertation. The University of Texas at Austin.

Valle-Molina, C. and Stokoe, K. H., II. (2012). Seismic measurements in sand specimens with varying degrees of saturation using piezoelectric transducers. *Canadian Geotechnical Journal*. 49:671-685, https://doi.org/10.1139/t2012-033

Van Ballegooy, S., Roberts, J.N., Stokoe, K.H., Cox, B.R., Wentz, F.J., Hwang, S., (2015). "Large-Scale Testing of Shallow Ground Improvements using Controlled Staged-Loading with T-Rex," presented at the *6th International Conference on Earthquake Geotechnical Engineering,* 1-4 November 2015, Christchurch, New Zealand.

Wagner, W. & Prußß, A. (2002). The IAPWS Formulation 1995 for the Thermodynamic Properties of Ordinary Water Substance for General and Scientific Use. *Journal of Physical and Chemical Reference Data* 31, 387. doi: 10.1063/1.1461829

Wentz, F.J., van Ballegooy, S., Rollins, K.M., Ashford, S.A., Olsen, M.J., (2015). " Large Scale Testing of Shallow Ground Improvements using Blast-Induced Liquefaction," presented at the *6th International Conference on Earthquake Geotechnical Engineering,* 1-4 November 2015, Christchurch, New Zealand.

Wichtmann, T., & Triantafyllidis, T. (2010). On the influence of the grain size distribution curve on P-wave velocity, constrained elastic modulus Mmax and Poisson's ratio of quartz sands. *Soil Dynamics and Earthquake Engineering*, 30(8), 757-766.

Woods, R. D., (1978). "Measurement of Dynamic Soil Properties," *Proceedings of the ASCE Geotechnical Engineering Division Specialty Conference on Earthquake Engineering and Soil Dynamics*, ASCE, Vol I, 19–21 June 1978, pp. 91–178.

Wotherspoon, L. M., Cox, B. R., Stokoe, K. H., II, Ashfield, D. J., and Philips, R. A., (2015). "Utilizing Direct-Push Crosshole Testing to Assess the Effectiveness of Soil Stiffening Caused by Installation of Stone Columns and Rammed Aggregate Piers," presented at the *6th International Conference on Earthquake Geotechnical Engineering*, 1-4 November 2015, Christchurch, New Zealand

Wotherspoon, L.M., Cox, B.R., Stokoe, K.H., Ashfield, D.J., Phillips, R., (2017). "Assessment of the Degree of Soil Stiffening from Stone Column Installation using Direct Push Crosshole Testing," presented at the *16th World Conference on Earthquake Engineering*, Santiago, Chile, 9-13 January 2017.

Wyllie, M. R., Gregory, A. R. & Gardner, G. H. F. (1956). Elastic wave velocity in heterogeneous and porous media. *Geophysics* 21, 41–70.

Vita

Andrew Christopher Stolte was born in Las Vegas, Nevada. He grew up in Henderson, Nevada and graduated valedictorian from Basic High School in 2006. He entered the University of Nevada, Reno in 2006 and graduated Magna Cum Laude, receiving the degree of Bachelor of Science in 2010. He received the degree of Master of Science from the University of California, Berkeley in 2011. In September, 2012, he entered the Graduate School at the University of Texas at Austin to pursue his doctorate studies in Civil Engineering.

Email: a.c.stolte@utexas.edu

This dissertation was typed by Andrew Christopher Stolte.